

POLYMERIC TEXTILE STENTS: PROTOTYPING AND MODELING

Except where reference is made to the work of others, the work described in this dissertation is my own or was done in collaboration with my advisory committee. This dissertation does not include proprietary or classified information.

Swagat Appasaheb Irsale

Certificate of Approval:

Peter Schwartz
Professor
Textile Engineering

Sabit Adanur, Chair
Professor
Textile Engineering

B. Lewis Slaten
Associate Professor
Consumer Affairs

Stephen L. McFarland
Dean
Graduate School

POLYMERIC TEXTILE STENTS: PROTOTYPING AND MODELING

Swagat Appasaheb Irsale

A Dissertation

Submitted to

the Graduate Faculty of

Auburn University

in Partial Fulfillment of the

Requirements for the

Degree of

Doctor of Philosophy

Auburn, Alabama
December 16, 2005.

POLYMERIC TEXTILE STENTS: PROTOTYPING AND MODELING

Swagat Appasaheb Irsale

Permission is granted to Auburn University to make copies of this dissertation at its discretion, upon request of individuals or institutions and at their expense. The author reserves all publication rights.

Signature of Author

Date of Graduation

VITA

Swagat Appasaheb Irsale, son of Mr. Appasaheb Kallappa Irsale and Mrs. Vasanti Appasaheb Irsale, was born on February 6, 1978 in Ichalkaranji MS, India. He graduated with a Bachelors degree in Man Made Textile Technology from Textile and Engineering Institute (D. K. T. E.), Ichalkaranji MS, India in 1999. He completed his Master of Textile in Textile Technology from Textile and Engineering Institute (D. K. T. E.), Ichalkaranji MS, India in 2002. He joined the graduate program in Textile Engineering at Auburn University in Fall 2002 and graduated with a Master of Science degree in Spring 2004. He enrolled in the PhD program at Auburn University in Summer 2004.

DISSERTATION ABSTRACT

POLYMERIC TEXTILE STENTS: PROTOTYPING AND MODELING

Swagat Appasaheb Irsale

Doctor of Philosophy, December 16, 2005

(M. S., Auburn University, 2004)

(M. Text., Textile and Engineering Institute, India, 2002)

(B. Text., Textile and Engineering Institute, India, 1999)

147 TYPED PAGES

Directed by Dr. Sabit Adanur

Although metal stents have been implanted for more than a decade, performance deficiencies still exist. The current study focuses on prototyping and modeling of braided structures to be used as stents, hence called ‘textile stents’. Textile stents are self-expanding stents. The objective is to establish guidelines for commercial manufacturing of textile stents which can become major substitutes for metal stents. Textile stents and bifurcated textile stents were manufactured. Manufacturing variables braid angle, braid diameter, and heatset time had statistically significant effects ($p= 0.0001$) on the compression force of textile stents. A chart is compiled which categorizes factors affecting the performance of textile stents. Strong correlation (*adjusted* $R^2= 0.9999$) between radial and *in vitro* (unidirectional) compressions of textile stents was observed. Agreement between values of Young’s modulus of textile stents derived by the mechanical model (strain energy method) to those of the experimental was good

(*adjusted R*²= 0.7955). Stress-strain curves were obtained by strip testing of textile stents on an Instron[®]. The empirical model showed strong correlation between theoretical and experimental values of compression force for 1.27 cm (*adjusted R*²= 0.8669) and 1.9 cm (*adjusted R*²= 0.9251) diameter textile stents. Two-Factor ANOVA showed statistically significant effect ($p = 0.00051$ for 0.4 cm artery diameter, $p = 0.00013$ for 0.8 cm artery diameter, $p = 0.01716$ for 1.2 cm artery diameter, $p = 0.01240$ for 1.6 cm artery diameter, $p = 0.0309$ for 2.5 cm artery diameter) of blood input velocity on exit velocity, determined by Ansys[®] FLOTRAN. Monofilament denier also showed statistically significant effect ($p = 0.04395$ for 0.4 cm, $p = 0.03814$ for 0.8 cm, $p = 0.01491$ for 1.2 cm) on exit velocity for all mentioned artery diameters except 1.6 and 2.5 cm. Textile stent entrance and exit effects and blood flow behavior in textile stented artery segment were helpful in understanding restenosis. Application of textile stents as substitute to metal stents is feasible.

KEYWORDS: Vascular disease, angioplasty, stent, restenosis, prototypes, monofilaments, *in vivo* and *in vitro* tests, braiding, strain energy method, Castigliano's theorem, empirical model, entrance and exit effects, platelets (thrombocytes), platelet plug formation.

DISCLAIMER

The results and applications are valid and limited only to this study. Author makes no representation, promise, or implies warranty concerning the suitability of 'textile stents' for implantation in any living organism. Author has no control over the information given in references and can not be held responsible for their content and authenticity.

ACKNOWLEDGEMENTS

I would like to thank my advisor Dr. Sabit Adanur for honoring me with a graduate research position and allowing to work with him on the project ‘Textile Prosthesis for Vascular Applications (NTC: F03-AE02)’. I will be always thankful to him for supervising my work. He has a lot to do with my transformation from an amateur graduate student to a researcher. I learned a bunch of technical details from him. I am also obligated to him for the time and other resources he spent on me.

I want to express sincere gratitude towards my Ph.D. committee members Dr. Peter Schwartz, Dr. Lewis Slaten and Dr. Anwar Ahmed (Department of Aerospace Engineering) for their comments and suggestions on my Ph.D. dissertation.

I would like to thank the United States Department of Commerce (USDC) through National Textile Center (www.ntcresearch.org) for financial support. I would like to thank Dr. Ramsis Farag, Dr. Moussa Traore, Mr. Jeff Thompson, and Mr. David Clark (all from Department of Textile Engineering) for their assistance with machine hardware. All in all, I would like to thank Auburn University, Graduate School, Department of Textile Engineering, Department of Consumer Affairs, and all Faculties, Staff, and graduate students related to the ‘Integrated Textiles and Apparel Science’ graduate studies for their cooperation.

Finally, everything I own is dedicated to my Mom, Dad, brother Abhinandan, sister-in-law Sujata, Rachana, and Rajat. They mean everything to me.

Swagat Appasaheb Irsale.

June 20, 2005.

swagat123@rediffmail.com, irsale123@yahoo.com.

Journal used

Textile Research Journal

Computer softwares used

Microsoft WORD[®], Microsoft EXCEL[®], Maple[®], Matlab[®], and Ansys[®]

FLOTRAN.

TABLE OF CONTENTS

	Page
LIST OF TABLES	xiii
LIST OF FIGURES	xiv
Chapter 1. INTRODUCTION AND BACKGROUND	1
1.1 Textiles and Implants	1
1.2 Stents and Angioplasty	4
1.3 Evolution of Endovascular Therapy	6
1.4 Objective	7
1.5 Literature Cited	8
Chapter 2. PROTOTYPE MANUFACTURING	15
2.1 Prototype Manufacturing of Braided Structures.....	15
2.2 Prototype Manufacturing of Tubular Narrow Woven Fabrics.....	19
2.3 Prototype Manufacturing of Bifurcated Braided Structures.....	23
2.4 Performance of Textile Stents	29
2.5 Literature Cited	33
Chapter 3. COMPRESSION FORCE OF POLYMERIC TEXTILE STENTS.....	34
3.1 Novel Compression Test	34
3.2 Tubular Narrow Woven Fabric Testing.....	36
3.3 Compression Force of Textile Stents	38
3.4 Correlating Compressions.....	46

3.5 Applications and Limitations	53
3.6 Literature Cited	54
Chapter 4. MODELING: PREDICTING YOUNG’S MODULUS AND COMPRESSION	
FORCE.....	55
4.1 Determination of Braid Structural Geometry	56
4.2 Definition of Strain Energy Function	62
4.3 Formulation of Interfilament Force	65
4.4 Determination of Braid Extension	68
4.5 Quantification of Young’s Modulus	69
4.6 Load- Strain Curves of Textile Stents.....	73
4.7 Formulation of Compression Force	78
4.8 Verification of the Empirical Model	81
4.9 Literature Cited	84
Chapter 5. BLOOD FLOW CHARACTERIZATION OF POLYMERIC TEXTILE	
STENTS	86
5.1 Rheology of Blood	86
5.2 Nature of the Blood Flow	87
5.3 Characterization of Blood Flow.....	87
5.4 Objective	88
5.5 Textile Stent Entrance and Exit Effects	90
5.6 Variation of Textile Stent Entrance and Exit Effects.....	100
5.7 General Linear Model.....	104
5.8 Results and Discussion.....	104

5.9 Literature Cited	116
Chapter 6. CONCLUSIONS AND RECOMMENDATIONS.....	119
6.1 Conclusions.....	119
6.2 Recommendations.....	120
6.3 Future Challenges.....	123
APPENDICES.....	124
A.1 Exit Velocity Results for 0.4 cm Artery Diameter Combinations.....	124
A.2 Exit Velocity Results for 0.8 cm Artery Diameter Combinations.....	128
A.3 Exit Velocity Results for 1.2 cm Artery Diameter Combinations.....	131
A.4 Exit Velocity Results for 1.6 cm Artery Diameter Combinations.....	134
A.5 Exit Velocity Results for 2.5 cm Artery Diameter Combinations.....	137
A.6 Prototype Manufacturing of Braided Hand	140
A.7 Terminology Used	145

LIST OF TABLES

	Page
3.1 SPSS [®] results for compression force (three-way ANOVA).....	44
4.1 Notations for strain energy model	56
4.2 Respective values of m and C	79
5.1 Two-factor ANOVA output for 0.4 cm artery diameter	112
5.2 Two-factor ANOVA output for 0.8 cm artery diameter	112
5.3 Two-factor ANOVA output for 1.2 cm artery diameter	112
5.4 Two-factor ANOVA output for 1.6 cm artery diameter	112
5.5 Two-factor ANOVA output for 2.5 cm artery diameter	112

LIST OF FIGURES

	Page
1.1: Ultramax™ vascular grafts	3
1.2: CorCap™ cardiac support device	3
1.3: Stent inside an artery	5
1.4: Angioplasty procedure	5
2.1: Stent	17
2.2: Wardwell braiding machine at Auburn University.....	18
2.3 Weave for seamless tubular narrow woven fabric.....	19
2.4 West-Point USA mini warping and sizing machine at Auburn University.....	20
2.5 Jakob-Muller fabric needle loom at Auburn University.....	21
2.6 Textile stent prototypes.....	22
2.7 <i>In vivo</i> application of bifurcated stent graft.....	24
2.8 Bifurcated stent graft.....	24
2.9 Dismantled wooden mandrel used for braiding bifurcated textile stents.....	26
2.10 Unbraided monofilaments to be braided into second leg.....	27
2.11 Prototype bifurcated braided stents	28
2.12 Factor groups affecting the performance of textile stents	30
2.13 Performance requirements of textile stents	32
3.1: Experimental arrangement	35
3.2: Novel compression test	35

3.3 Tubular narrow woven fabric testing on Instron (machine direction).....	37
3.4 Tubular narrow woven fabric testing on Instron (cross-machine direction).....	37
3.5 Compression force of 6.3 mm (diameter) textile stents	39
3.6 Compression force of 12.7 mm (diameter) textile stents	40
3.7 Compression force of 19 mm (diameter) textile stents	41
3.8 Compression force of 25.4 mm (diameter) textile stents	42
3.9 Estimated marginal means for compression force	45
3.10 <i>In vitro</i> novel compression test (unidirectional compression)	47
3.11 Radial compression	48
3.12 Calculating compression during novel compression (<i>in vitro</i>) test	50
3.13 Comparison of radial and unidirectional (novel test) compressions.....	52
4.1 Braided structure	57
4.2 Cut and opened braided structure	58
4.3 Diamond trellis as repeating unit	59
4.4 Cross-section showing ‘braid inclination angle’	60
4.5 Monofilaments intersection as a unit of braided structure	63
4.6 Cross-section of monofilaments intersection	66
4.7 Comparison of Young’s moduli	70
4.8 Comparison of Young’s moduli (12 mm textile stents diameter)	71
4.9 Load-strain curves (4 mm diameter textile stents)	74
4.10 Load-strain curves (8 mm diameter textile stents)	75
4.11 Load-strain curves (12 mm diameter textile stents)	76
4.12 Load-strain curves (16 mm diameter textile stents)	77

4.13 Trends for 60 degree braid angle textile stents	79
4.14 Trends for m and C	80
4.15 Verification of empirical model (EM)	83
5.1 Longitudinally irregular plaque	89
5.2 Radially irregular plaque	89
5.3 Textile stent entrance effect	92
5.4 Textile stent exit effect	93
5.5 Textile stent entrance and exit effects (0.4 cm artery diameter, 600 denier, 6 cm/s)	95
5.6 Blood flow in the human abdominal aortic bifurcation (blood input velocity= 38 cm/s)	97
5.7 Bifurcated textile stent entrance and exit effects (blood input velocity= 28 cm/s).	98
5.8 Joint of textile stented abdominal aortic bifurcation (blood input velocity= 28 cm/s)	99
5.9 Variation of textile stent entrance and exit effects (0.4 cm artery diameter, 1100 denier).....	101
5.10 Variation of bifurcated textile stent entrance and exit effects (1100 denier)	103
5.11 Three-dimensional graph of exit velocity for artery of 0.4 cm diameter	106
5.12 Three-dimensional graph of exit velocity for artery of 0.8 cm diameter	107
5.13 Three-dimensional graph of exit velocity for artery of 1.2 cm diameter	108
5.14 Three-dimensional graph of exit velocity for artery of 1.6 cm diameter	109
5.15 Three-dimensional graph of exit velocity for artery of 2.5 cm diameter	110
6.1 Proposed flow model	121

6.2 Proposed <i>in vitro</i> stent-artery-plaque simulator	122
A.1 Exit velocity for combination of 0.4 cm, 150 denier, and 1 cm/s.....	124
A.2 Exit velocity for combination of 0.4 cm, 150 denier, and 3 cm/s.....	124
A.3 Exit velocity for combination of 0.4 cm, 150 denier, and 6 cm/s.....	125
A.4 Exit velocity for combination of 0.4 cm, 600 denier, and 1 cm/s.....	125
A.5 Exit velocity for combination of 0.4 cm, 600 denier, and 3 cm/s.....	125
A.6 Exit velocity for combination of 0.4 cm, 600 denier, and 6 cm/s.....	126
A.7 Exit velocity for combination of 0.4 cm, 1100 denier, and 1 cm/s.....	126
A.8 Exit velocity for combination of 0.4 cm, 1100 denier, and 3 cm/s.....	126
A.9 Exit velocity for combination of 0.4 cm, 1100 denier, and 6 cm/s.....	127
A.10 Exit velocity for combination of 0.8 cm, 150 denier, and 1 cm/s.....	128
A.11 Exit velocity for combination of 0.8 cm, 150 denier, and 3 cm/s.....	128
A.12 Exit velocity for combination of 0.8 cm, 150 denier, and 6 cm/s.....	128
A.13 Exit velocity for combination of 0.8 cm, 600 denier, and 1 cm/s.....	129
A.14 Exit velocity for combination of 0.8 cm, 600 denier, and 3 cm/s.....	129
A.15 Exit velocity for combination of 0.8 cm, 600 denier, and 6 cm/s.....	129
A.16 Exit velocity for combination of 0.8 cm, 1100 denier, and 1 cm/s.....	130
A.17 Exit velocity for combination of 0.8 cm, 1100 denier, and 3 cm/s.....	130
A.18 Exit velocity for combination of 0.8 cm, 1100 denier, and 6 cm/s.....	130
A.19 Exit velocity for combination of 1.2 cm, 150 denier, and 8 cm/s.....	131
A.20 Exit velocity for combination of 1.2 cm, 150 denier, and 10 cm/s.....	131
A.21 Exit velocity for combination of 1.2 cm, 150 denier, and 12 cm/s.....	131
A.22 Exit velocity for combination of 1.2 cm, 600 denier, and 8 cm/s.....	132

A.23 Exit velocity for combination of 1.2 cm, 600 denier, and 10 cm/s.....	132
A.24 Exit velocity for combination of 1.2 cm, 600 denier, and 12 cm/s.....	132
A.25 Exit velocity for combination of 1.2 cm, 1100 denier, and 8 cm/s.....	133
A.26 Exit velocity for combination of 1.2 cm, 1100 denier, and 10 cm/s.....	133
A.27 Exit velocity for combination of 1.2 cm, 1100 denier, and 12 cm/s.....	133
A.28 Exit velocity for combination of 1.6 cm, 150 denier, and 12 cm/s.....	134
A.29 Exit velocity for combination of 1.6 cm, 150 denier, and 16 cm/s.....	134
A.30 Exit velocity for combination of 1.6 cm, 150 denier, and 20 cm/s.....	134
A.31 Exit velocity for combination of 1.6 cm, 600 denier, and 12 cm/s.....	135
A.32 Exit velocity for combination of 1.6 cm, 600 denier, and 16 cm/s.....	135
A.33 Exit velocity for combination of 1.6 cm, 600 denier, and 20 cm/s.....	135
A.34 Exit velocity for combination of 1.6 cm, 1100 denier, and 12 cm/s.....	136
A.35 Exit velocity for combination of 1.6 cm, 1100 denier, and 16 cm/s.....	136
A.36 Exit velocity for combination of 1.6 cm, 1100 denier, and 20 cm/s.....	136
A.37 Exit velocity for combination of 2.5 cm, 150 denier, and 28 cm/s.....	137
A.38 Exit velocity for combination of 2.5 cm, 150 denier, and 33 cm/s.....	137
A.39 Exit velocity for combination of 2.5 cm, 150 denier, and 38 cm/s.....	137
A.40 Exit velocity for combination of 2.5 cm, 600 denier, and 28 cm/s.....	138
A.41 Exit velocity for combination of 2.5 cm, 600 denier, and 33 cm/s.....	138
A.42 Exit velocity for combination of 2.5 cm, 600 denier, and 38 cm/s.....	138
A.43 Exit velocity for combination of 2.5 cm, 1100 denier, and 28 cm/s.....	139
A.44 Exit velocity for combination of 2.5 cm, 1100 denier, and 33 cm/s.....	139
A.45 Exit velocity for combination of 2.5 cm, 1100 denier, and 38 cm/s.....	139

A.46 Making braided structure with 16 monofilaments.....	141
A.47 Sixteen monofilaments braided structure made on 64 spindle machine.....	141
A.48 Making braided structure with 12 monofilaments.....	142
A.49 Twelve monofilaments braided structure made on 64 spindle machine.....	142
A.50 Making braided structure with 48 monofilaments.....	143
A.51 Human hand.....	144
A.52 Braided hand prototype.....	144

CHAPTER 1

INTRODUCTION AND BACKGROUND

1.1 *Textiles and Implants*

The idea of implanting textile materials, structures, or their combinations is hardly new. ‘Textile endovascular prosthetic devices’ were defined as the textile biomaterial structures implanted inside the arteries or vessels to keep the vessel lumen open for a longer time [19]. Researchers implanted structures made from polyester [17, 3], nylon [40, 48, 14], polyethylene [18], Teflon[®] [13] as well as Lycra[®] [20] as vascular implants. Shumway *et al.* [41] implanted Ivalon[®] tubes as artificial vessels in dogs. Eisenbud *et al.* [6] developed and implanted polyester mesh stents in the abdominal aorta of dogs. Sharafuddin *et al.* [39] added polyester fillings to nitinol self-expanding stents and observed enhanced thrombogenicity. Grindley [10] mentioned application of polyethylene tubes for anastomosis of common bile duct, trachea, and pelvic colon. Combined metal and textile structure implants viz. Palmaz stents covered with polytetrafluoroethylene (PTFE) [28], self-expanding z-stents covered with polyester [30], stents sutured to expanded-polytetrafluoroethylene (ePTFE) membrane [38, 2], as well as nitinol-polyester self expanding stent grafts [8] were found in the literature. These

various types of stents and stent-grafts are designed and being implanted to combat artery diseases.

Textiles have also been implanted as hernia repair meshes, heart valve components and nerve guides [24]. Tis *et al.* [45] studied *in vitro* biomechanical performance of braided hamstring tendons. Nicklin *et al.* [32] examined biomechanical properties of braided tendon grafts. Simoes *et al.* [43] developed prototypes of braided composites to be used for femoral hip prosthesis. Veerabagu *et al.* [49] and Fujihara *et al.* [9] examined compatibility of textile composites for bone plate applications. Ingraham *et al.* [18] mentioned applications of poly-vinyl chloride (PVC) for plastic surgery prosthesis, acrylic for repairing skull defects, and nylon as sutures. Kawaguchi *et al.* [22] studied mechanical properties of collagen coated polypropylene cylindrical mesh to be used as artificial tracheas and suggested that the chosen materials comply with the requirements in terms of mechanical properties.

Textiles emerged as an integrated part of the most advanced artificial implants and organs. Akutsu *et al.* [1] and Kolff [25] developed artificial heart valves from polyurethane. Atrium Medical Corporation™ has various vascular grafts (Figure 1.1), and hernia repair meshes made up of textile materials. Acorn Cardiovascular™ invented a cardiac support device (Figure 1.2) made up of a knitted polyester mesh [29, 33] for patients with symptomatic heart failure. All in all, human hearts and arteries can be envisioned as wearing advanced textiles or polymers, and in the near future kidneys, bones, and others will follow. All these textile or polymeric biomaterials can be defined as ‘bio-apparels’. As a summary statement, several commercially available and research

level applications were and will be feasible due to a pool of biocompatible textile materials offering versatile properties.

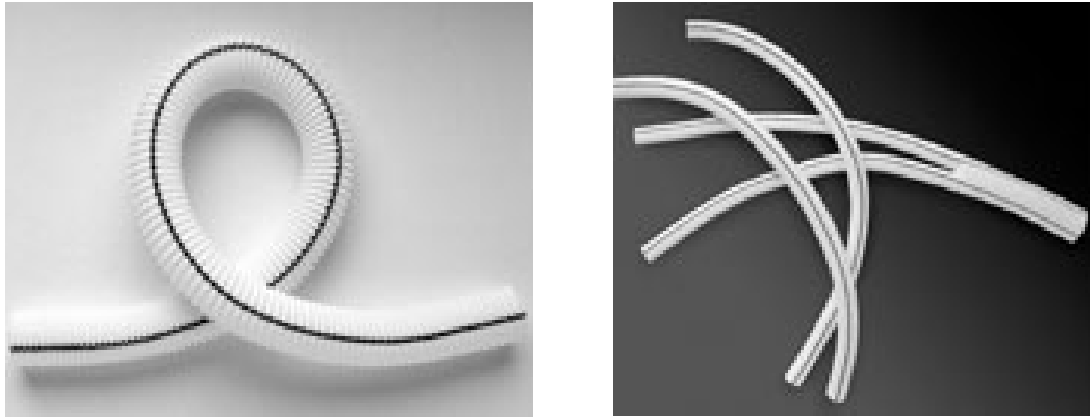


FIGURE 1.1: Ultramax™ vascular grafts.

Source: www.atriummed.com, access date: April 11, 2005.



FIGURE 1.2: CorCap™ cardiac support device.

Source: www.acorncv.com, access date: April 10, 2005.

Apart from implants and related applications, nano-capsule coated apparels [15] and wound dressings made up of nanofibrous membranes [23] are available. Advanced healthcare applications include intelligent biomedical clothing (IBC), an integration of textiles with sensors, actuators, and computing [27]. These clothings gather and transmit data to doctor or health surveying station, where immediate action can be taken if necessary [16]. These advanced healthcare textiles will become an integral part of the most advanced 'telemedicine' approach.

1.2 Stents and Angioplasty

Stents (Figure 1.3) serve to hold the diseased artery lumen open and preserve it after angioplasty (Figure 1.4). These tubular mesh structures have evolved as a less invasive treatment for the occlusive artery disease. In 1998, over 800,000 stents were implanted in more than 500,000 patients [46], and in 2001, over 1 million angioplasties were done in the United States [52]. Carotid arteries, coronary arteries, abdominal aorta, and femoral arteries are very much prone to the artery diseases [26]. Atherosclerosis is one of the artery diseases, which means hardening of the intima or media layers of the arteries. Atherogenesis is defined as beginning of the plaque deposition within the diseased artery sections, mainly due to atherosclerosis [12]. Plaque depositions cause the artery lumen to narrow, known as stenosis.

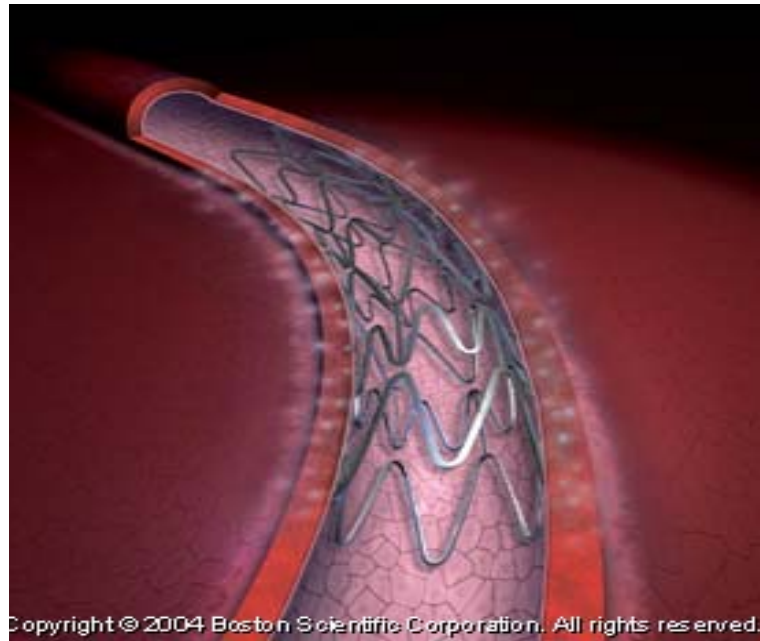


FIGURE 1.3: Stent inside an artery.

Source: www.bostonscientific.com, access date: April 12, 2005.

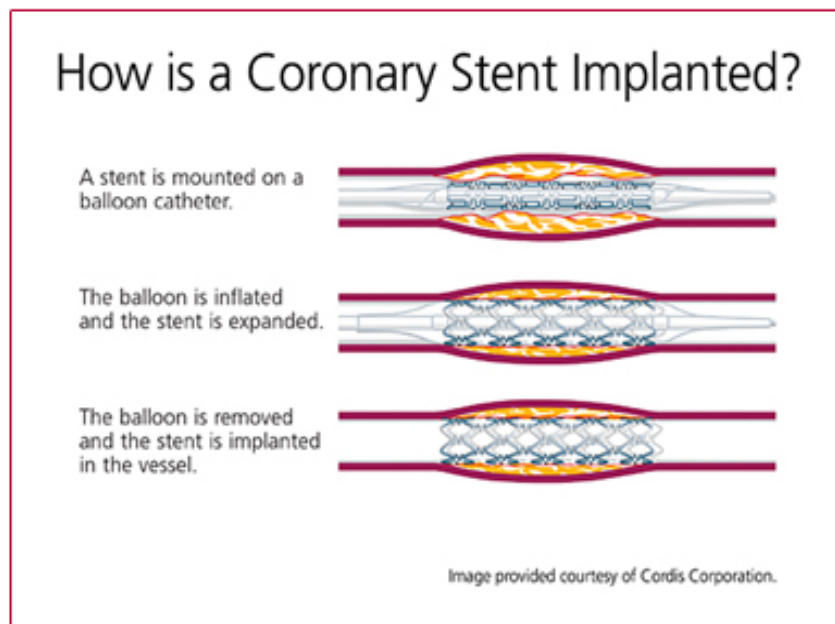


FIGURE 1.4: Angioplasty procedure.

Source: www.cordisendovascular.com, access date: June 18, 2003.

Even after treatment by stents, the artery lumen may clog again, termed as restenosis. This is one of the drawbacks of metal stents. Others include slippage of the stent frames [36], morphological changes in stent graft material [35], foreign body contamination [51], and changes in physical properties of stents due to balloon dilatation [37]. Metal stents may even cause substantial heating or possible dislodgement when exposed to certain imaging modalities [5]. In 1994, hospital charges associated with percutaneous transluminal coronary revascularizations in the United States exceeded \$6 billion [7]. However, close to 100 different stent designs are under evaluation or being marketed worldwide and compete in a \$3 billion stent industry [44]. To understand and predict future of stents, and develop novel stents, it is very much necessary to take a closer look at the evolution of endovascular therapy.

1.3 Evolution of Endovascular Therapy

One of the initial steps in the evolution of endovascular therapy was the surgical implantation of nylon tubes as vascular prosthesis by Voorhees *et al.* [50]. This was followed by the invention of catheter deliverable coil springs by Dotter and Judkins [4]. This was a milestone towards the less invasive endovascular therapy, which avoided open body surgeries. Later, Gruntzig *et al.* [11] proved that inserting a deflated balloon with the catheter and inflating it at the diseased artery site gave better results. Authors termed the procedure as percutaneous transluminal coronary angioplasty (PTCA). After that, Sigwart *et al.* [42] invented a catheter deliverable metal scaffold to avoid abrupt closure of arteries, known as stents. However, just implanting stents was not sufficient, as it could not stop or eliminate restenosis. Zilberman *et al.* [56], Topol and Serruys [47], Reed *et al.* [34], and Karoussos *et al.* [21] worked on preliminary models of drug-eluting

stents. Drug-eluting stents (DES) slowly release a drug which prevents build up of new tissues and avoids restenosis, making the stents more efficient. Morice *et al.* [31] observed significant prevention of neointimal proliferation and restenosis due to sirolimus-eluting stents implanted in 238 patients, when compared to standard stents. On April 24, 2003, the United States Food and Drug Administration (FDA) approved [53] first drug-eluting stent by Cordis[®] Corporation. Cypher[™] [54], and Taxus[®] Express^{2™} [55] are examples of commercially available drug-eluting stents in the United States.

Stents of future are ‘drug-eluting stents’. In order to deliver drugs at targeted sites, and release it over longer period of time, these drugs must be integrated into stent materials. It is very much likely that textiles or polymers can be advantageous in integrating, holding, binding, as well as releasing drugs rather than metals. So, future stents will be made of ‘intelligent textile and/or polymeric structures’ capable of functioning as a ‘drug delivery and controlled release system’ in addition to their traditional function as a mechanical scaffold.

1.4 Objective

Current study focuses on prototyping and modeling of braided structures to be used as stents, hence called ‘textile stents’. The objective was to establish guidelines for commercial manufacturing of polymeric textile stents which can become major substitutes for metal stents. The study comprises prototype manufacturing of textile stents, a chart to understand their performance, correlation of radial and unidirectional (*in vitro*) compressions, a mechanical model to predict Young's modulus, an empirical model to formulate compression force, and blood flow characterization of polymeric textile stents.

1.5 Literature Cited

1. Akutsu, T., Dreyer, B., and Kolff, W., "Polyurethane Artificial Heart Valves in Animals", *J. Appl. Physiol.*, **14**(6), 1045-1048 (1959).
2. Birgelen, C., Haude, M., Hermann, J., Altmann, C., Klinkhart, W., Welge, D., Wieneke, H., Baumgart, D., Sack, S., and Erbel, R., "Early Clinical Experience with the Implantation of a Novel Synthetic Coronary Stent Graft", *Cathet. Cardiovasc. Intervent.*, **47**(4), 496-503 (1999).
3. Deterling, R., and Bhonslay, S., "An Evaluation of Synthetic Materials and Fabrics Suitable for Blood Vessel Replacement", *Surg.*, **38**(1), 71-91 (1955).
4. Dottor, C., and Judkins, M., "Transluminal Treatment of Atherosclerotic Obstruction: Description of a New Technique and a Preliminary Report of its Application", *Cir.*, **30**, 654-670 (1964).
5. Edwards, M., Taylor, K., and Shellock, F., "Prosthetic Heart Valves: Evaluation of Magnetic Field Interactions, Heating, and Artifacts at 1.5 T", *J. Magn. Reson. Imaging*, **12**(2), 363-369 (2000).
6. Eisenbud, D., Parsonnet, V., Wiktor, D., Ferrara-Ryan, M., and Villanueva, A., "A Polyester Intravascular Stent for Maintaining Luminal Patency: A Gross and Microscopic Study of the Device's Incorporation, Early Maturation, and Thrombogenicity", *Tex. Heart Inst. J.*, **15**(1), 12-16 (1988).
7. Ellis, S., Miller, D., Brown, K., Omoigni, N., Howell, G., Kutner, M., and Topol, E., "In-Hospital Cost of Percutaneous Coronary Revascularization: Critical Determinants and Implications", *Circ.*, **92**(4), 741-747 (1995).

8. Formichi, M., Marois, Y., Roby, P., Marinov, G., Stroman, P., King, M., Douville, Y., and Guidoin, R., "Endovascular Repair of Thoracic Aortic Aneurysm in Dogs: Evaluation of a Nitinol-Polyester Self Expanding Stent-Graft", *J. Endovasc. Ther.*, **7**(1), 47-67 (2000).
9. Fujihara, K., Huang, Z., Ramkrishna, S., Satknanantham, K., and Hamada, H., "Performance Study of Braided Carbon/PEEK Composite Compression Bone Plates", *Biomater.*, **24**(15), 2661-2667 (2003).
10. Grindley, J., "Method of Making Tubes of Polyethylene Film for Use in Anastomosis of the Common Bile Duct", *Surg.*, **24**, 22-29 (1948).
11. Gruntzig, A., Senning, A., and Siegenthaler, W., "Non-operative Dilatation of Coronary-Artery Stenosis: Percutaneous Transluminal Coronary Angioplasty", *N. Engl. J. Med.*, **301**(2), 61-68 (1979).
12. Guyton, A., *Textbook of Medical Physiology*, Tenth Edition, Saunders, Philadelphia, 2000.
13. Harrison, J., "Use of Teflon as Blood Vessel Replacement", *Surg. Gynecol. Obst.*, **104**(1), 80-87 (1957).
14. Harrison, J., and Adler, R., "Nylon as a Vascular Prosthesis in Experimental Animals with Tensile Strength Studies", *Surg. Gynecol. Obst.*, **103**(5), 613-617 (1956).
15. Hofer, D., and Swerev, M., "Medical Textiles and Skin Equivalents", *J. Textile Apparel Tech. Manag.*, **3**(2), 1-4 (2003).
16. Hofer, D., and Swerev, M., "The Future of Medical Textiles: High-tech for the Well-being of the Patient", *J. Textile Apparel Tech. Manag.*, **3**(2), 1-3 (2003).

17. Hufnagel, C., and Rabil, P., "Replacement of Arterial Segments- Utilizing Flexible Orlon Prostheses", *A.M.A. Arch. Surg.*, **70**(1), 105-110 (1955).
18. Ingraham, F., Alexander, E., and Matson, D., "Synthetic Plastic Materials in Surgery", *N. Eng. J. Med.*, **236**, 362-368 (1947).
19. Irsale, S., Masters Thesis, Auburn University, 2004.
20. Izhar, U., Schwalb, H., Borman, J., Hellener, G., Solomon, A., Marom, G., Stern, T., and Cohn, D., "Novel Synthetic Selectively Degradable Vascular Prostheses: A Preliminary Implantation Study", *J. Surg. Res.*, **95**(2), 152-160 (2001).
21. Karoussos, I., Wieneke, H., Sawotowski, T., Wnendt, S., Fischer, A., Dirsch, O., Dahmen, U., and Erbel, R., "Inorganic Materials as Drug Delivery Systems in Coronary Artery Stenting", *Inorg. Mat.*, **33**(12), 738-746 (2002).
22. Kawaguchi, S., Nakamura, T., Shimizu, Y., Masuda, T., Takigawa, T., Liu, Y., Hiroki, U., Sekine, T., and Matsumoto, K., "Mechanical Properties of Artificial Tracheas Composed of a Mesh Cylinder and a Spiral Stent", *Biomat.*, **22**, 3085-3090 (2001).
23. Khil, M., Cha, D., Kim, H., Kim, I., and Bhattarai, N., "Electrospun Nanofibrous Polyurethane Membrane as Wound Dressing", *J. Biomed. Mater. Res.*, **67B**(2), 675-679 (2003).
24. King, M., "Overview of Opportunities in Medical Textiles", *Can. Textile J.*, **118**(4), 34-36 (2001).
25. Kolff, W., "The Invention of the Artificial Heart", *Int. J. Art. Org.*, **13**(7), 396-403 (1990).
26. Lighfoot, E., *Transport Phenomena and Living Systems*, Wiley, New York, 1972.

27. Lymberis, A., and Olsson, S., “Intelligent Biomedical Clothing for Personal Health and Disease Management: State of the Art and Future Vision”, *Telemed. J. E-health*, **9**(4), 379-386 (2003).
28. Marin, M., Veith, F., Cynamon, J., Sanchez, L., Bakal, C., Suggs, W., Lyon, R., Schwartz, M., Parsons, R., Wengerter, K., and Parodi, J., “Human Transluminally Placed Endovascular Stented Grafts: Preliminary Histopathologic Analysis of Healing Grafts in Aortoiliac and Femoral Artery Occlusive Disease”, *J. Vasc. Surg.*, **21**(4), 595-604 (1995).
29. Mehmet, C., Konertz, W., Kleber, F., Mohr, F., Gummert, J., Ostermeyer, J., Lass, M., Raman, J., Acker, M., and Smedira, N., “Global Surgical Experience with the Acorn Cardiac Support Device”, *J. Thorac. Cardiovasc. Surg.*, **126**(4), 983-991 (2003).
30. Mitchell, R., Miller, D., Dake, M., Semba, C., Moore, K., and Sakai, T., “Thoracic Aortic Aneurysm Repair with an Endovascular Stent Graft: The First Generation”, *Ann. Thorac. Surg.*, **67**(6), 1971-1974 (1999).
31. Morice, M., Serruys, P., Sousa, E., Fajadet, J., Hayashi, E., Perin, M., Colombo, A., Schuler, G., Barragán, P., Guagliumi, G., Molnar, F., and Falotico, R., “A Randomized Comparison of a Sirolimus-eluting Stent with a Standard Stent for Coronary Revascularization”, *N. Engl. J. Med.*, **346**(23), 1773-1780 (2002).
32. Nicklin, S., Waller, C., Walker, P., Chung, W., and Walsh, W., “In Vitro Structural Properties of Braided Tendon Grafts”, *Am. J. Sports Med.*, **28**(6), 790-793 (2000).

33. Raman, J., Hata, M., Storer, M., Power, J., Buxton, B., Alferness, C., and Hare, D.,
 “The Mid-term Results of Ventricular Containment (ACORN WRAP) for End-stage
 Ischemic Cardiomyopathy”, *Ann. Thorac. Cardiovasc. Surg.*, **7**(5), 278-281 (2001).
34. Reed, M., Wu, C., Kneller, J., Watkins, S., Vorp, D., Nadeem, A., Weiss, L.,
 Rebello, K., Mescher, M., Smith, A., Rosenblum, W., and Feldman, M.,
 “Micromechanical Devices for Intravascular Drug Delivery”, *J. Pharm. Sci.*, **87**(11),
 1387-1394 (1998).
35. Riepe, G., Heilberger, P., Umscheid, T., Chakfe, N., Raithel, D., Stelter, W.,
 Morlock, M., Kretz, J., Schroder, A., and Imig, H., “Frame Dislocation of Body
 Middle Rings in Endovascular Stent Tube Grafts”, *Eur. J. Endovasc. Surg.*, **17**(1),
 28-34 (1999).
36. Riepe, G., Heintz, C., Kaiser, E., Chakfe, N., Morlock, M., Delling, M., and Imig, H.,
 “What Can We Learn from Explanted Endovascular Devices?”, *Euro. J. Endovasc.
 Surg.*, **24**(2), 117-122 (2002).
37. Salzmann, D., Yee, D., Roach, D., Berman, S., and Williams, S., “Effect of Balloon
 Dilatation on ePTFE Structural Characteristics”, *J. Biomed. Mater. Res.*, **36**(4), 498-
 507 (1997).
38. Sambeek, M., Gussenhoven, E., Lugt, A., Honnkop, J., Bios, N., and Urk, H.,
 “Endovascular Stent Grafts for Aneurysms of the Femoral and Popliteal Arteries”,
Ann. Vasc. Surg., **13**(3), 274-253 (1999).
39. Sharafuddin, M., Gu, X., Titus, J., Urness, M., Cervera-Ceballos, J., and Amplatz,
 K., “Transvenous Closure of Secundum Atrial Septal Defects: Preliminary Results

- with a New Self-expanding Nitinol Prosthesis in a Swine Model”, *Cir.*, **95**(8), 2162-2168 (1997).
40. Shumacker, H., and King, H., “The Use of Pliable Plastic Tubes as Aortic Substitutes in Man”, *Surg. Gynec. Obst.*, **99**(3), 287-294 (1954).
 41. Shumway, N., Gliedman, M., and Lewis, J., “An Experimental Study of the Use of Polyvinyl Sponge for Aortic Grafts”, *Surg. Gynec. Obst.*, **100**(5), 703-706 (1955).
 42. Sigwart, U., Puel, J., Mirkovitch, V., Joffre, F., and Kappenberger, L., “Intravascular Stents to Prevent Occlusion and Restenosis after Transluminal Angioplasty”, *N. Eng. J. Med.*, **316**(12), 701-706 (1987).
 43. Simoes, J., and Marques, A., “Determination of Stiffness Properties of Braided Composites for the Design of a Hip Prosthesis”, *Composites* **32A**, 655-662 (2001).
 44. Stoeckel, D., Bonsignore, C., and Duda, S., “A Survey of Stent Designs”, *Min. Invas. Ther. Allied Technol.*, **11**(4), 137-147 (2002).
 45. Tis, J., Klemme, W., Kirk, K., Murphy, K., and Cunningham, B., “Braided Hamstring Tendons for Reconstruction of the Anterior Cruciate Ligament: A Biomechanical Analysis”, *Am. J. Sports Med.*, **30**(5), 684-688 (2002).
 46. Topol, E., “Coronary Artery Stents Gauging, Gorging, and Gouging”, *N. Engl. J. Med.*, **339**(23), 1702-1704 (1998).
 47. Topol, E., and Serruys, P., “Frontiers in Interventional Cardiology”, *Circ.*, **98**(17), 1802-1820 (1998).
 48. Vargas, E., and Deterling, R., “The Use of Nylon Net for the External Support of Blood Vessel Graft and Aneurysms”, *Surg.*, **34**(6), 1061-1075 (2003).

49. Veerabagu, S., Fujihara, G., Dasari, G., and Ramakrishna S., “Strain Distribution Analysis of Braided Composite Bone Plates”, *Comp. Sci. Tech.*, **63**(3), 427-435 (2002).
50. Voorhees, A., Jaretzki, A., and Blakemore, A., “The Use of Tubes Constructed from Vinyon N Cloth in Bridging Arterial Defects”, *Ann. Surg.*, **135**(3), 332-337 (1952).
51. Whelan, D., Beusekom, H., and Gissen, W., “Foreign Body Contamination during Stent Implantation”, *Cathet. Cardiovasc. Diagn.*, **40**(3), 328-332 (1997).
52. www.americanheart.org, American Heart Association® webpage, access date: October 1, 2004.
53. www.fda.gov, News release of April 24, 2003, ‘FDA Approves Drug-Eluting Stent for Clogged Heart Arteries’, access date: April 13, 2005.
54. www.jnj.com, access date: June 1, 2004.
55. www.taxus-stent.com, access date: April 12, 2005.
56. Zilberman, M., Schwade, N., and Eberhart, R., “Protein-Loaded Bioresorbable Fibers and Expandable Stents: Mechanical Properties and Protein Release”, *J. Biomed. Mater. Res.: Appl. Biomater.*, **69B**(1), 1-10 (2004).

CHAPTER 2

PROTOTYPE MANUFACTURING

It was noticeable that all stents (Figure 2.1) were made up of either metal or combined metal and textile material. The present study describes prototype manufacturing of endovascular stents fully made up of textile materials. The prototype textile stents had a braided structure (reinforcing component) covered with a tubular narrow woven fabric (sealing component). However, the sealing component was optional. Although, prototypes of both reinforcing and sealing components were made, models were exclusively developed by considering braided structures as the only component of polymeric textile stents.

2.1 Prototype Manufacturing of Braided Structures

Polyester monofilaments of 1100 and 2400 denier were selected. Thread strength, knot strength and loop strength of both monofilaments were tested on Uster Tensorapid 3. Monofilament samples were then heatset for one hour at seven different temperatures: 93, 118, 138, 160, 182, 204 and 227 °C (200, 240, 280, 320, 360, 400 and 440 °F respectively). Again thread strength, knot strength and loop strength of all monofilament samples were tested on Uster Tensorapid 3. Depending on the results of Tensorapid tests, optimum temperature for further experimentation was chosen as 182 °C (360 °F). By

comparing strength results of both monofilaments, 1100 denier was selected as the best and used for manufacturing of braided structures.

Sixty-four fault and breakage free spools were wound on Wardwell quill winding machine and selected for braiding. The spools were mounted on Wardwell braiding machine (Figure 2.2) and monofilaments were threaded through respective guides. All monofilaments were pulled forward and passed through the former ring. Monofilaments were then fixed on a long base mandrel with a tape. Four mandrels 6.3, 12.7, 19, and 25.4 mm in diameter were used. These mandrels were used to slide on the long base mandrel. Braided structures were manufactured on the movable outer mandrels. The speed of spools and traverse of monofilament carriers were varied and adjusted to manufacture braids of the required braid angle. The braid angle was measured with 'a' dial. Horgears were set to braid regular (2/2) braid. For each of four braiding mandrel diameters, braided structures were manufactured for four different braid angles: 30°, 45°, 60°, and 75° (braid angle = 2β). Braided structures of each respective braid diameter and braid angle were heatset at 182°C and at seven different heat set times (0, 20, 40, 60, 80, 100, and 120 minutes). Braided structures were heatset on mandrels to maintain their structural integrity.

Braid angle and braid diameter each had four levels and heatset time had seven levels. Therefore, the experimental design was:

$$\text{number of experimental combinations} = (\text{levels})^{\text{factors}} = (4)^2 (7)^1 = 112.$$

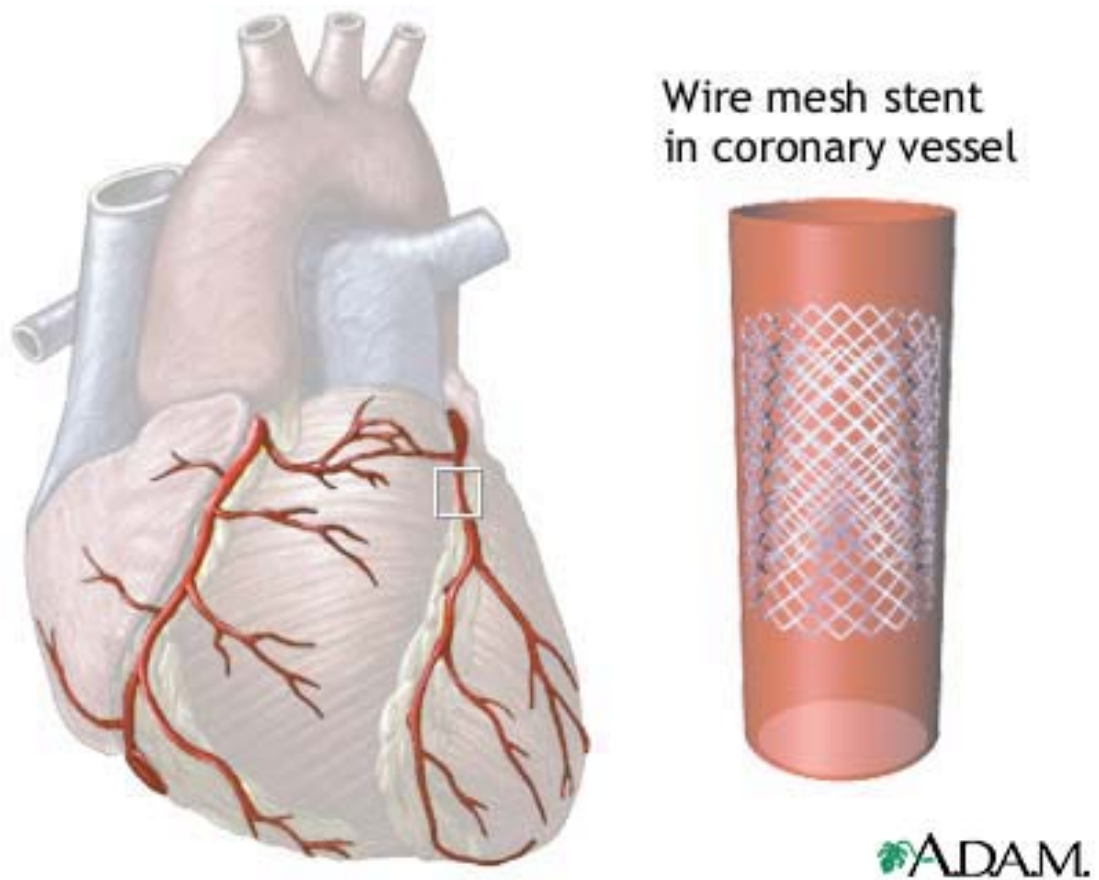


FIGURE 2.1: Stent.

www.nlm.nih.gov, access date: June 20, 2005.

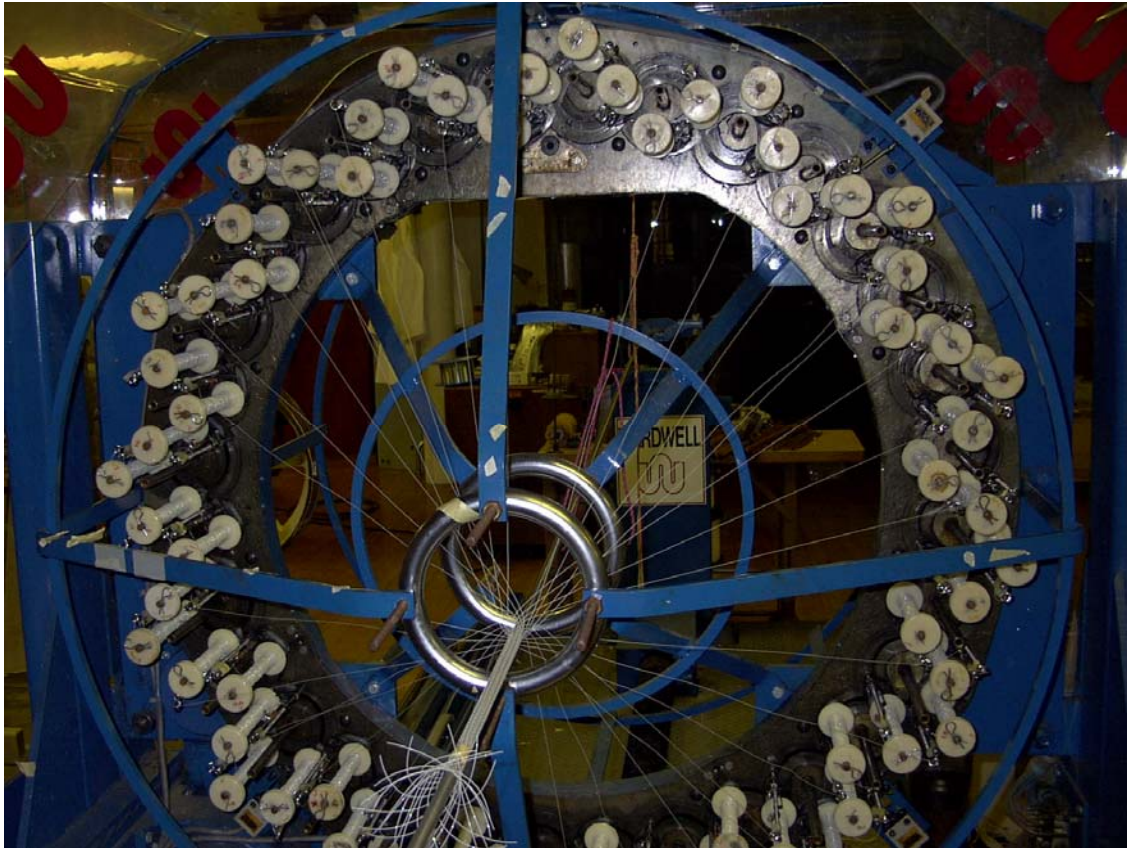


FIGURE 2.2: Wardwell braiding machine at Auburn University.

2.2 Prototype Manufacturing of Tubular Narrow Woven Fabrics

Polyester multifilaments of 150 denier were selected as warp for weaving tubular narrow woven fabrics. 4% solution of cold size (plasticryl M-30) was prepared and used for sizing of warp on West-Point USA mini sizing machine (Figure 2.4). The sized warp beam was mounted on Jakob-Muller fabric needle loom (Figure 2.5) and pattern chain was prepared to manufacture tubular fabric. The weave repeat for tubular fabric is shown in Figure 2.3; U stands for upper shed and L stands for lower shed. The weave in each shed was plain. Thus the fabric has two plain woven surfaces with no interlacements between them except at edges, forming a tubular fabric.

	U	L	U	L
L	×		×	×
U			×	
L	×	×	×	
U	×			

FIGURE 2.3: Weave for seamless tubular narrow woven fabric.

Polyester multifilament of 150 denier was used as weft to make non-elastic tubular fabrics. Nylon-lycra yarn of 150 denier was used as weft to make elastic tubular fabrics. Tubular narrow woven fabrics were tested for their mechanical properties on an Instron machine. Prototype textile stents are shown in Figure 2.6.

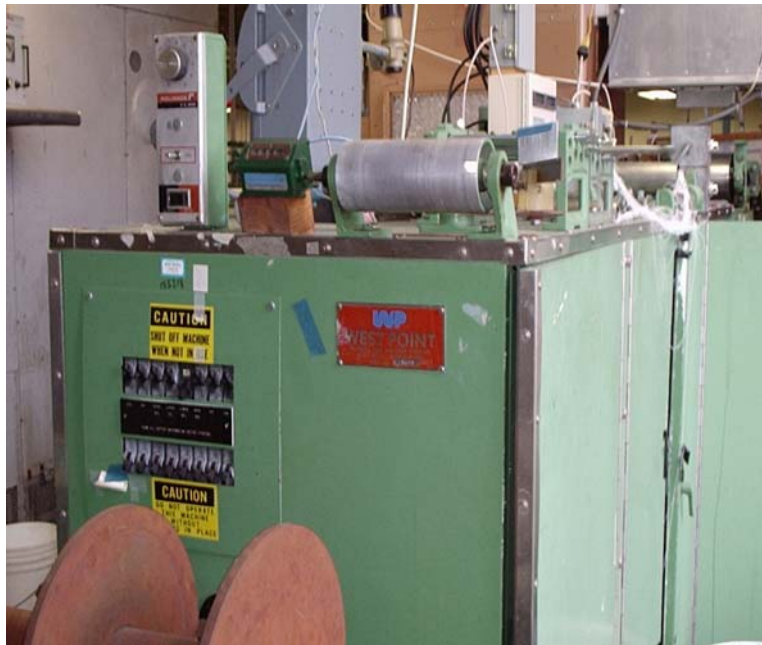


FIGURE 2.4: West-Point USA mini warping and sizing machine at Auburn University.

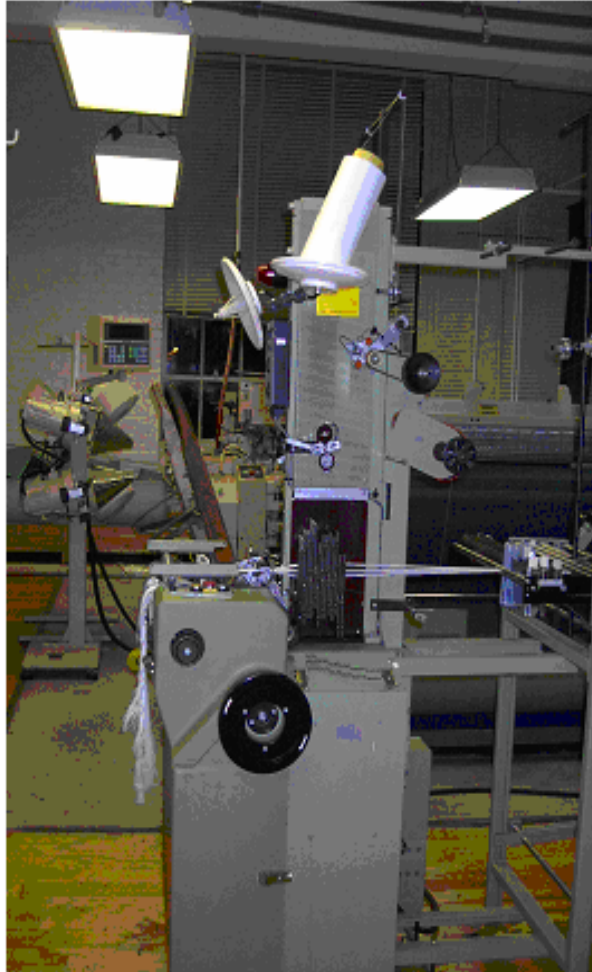


FIGURE 2.5: Jakob-Muller fabric needle loom at Auburn University.

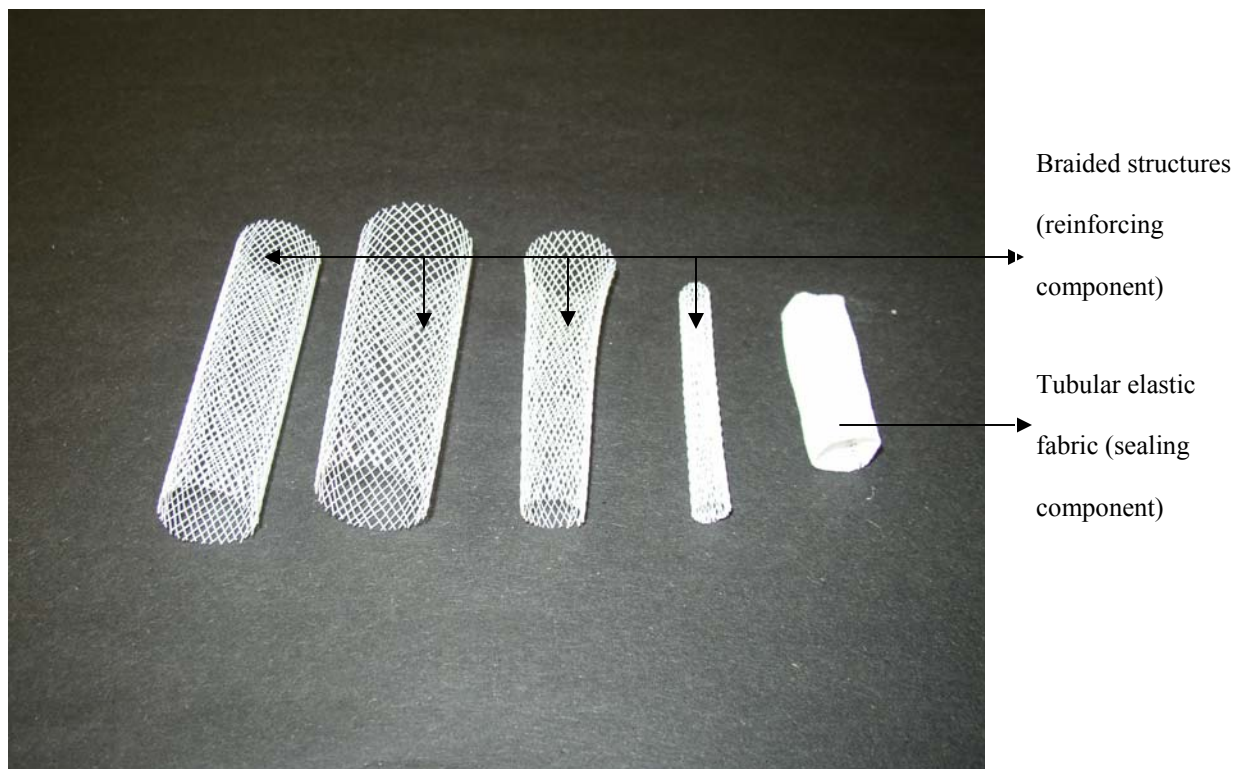


FIGURE 2.6: Textile stent prototypes.

2.3 Prototype Manufacturing of Bifurcated Braided Structures

Bifurcated braided structures can be explored for their application in abdominal aortic aneurysm implantation in humans. Bifurcated stent grafts (Figure 2.7) offer great potential for reduced morbidity, mortality and hospital stay because of minimally invasive endovascular placement through catheters. Most abdominal aortic aneurysms extend into one or both iliac arteries. Therefore bifurcated braided stents were designed consisting of proximal aortic trunk divided into two distinct lumens or sockets of smaller and equal diameter.

All commercially available bifurcated stent grafts (Figure 2.8) are of metal or combination of metal and textile materials. In this study prototypes of ‘bifurcated braided stent’ were manufactured. The prototype consisted of one single braided structure divided further into two smaller and equal diameter legs. Bifurcated braided structures were manufactured such that the monofilaments were continuous in length throughout the braided structure. The bifurcated braided stents were manufactured on a sixty-four spindle Wardwell braiding machine using two methods labeled herein as A and B. These two methods differed in selection and arrangement of monofilament spools braided into two smaller and equal diameter legs as well as into a single braided structure.



FIGURE 2.7: *In vivo* application of bifurcated stent graft.

Source: www.uphs.upenn.edu, access date: October 10, 2003.



FIGURE 2.8: Bifurcated stent graft.

Source: *Tex. Heart Inst J.* **27**(2), 128–135 (200).

To manufacture bifurcated braided stents, first a single braided structure with 64 monofilaments (1100 denier polyester) was manufactured using a Wardwell braiding machine. Then, without breaking any yarns, half of the spools on one side of the machine were taken off. The remaining 32 spools on the machine were rearranged such that they braid the exact same structure without missing any interlacement or creating additional floats. Figure 2.9 shows dismantled wooden mandrel used for braiding of bifurcated textile stents. With 32 spools on the machine, one leg of “Y” shaped structure was braided (Figure 2.10) and then those 32 spools were taken off the machine. The remaining set of 32 spools was mounted and rearranged on the machine and the other leg was braided. The position of spools was carefully monitored and maintained for proper interlacement of monofilaments while braiding each leg. The smaller diameter wooden mandrels were used for braiding smaller diameter legs. The wooden mandrel was designed such that it can be assembled or dismantled easily. The design used for bifurcated braided structures (Figure 2.11) was a 2/2 braid. Care was taken such that there were no monofilament entanglements. Two sets of monofilaments-- one on and other off the machine-- were changed flawlessly after braiding one leg. For method A, 64 monofilaments on the machine were divided into two sections as left and right, each having 32. For method B, monofilaments were selected from all four quadrants where each quadrant contributed eight monofilaments. After selecting 32 spools for both methods, the spools were rearranged at the exact same position they had while manufacturing single braided structure with all 64 monofilaments. Bifurcated structures were heatset on mandrels to maintain their structural integrity.



FIGURE 2.9: Dismantled wooden mandrel used for braiding bifurcated textile stents.

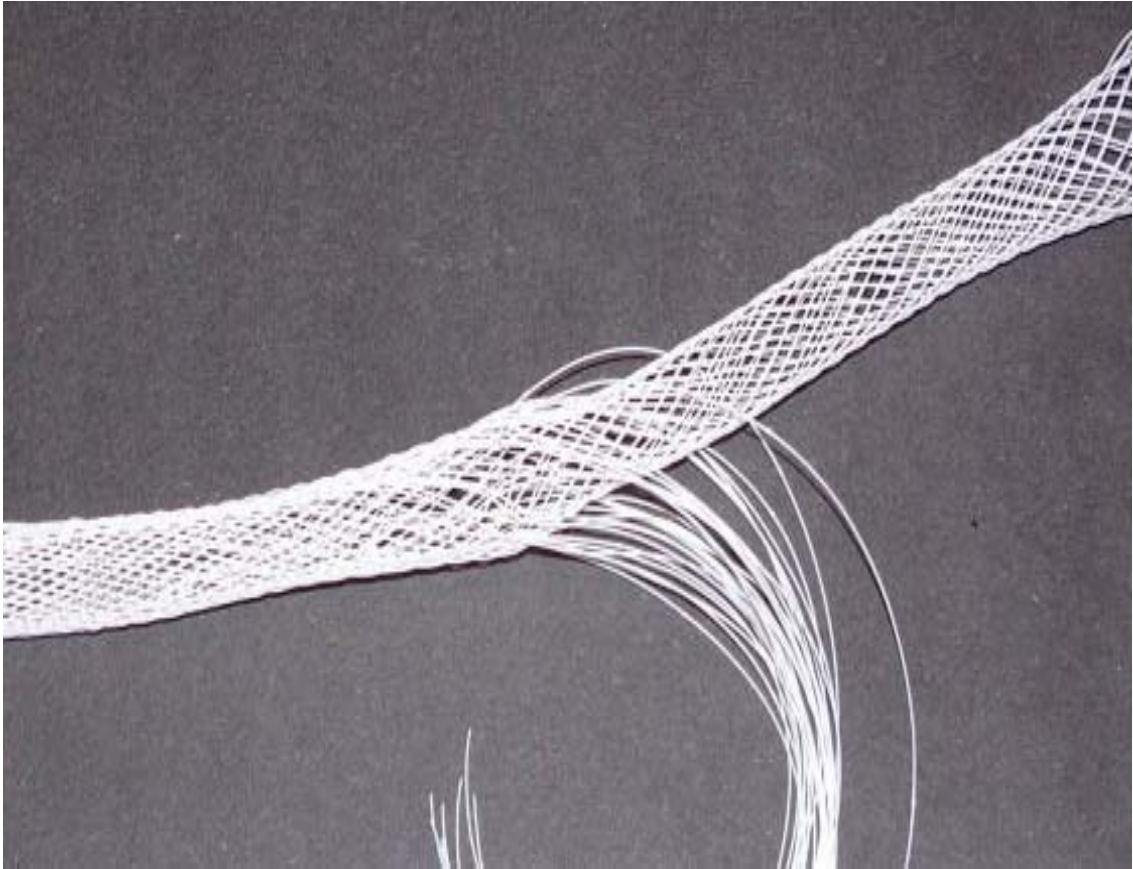


FIGURE 2.10: Unbraided monofilaments to be braided into second leg.

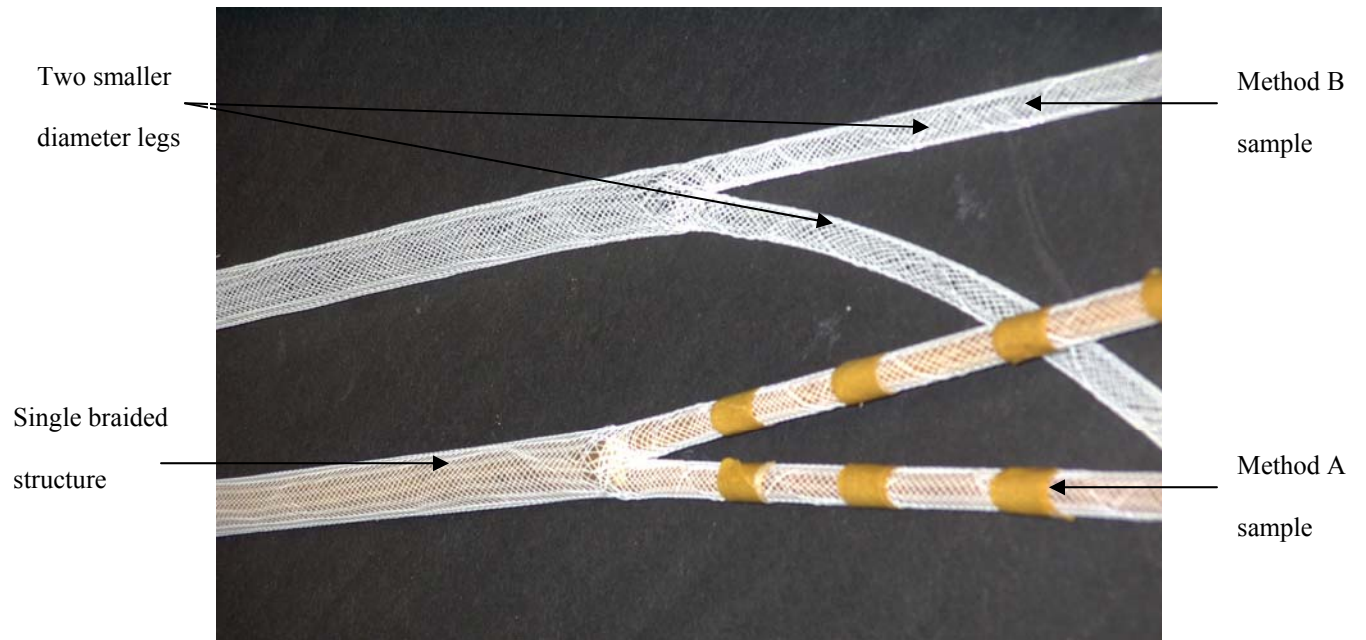


FIGURE 2.11: Prototype bifurcated braided stents.

2.4 Performance of Textile Stents [3]

After implantation, stents undergo various forces due to pulsatile blood flow, vessel wall movements, as well as external force applied by the plaque itself. In general, a stent implanted in an artery of a person endures $1.5-2 \times 10^9$ cardiac cycles [1]. During angioplasty, surface load of approximately 13.3 kPa is applied on the inner boundary surface of the artery [2].

Textile stents must exert sufficient pressure on the artery wall to reestablish patency, but should not cause damage or rupture. The final radius into which textile stent expands within an artery depends on the pressure exerted by the artery on the stent. Textile stents must be designed to withstand normal pressures encountered in an artery without occluding or permanently deforming. Pressures caused by an artery spasm may rise up to 20.26 kPa [4]. Textile stents should not fail under pressure peaks generated by such spasms. Textile stents cannot be made bulky. They must offer minimum resistance to the blood flow, and be able to pass through tortuous arterial path. As a summary statement, textile stents must achieve an optimum balance between material properties and structural design.

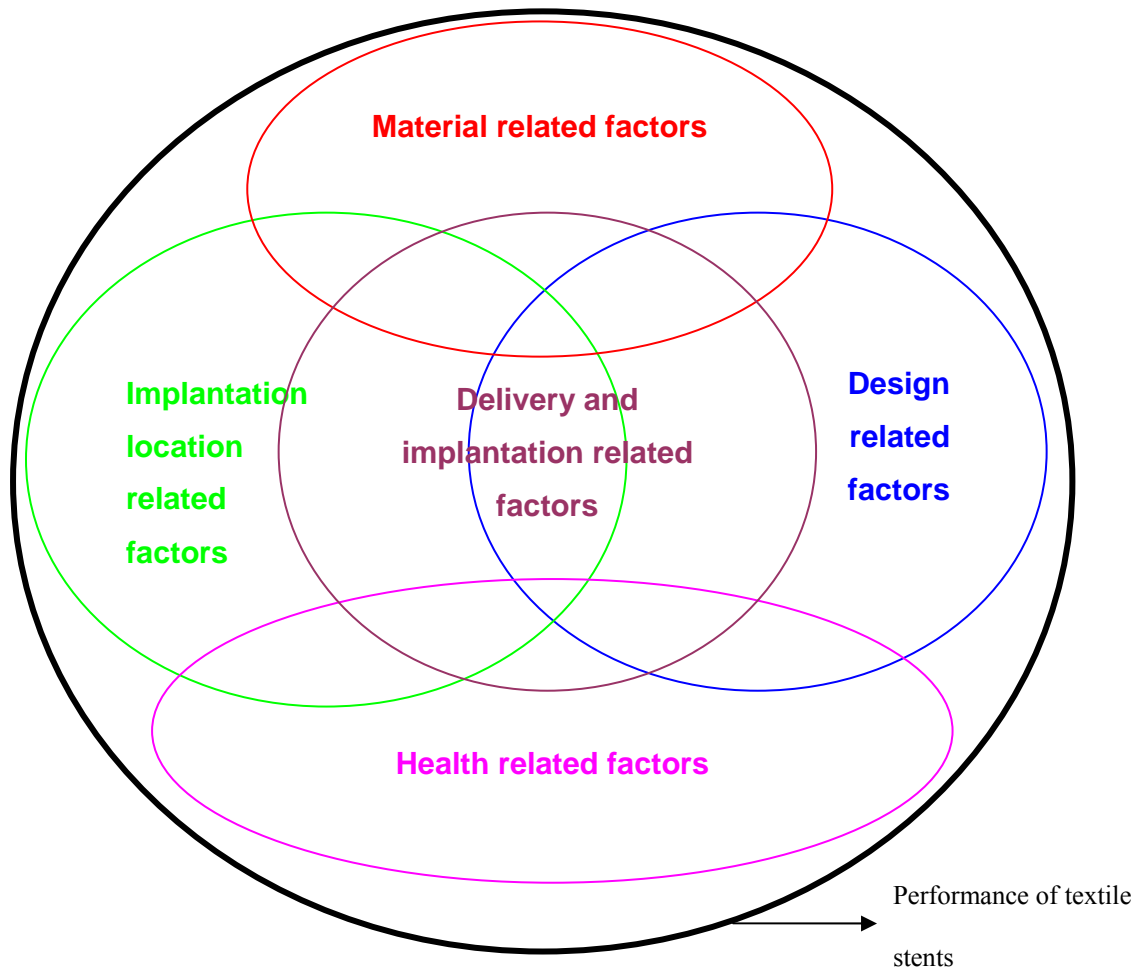


FIGURE 2.12: Factor groups affecting the performance of textile stents.

A comprehensive categorization of factors affecting the performance of textile stents was not observed in the literature and hence is addressed in this study. All known factors affecting the performance of textile stents were classified into five major factor groups: material related factors, design related factors, delivery and implantation related factors, implantation location related factors, and patient's health related factors. All these factor groups were interrelated to each other in a complex manner. Contribution of each factor group to the performance of textile stents can be seen in Figure 2.12. Implantation location related factors, delivery and implantation related factors, and design related factors showed inter-relation with each other as well as with the remaining two factor groups. Material related factors and health related factors had no relation.

Theoretical chart depicting factors affecting the performance of textile stents was somewhat intricate due to involvement of large number of factors and their variability from patient to patient depending on the patient's age, sex, health status, eating habits, lifestyle, etc. Several researchers from various fields contributed significantly on all factors; but a comprehensive chart was not observed and hence addressed in this study which is given in Figure 2.13. The factors groups and chart are suggested as performance determinants of textile stents and will be helpful in further research activities.

The factor groups are also applicable to most biomedical implants.

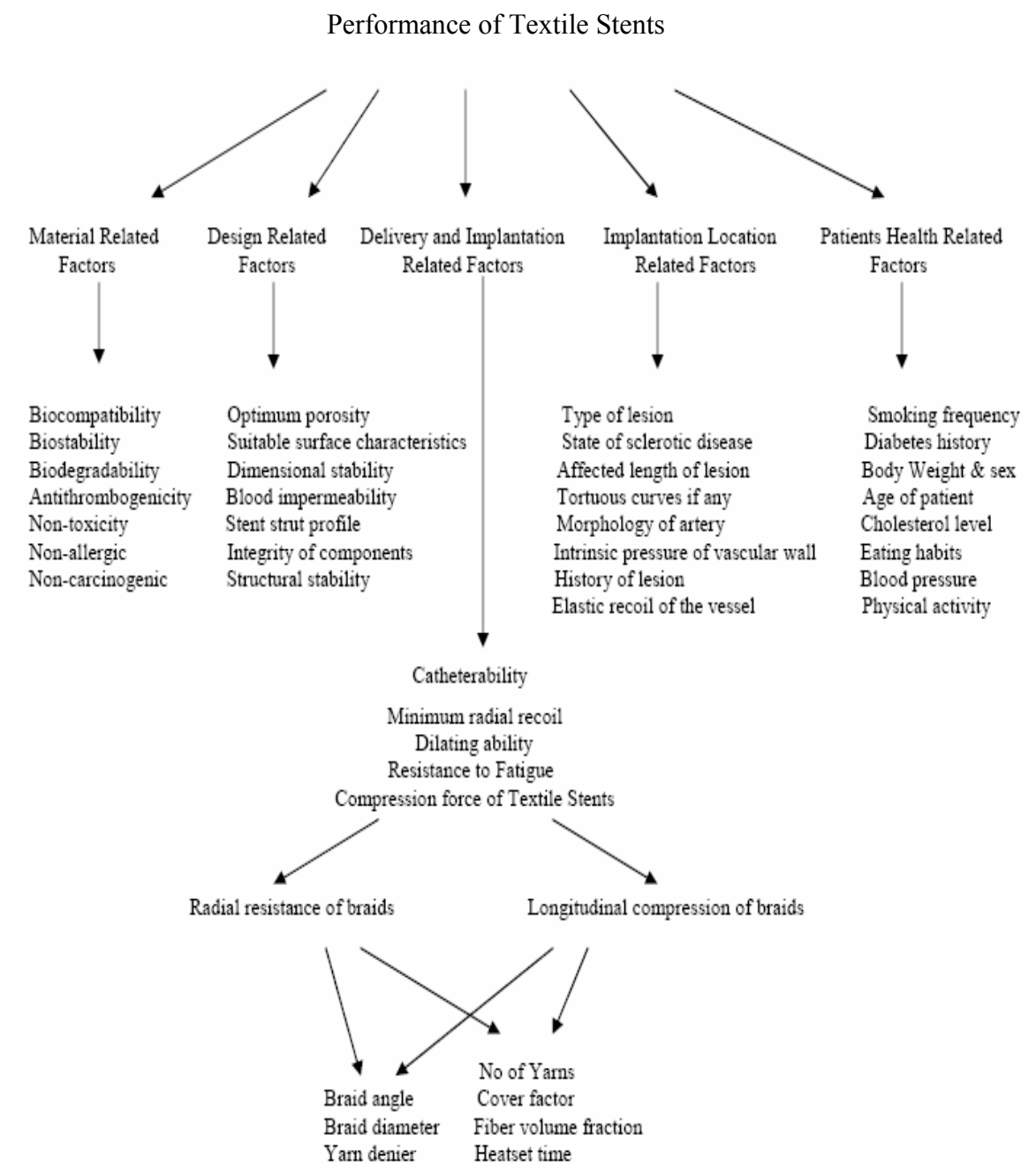


FIGURE 2.13: Performance requirements of textile stents.

2.5 Literature Cited

1. Dumoulin, C., and Cochelin, B., “Mechanical Behavior Modeling of Balloon-expandable Stents”, *J. Biomech.*, **33**(11), 1461-1470 (2000).
2. Holzapfel, G., Stadler, M., and Schulze-Bauer C., “A Layer Specific Three-Dimensional Model for the Simulation of Balloon Angioplasty using Magnetic Resonance Imaging and Mechanical Testing”, *Ann. Biomed. Eng.*, **30**(6), 753-767 (2002).
3. Irsale, S., and Adanur, S., “Compression Force Modeling of Braided Textile Stents”, The Proc. Southeastern Conference on Theoretical and Applied Mechanics, **22**, Mahfuz, H., and Hosur, M., eds., Tuskegee, Alabama, 2004, pp. 632-641.
4. Schrader, S., and Beyar, R., “Evaluation of the Compressive Mechanical Properties of Endoluminal Metal Stents”, *Cathet. Cardiovasc. Diagn.*, **44**(2), 179-187 (1998).

CHAPTER 3

COMPRESSION FORCE OF POLYMERIC TEXTILE STENTS

3.1 Novel Compression Test

Compression properties of textile stents significantly affect their performance. Several metal stent compression tests including longitudinal compression [4], constricted ends compression [2], wrap around collar compression [1], and pressure chamber compression [5] were found in the literature. A compression test was conceived for polymeric textile stents in the textile testing environment. The experimental arrangement for novel compression test on the Instron is shown in Figure 3.1. With this arrangement, it was possible to test different diameter textile stents. As the test started, the lower jaw moved upwards and compressed the textile stent (Figure 3.2). A specific distance between the upper and lower jaw was maintained as the end point of the test. The ‘test end distance’ was kept the same for all compression tests.



FIGURE 3.1: Experimental arrangement.



FIGURE 3.2: Novel compression test.

3.2 Tubular Narrow Woven Fabric Testing

Non-elastic (polyester multifilament weft) and elastic (nylon-lycra blend weft) tubular fabric samples were tested on Instron materials tester for the mechanical properties. Three samples of each were tested. The gauge length was 76.2 mm for the machine direction (Figure 3.3) and 3.2 mm for the cross machine direction (Figure 3.4) testing. Values of maximum load and % strain were recorded and statistical analysis was carried out. Bifurcated braided structures were compared for tactile properties and better monofilament interlacements throughout their length.

There was no statistically significant effect of change in weft from 150 denier polyester multifilament to 150 denier nylon-lycra blend elastic yarn on load at break of the sealing component when tested in both machine ($p = 0.2249$) and cross-machine ($p = 0.3170$) directions. However, there was a statistically significant effect of change of weft on % strain when tested in both machine ($p = 0.00125$) and cross-machine ($p = 0.01784$) directions. This was because nylon-lycra blend yarn had much more elongation than that of polyester. All results were analyzed by one-way ANOVA (analysis of variance) using Microsoft EXCEL[®].



FIGURE 3.3: Tubular narrow woven fabric testing on Instron (machine direction).



FIGURE 3.4: Tubular narrow woven fabric testing on Instron (cross-machine direction).

3.3 Compression Force of Textile Stents

Textile stents (5 samples each for 112 combinations) were tested for compression with the novel compression test. Three-dimensional graphs (Figures 3.5, 3.6, 3.7, and 3.8) were plotted for different diameter textile stents to predict their compression force over a broader range. Metal stents are commercially sold and manufactured depending on their diameter and length. Therefore, it was convenient to predict compression force of textile stents based on their diameters.

For 12.7 and 25.4 mm braid diameters, higher compression force was observed as braid angle was increased (Figure 3.6 and 3.8). But certainly an interesting trend was observed for 19 mm braided structures because there was no increase in compression force as braid angle was increased. It was concluded that 19 mm braided structures were unstable even after heatsetting. Due to structural instability, the compression force observed for 60° braid angle was less than those of 30°, 45°, and 75° (Figure 3.7). For 6.3 mm textile stents, compression force increased as braid angle was increased. These three-dimensional surfaces provided useful guidelines for manufacturing of braided structures.

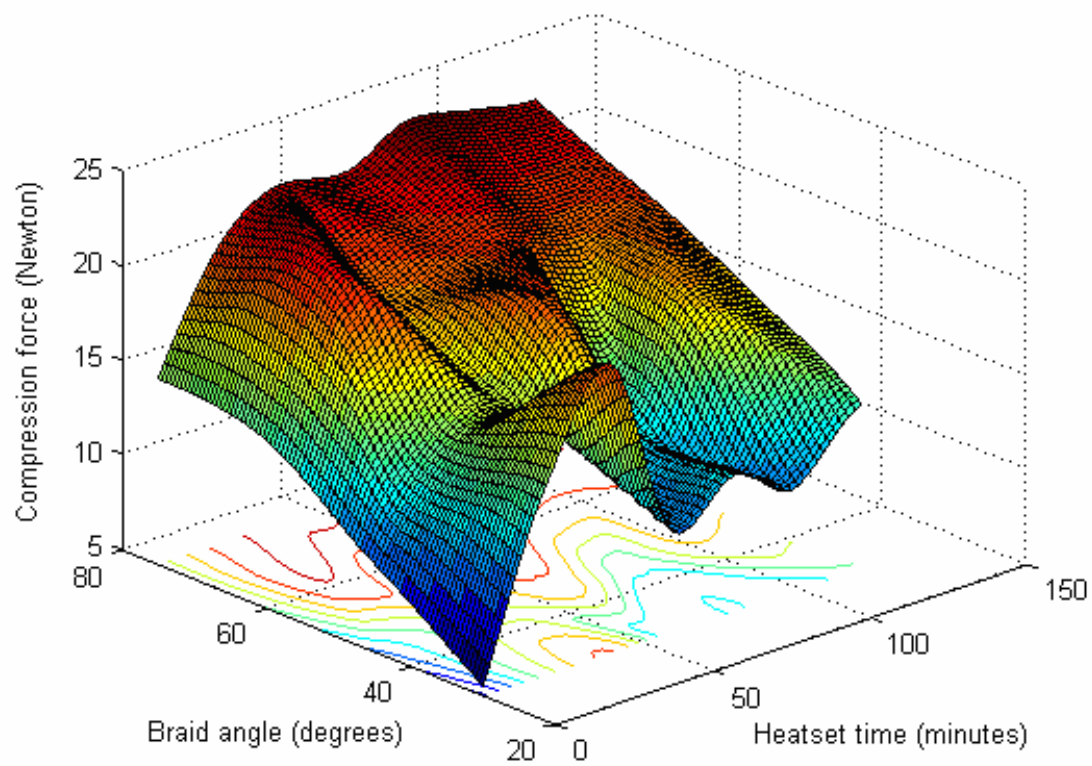


FIGURE 3.5: Compression force of 6.3 mm (diameter) textile stents.

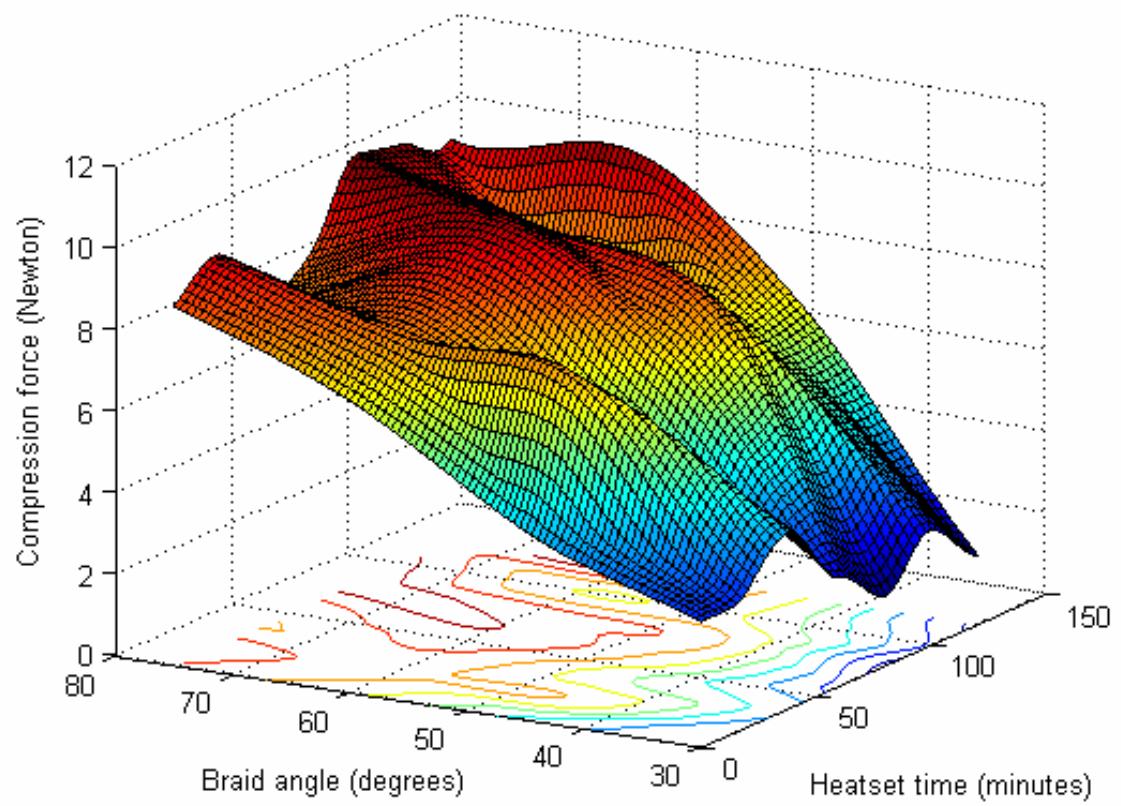


FIGURE 3.6: Compression force of 12.7 mm (diameter) textile stents.

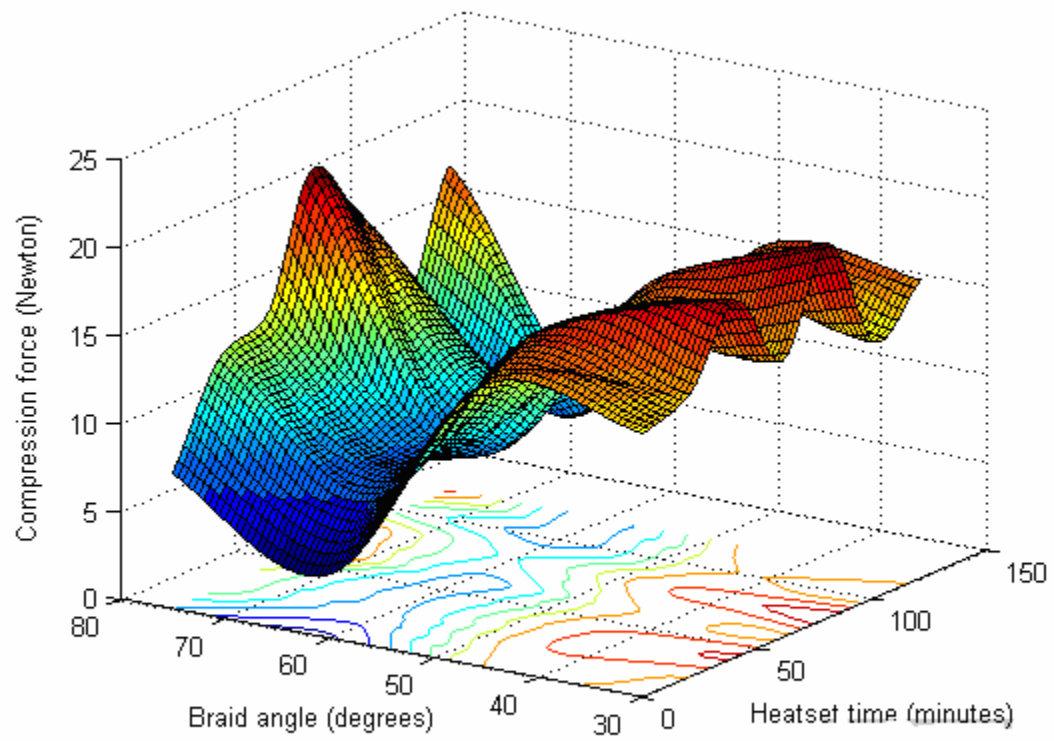


FIGURE 3.7: Compression force of 19 mm (diameter) textile stents.

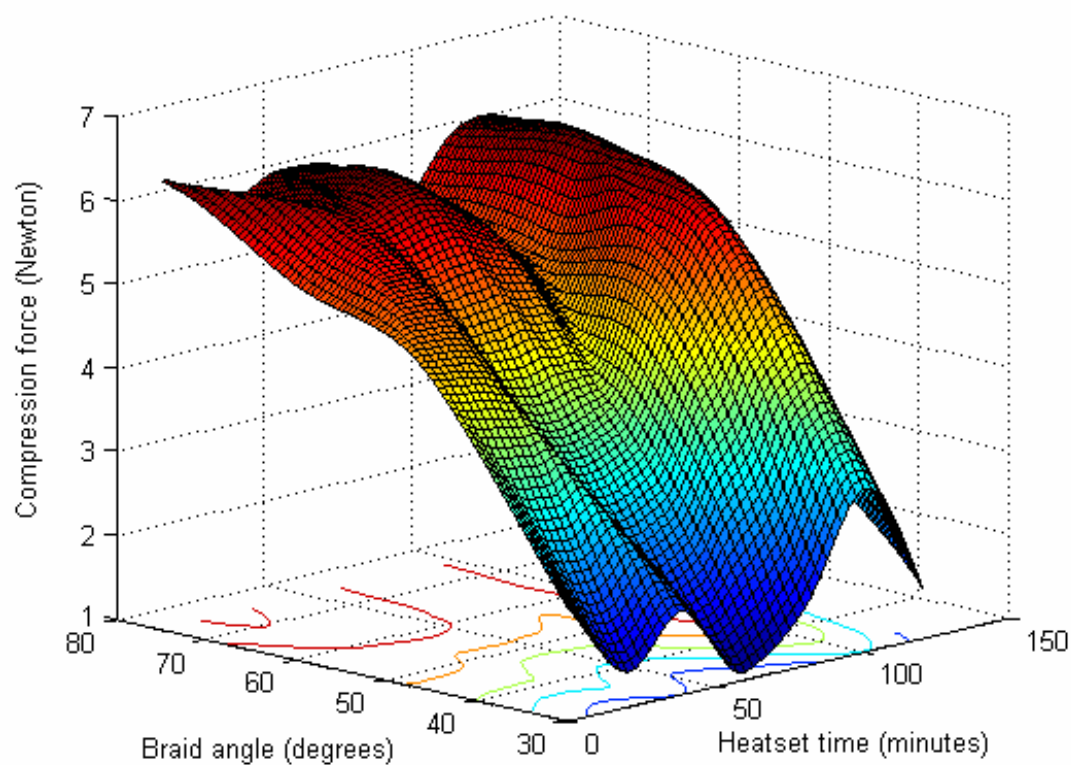


FIGURE 3.8: Compression force of 25.4 mm (diameter) textile stents.

Table 3.1 shows three-way ANOVA results for compression force in Statistical Package for Social Sciences (SPSS®). Braid diameter, braid angle and heatset time showed statistically significant effect ($p = 0.0001$) on compression force. Interaction effects of any two and three variables were also statistically significant.

Monofilament size (in denier) showed statistically significant effect ($p=0.000538$) on compression force of textile stents. Estimated marginal means (Figure 3.9) were best for 75° textile stents. Although 60° structures showed lower values for 19 and 25 mm, key area for the stents is between 4 mm and 12 mm. Therefore, 60° samples were selected as the best textile stent samples. Post-hoc results were better for 60 minutes heatset samples. Therefore, it was concluded that 60° braid angle and 60 minutes heatset samples were the best. These results were further used in mechanical modeling of textile stents.

TABLE 3.1: SPSS® results for compression force (three-way ANOVA).

Response Variable: COMPRESSION FORCE

Source	Type III Sum of Squares	df	Mean Square	F	(p value)
Corrected Model	234484004.736	111	2112468.511	94.210	<.0001
Intercept	658382622.864	1	658382622.864	29361.961	<.0001
DIAMETER	151188960.436	3	50396320.145	2247.530	<.0001
ANGLE	14403720.893	3	4801240.298	214.121	<.0001
TIME	7571027.886	6	1261837.981	56.274	<.0001
DIAMETER * ANGLE	40266216.836	9	4474024.093	199.529	<.0001
DIAMETER * TIME	9173786.714	18	509654.817	22.729	<.0001
ANGLE * TIME	3741919.857	18	207884.437	9.271	<.0001
DIAMETER * ANGLE * TIME	8138372.114	54	150710.595	6.721	<.0001
Error	10045494.400	448	22422.979		
Total	902912122.000	560			
Corrected Total	244529499.136	559			

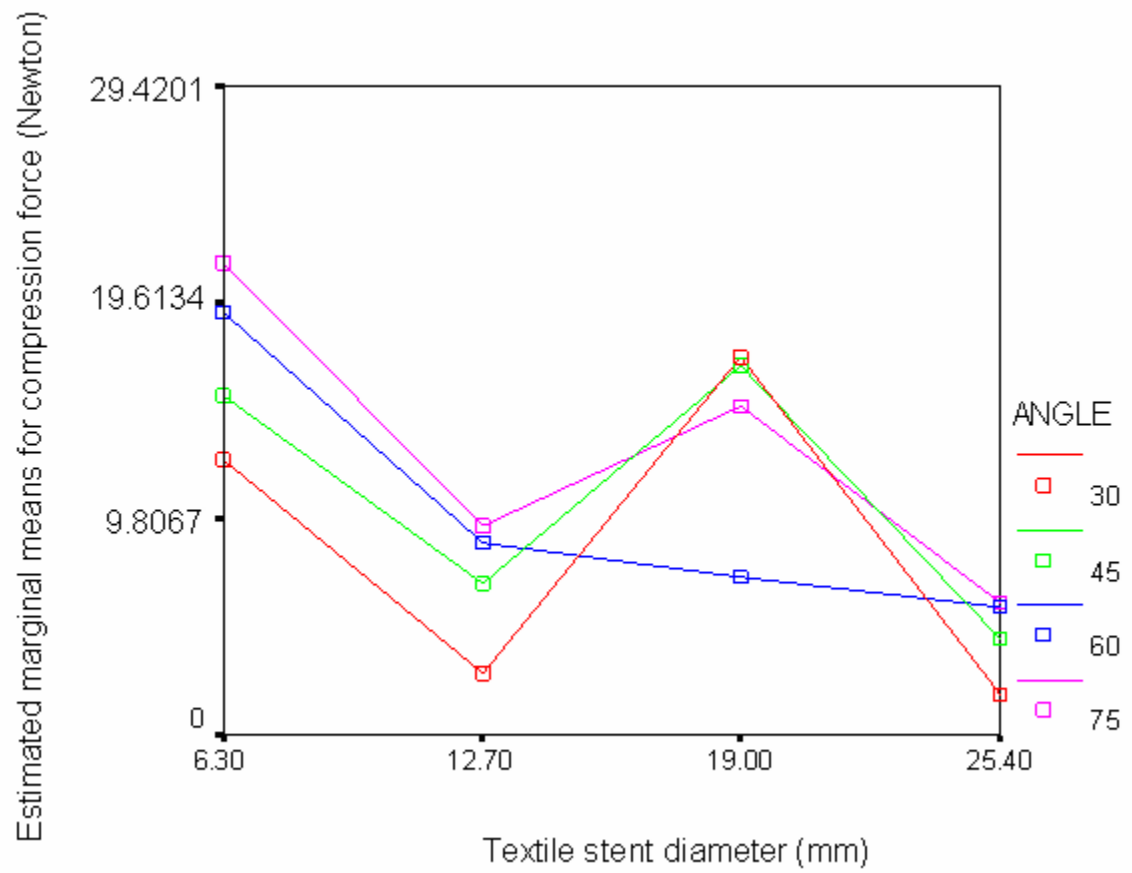


FIGURE 3.9: Estimated marginal means for compression force.

3.4 Correlating Compressions

Textile stent has to sustain various forces acting longitudinally as well as radially. The textile stent must have sufficient compression force to avoid compression and ultimate blockage of the artery. The majority of *in vivo* forces acting on stents are radial.

The correlation of *in vitro* (like novel compression test) and radial compression tests, which simulate *in vivo* conditions was not found in the literature, and hence is addressed in this study. In geometrical correlation, *in vitro* (unidirectional) compression was compared with radial compression. Figure 3.10A shows *in vitro* compression and Figure 3.11 shows radial compression.

ASSUMPTIONS

- For modeling, compression was defined and calculated as the distance traveled by individual monofilament intersections during deformation.
- Textile stents were uniformly compressed. The compression force was not permanently deforming textile stent or individual monofilaments.
- The monofilament intersections were distributed uniformly throughout the textile stent. During compression, monofilament intersections travel in a straight line.
- Cross-section of a textile stent is similar throughout the structure. Textile stent has 64 monofilaments and X_i represents a monofilament intersection.
- Textile stents are compressed up to the ‘test end distance’ (Figure 3.10B), which is the same for both compressions.

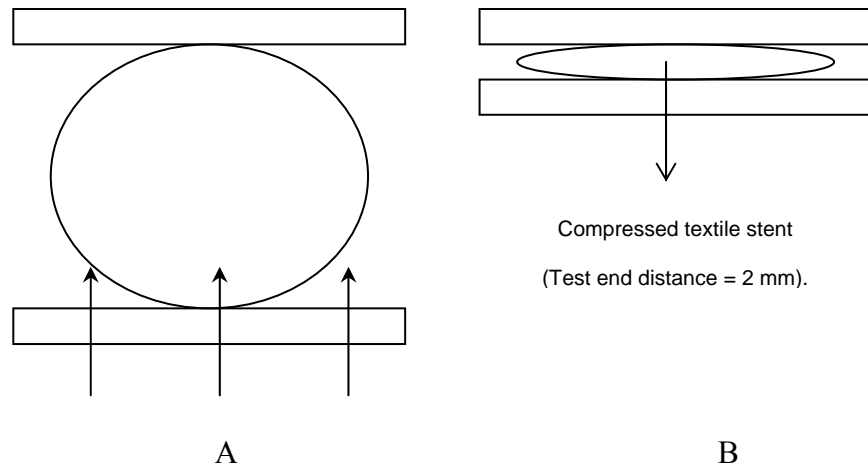


FIGURE 3.10: *In vitro* novel compression test (unidirectional compression).

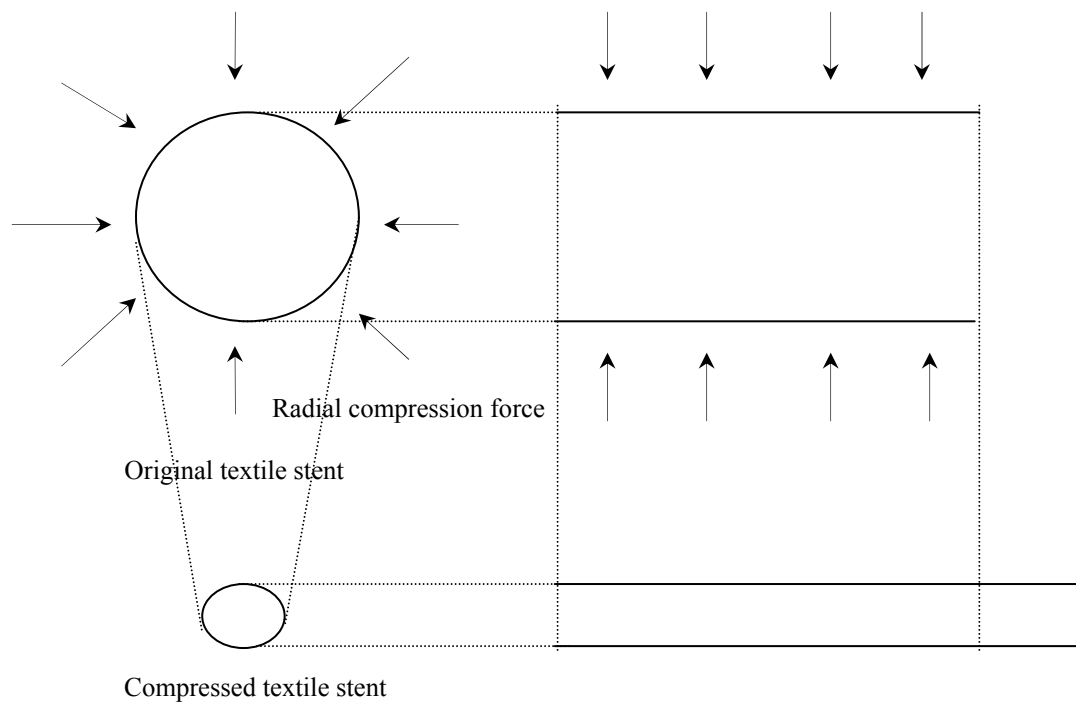


FIGURE 3.11: Radial compression.

The textile stent structure was divided equally in four quadrants, two of which (A and B) are shown in Figure 3.12. MO and NO are radii of textile stent. Q_i is a part of the distance traveled by monofilament intersections during deformation. During compression monofilament intersections were moved and the distance traveled by them was calculated. The total displacement of all monofilament intersections in the novel test (unidirectional compression) was compared to those in the radial compression.

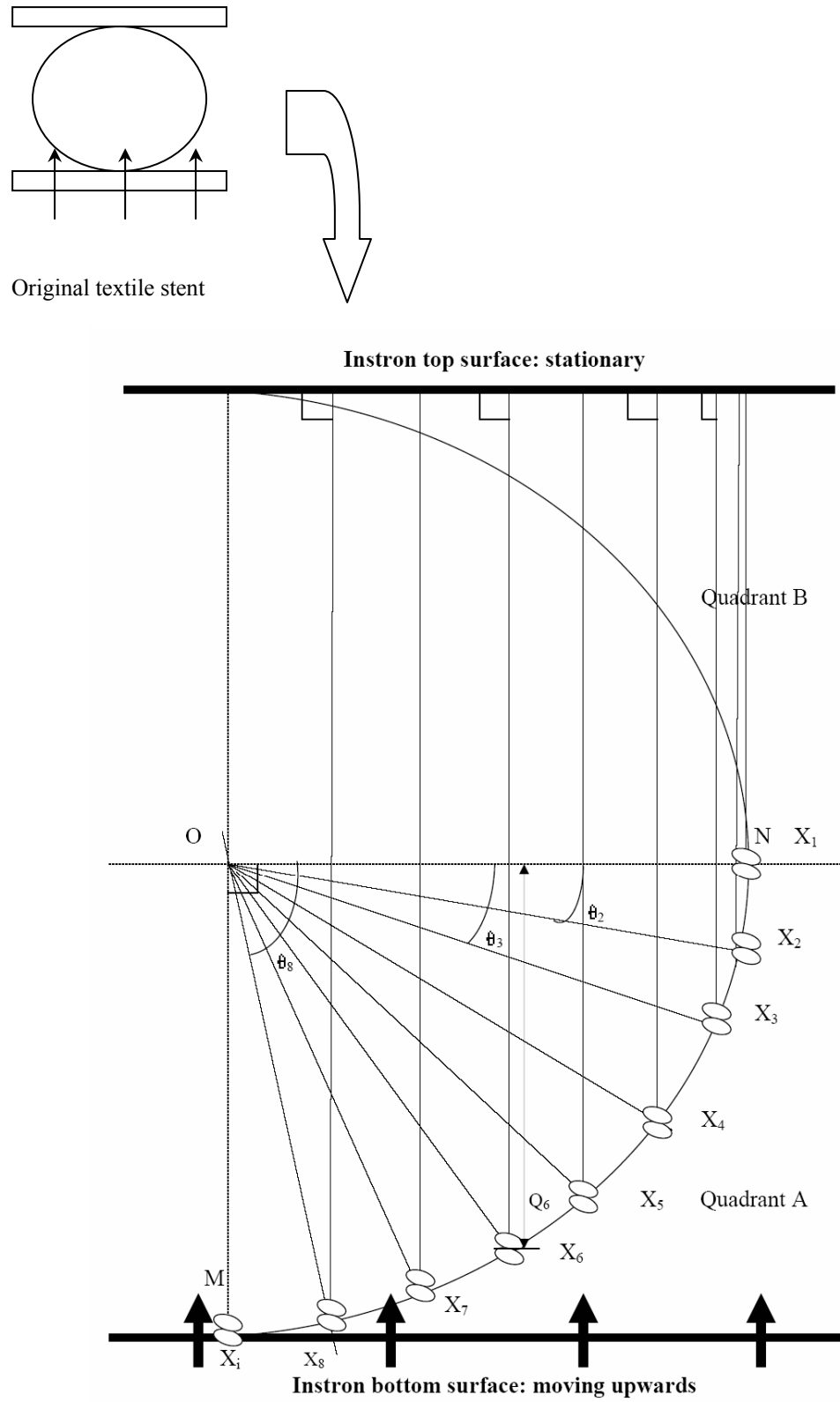


FIGURE 3.12: Calculating compression during novel compression (*in vitro*) test.

In the present study, 64 monofilaments formed 32 monofilament intersections. The total distance traveled by all monofilament intersections during radial compression was,

$$\text{total displacement} = 32 \times (r - 0.1) \text{ cm} \quad (3.1)$$

where r = radius of textile stent in cm.

Total distance traveled by all monofilament intersections during unidirectional (novel test) compression (Figure 3.10) was,

$$\text{total displacement} = [2 (Q_1 + \dots + Q_8) + Q_9 + 16 (r - 0.2)] + 2 (r - 0.2) + 7[(r - 0.2)] - (Q_1 + \dots + Q_8) \text{ cm.} \quad (3.2)$$

where $Q_i = \frac{2}{r} \sqrt{s (s - r)^2 (s - 2r(\sin \theta / 2))}$ cm (i varies from 1 to 8 for each quadrant).

$$\text{and } s = \frac{r + r + (NX_i)}{2} \text{ cm.}$$

From equations 3.1 and 3.2, radial and *in vitro* (unidirectional) compressions were calculated and compared (Figure 3.13) for 0.4, 0.6, 0.8, 1.2, 1.6, 1.9, and 2.54 cm textile stents. Linear regression showed strong correlation (*adjusted R*²=0.99999) between radial and *in vitro* (unidirectional) compressions.

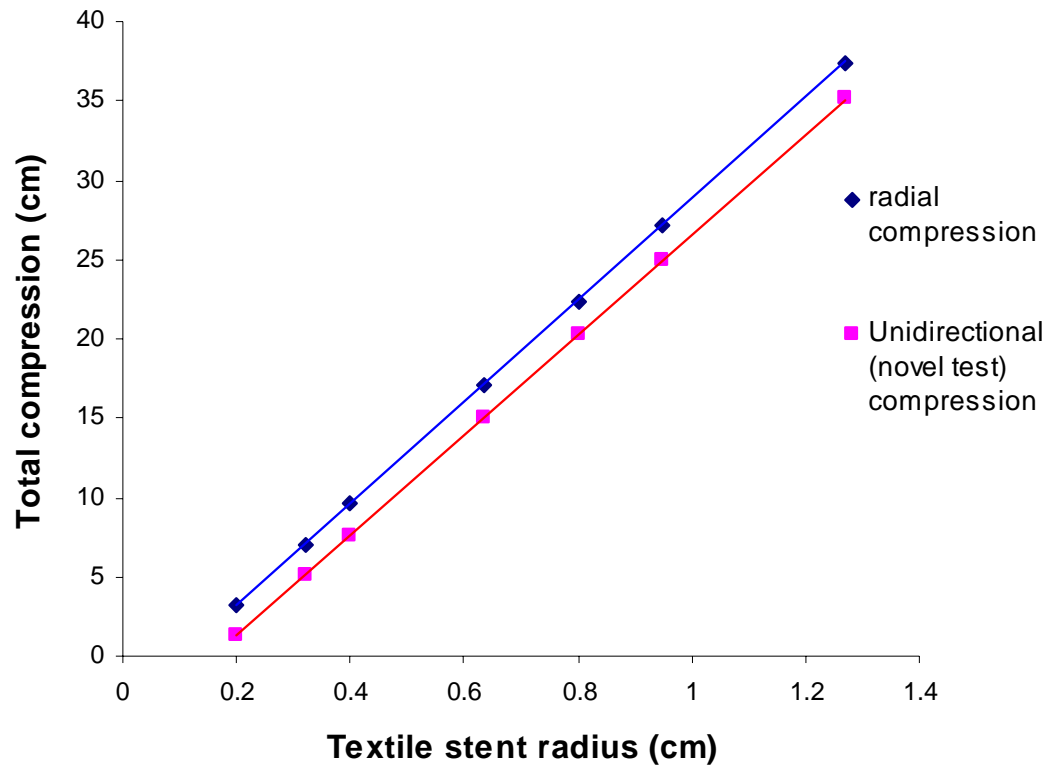


FIGURE 3.13: Comparison of radial and unidirectional (novel test) compressions.

3.5 Applications and Limitations

Strong correlation was observed between the radial and *in vitro*- unidirectional compressions. If *in vivo* compression forces are quantified, those can be compared with compression forces calculated by the novel compression test. However, for the purpose of calculating compressions it was assumed that monofilament intersections travel in a straight line during compression. But, due to friction between monofilaments they may deviate and change the compression. Calculating the actual total distance traveled by all monofilament intersections may be difficult after certain level of compression. Because of this, *in vitro* compression was less than the radial compression. Also, textile stents were not physically fixed during the test. The model did not take into account the gradual increase in radial compression forces applied over time by the plaque after implantation. *In vivo* compressive forces assumed in the geometrical correlation were uniform and unidirectional. But actual *in vivo* forces may be different. The stents are generally compressed at some point and then the load further spreads throughout the structure. The correlation could not describe the compressive forces due to a localized sharp spur of calcified plaque. However, the approach correlated radial and unidirectional compressions for textile stents. The novel compression test can also be used for metal stents.

3.6 Literature Cited

1. Agrawal, M., and Clark, H., “Deformation Characteristics of a Bioabsorbable Intravascular Stent”, *Invest. Radiol.*, **27**(12), 1020-1024 (1992).
2. Dyet, J., Watts, W., Ettles, D., and Nicholson, A., “Mechanical Properties of Metallic Stents: How Do These Properties Influence the Choice of Stents for Specific Lesions?”, *Cardiovasc. Intervent. Radiol.*, **23**(1), 47-54 (2000).
3. Irsale, S., and Adanur, S., “Compression Force Modeling of Braided Textile Stents”, The Proc. Twenty Second Southeastern Conference on Theoretical and Applied Mechanics, Mahfuz, H., and Hosur, M., eds., Tuskegee, Alabama, 2004, pp. 632-641.
4. Schrader, S., and Beyar, R., “Evaluation of the Compressive Mechanical Properties of Endoluminal Metal Stents”, *Cathet. Cardiovasc. Diagn.*, **44**(2), 179-187 (1998).
5. Zilberman, M., Schwade, N., and Eberhart, R., “Protein-Loaded Bioresorbable Fibers and Expandable Stents: Mechanical Properties and Protein Release”, *J. Biomed. Mater. Res.: Appl. Biomater.*, **69B**(1), 1-10 (2004).

CHAPTER 4

MODELING: PREDICTING YOUNG’S MODULUS AND COMPRESSION FORCE

Mechanical properties play decisive role towards the performance of textile stents, which are braided structures. Strain energy method is being used by textile researchers to understand various facets of the performance of fiber assemblies [9], fibrous composite materials [4], yarns [7], plain weave fabrics [11], and hybrid fabrics [1]. The objective of this model was to predict the Young’s modulus of textile stents, which are monofilament braids, by strain energy method. In the current study, strain energy method and Castigliano’s theorem [12] were applied for modeling. The equations needed to predict the Young’s modulus by strain energy method were divided into three parts: determination of structural geometry, definition of the strain energy function, and equations derived by strain energy method [5, 10]. The strain energy equations were derived from those of the plain weave [8]. Previous braid models developed by Heirigs and Schwartz [6] and Zang *et al.* [14] provided useful guidelines in understanding the structure and properties of braids.

TABLE 4.1: Notations for strain energy model.

2β = braid angle in degrees.	$x = A_1PA_2, y = C_1PC_2$ (Figure 4.5).
r = radius of braid in units.	$p = A_1QA_2$, and $t = C_1QC_2$ (Figure 4.5).
l = length of braid formed in one carrier rotation.	w = width of each diamond trellis.
m = total monofilaments in the braid.	g = length of each diamond trellis.
B_1, B_2 = flexural rigidities of monofilaments.	θ_1, θ_2 = respective braid inclination angles.
M = applied bending moment of the monofilament.	F_1, F_2 = applied forces on braid.
λ_1, λ_2 = elasticity modulus of monofilaments.	v_1, v_2 = inter-filament forces on individual monofilaments.
μ = coefficient of friction between monofilaments.	U = total strain energy of the unit.
E_1, E_2 = Young's modulus of braid.	U_b = bending strain energy of the unit.
	U_c = compression strain energy of the unit.
	U_e = extension strain energy of the unit.
	d = monofilament diameter in units.
	f_1, f_2 = forces on individual monofilaments.

4.1 Determination of Braid Structural Geometry

ASSUMPTIONS

- Each monofilament is perfectly circular throughout its length.
- Monofilaments are equally spaced throughout the braided structure.
- Braided structure can be laid flat when cut and opened.
- Monofilaments form diamond braid (1/1 intersection repeat) as shown in Figure

4.1.

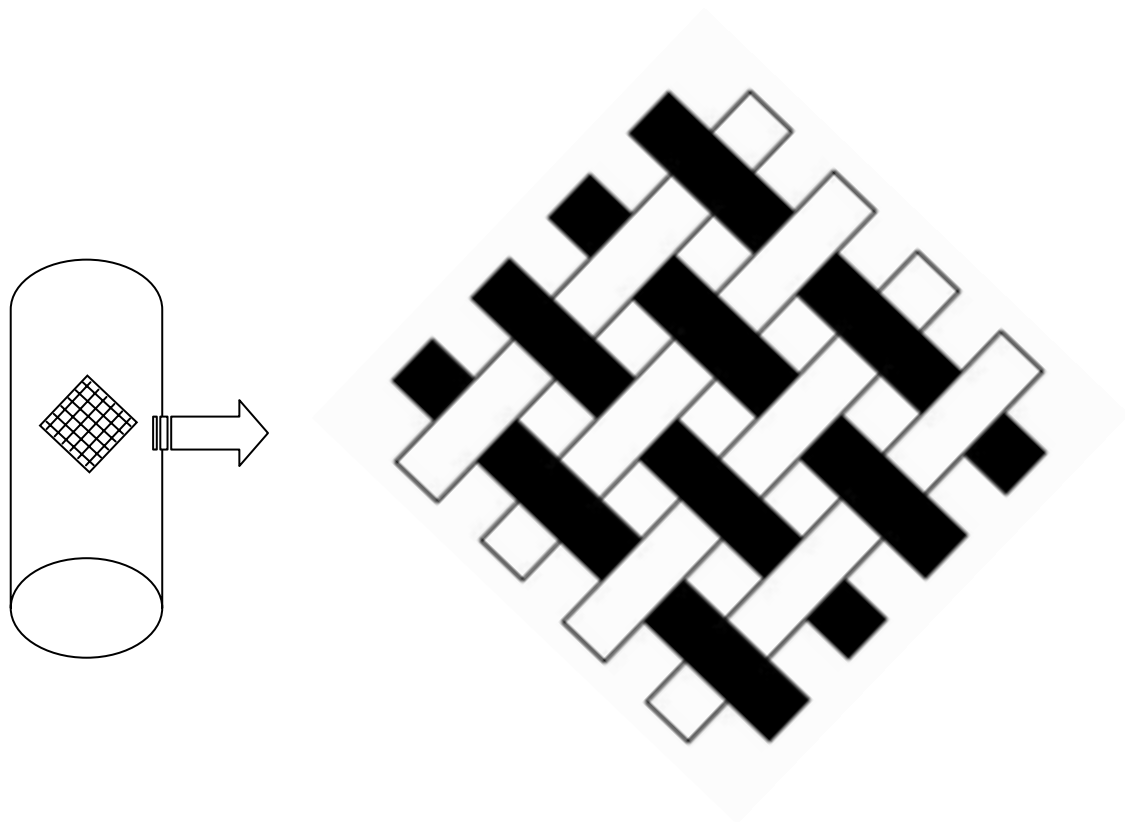


FIGURE 4.1: Braided structure.

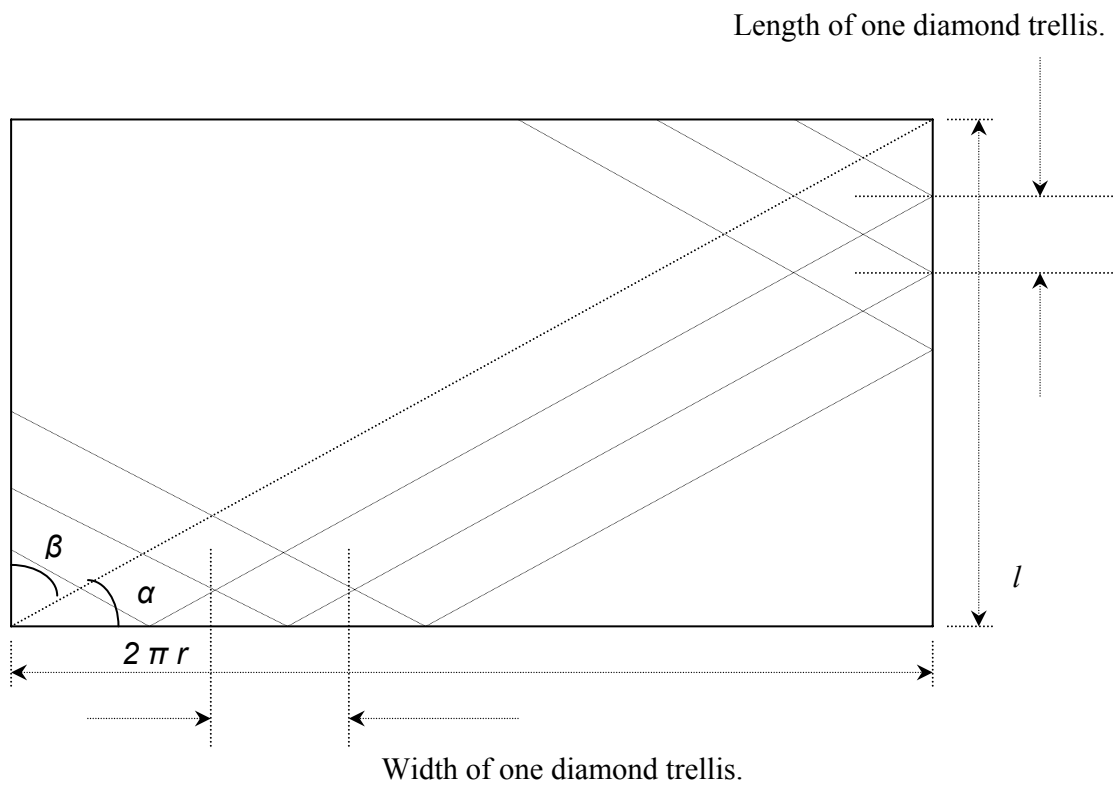


FIGURE 4.2: Cut and opened braided structure.

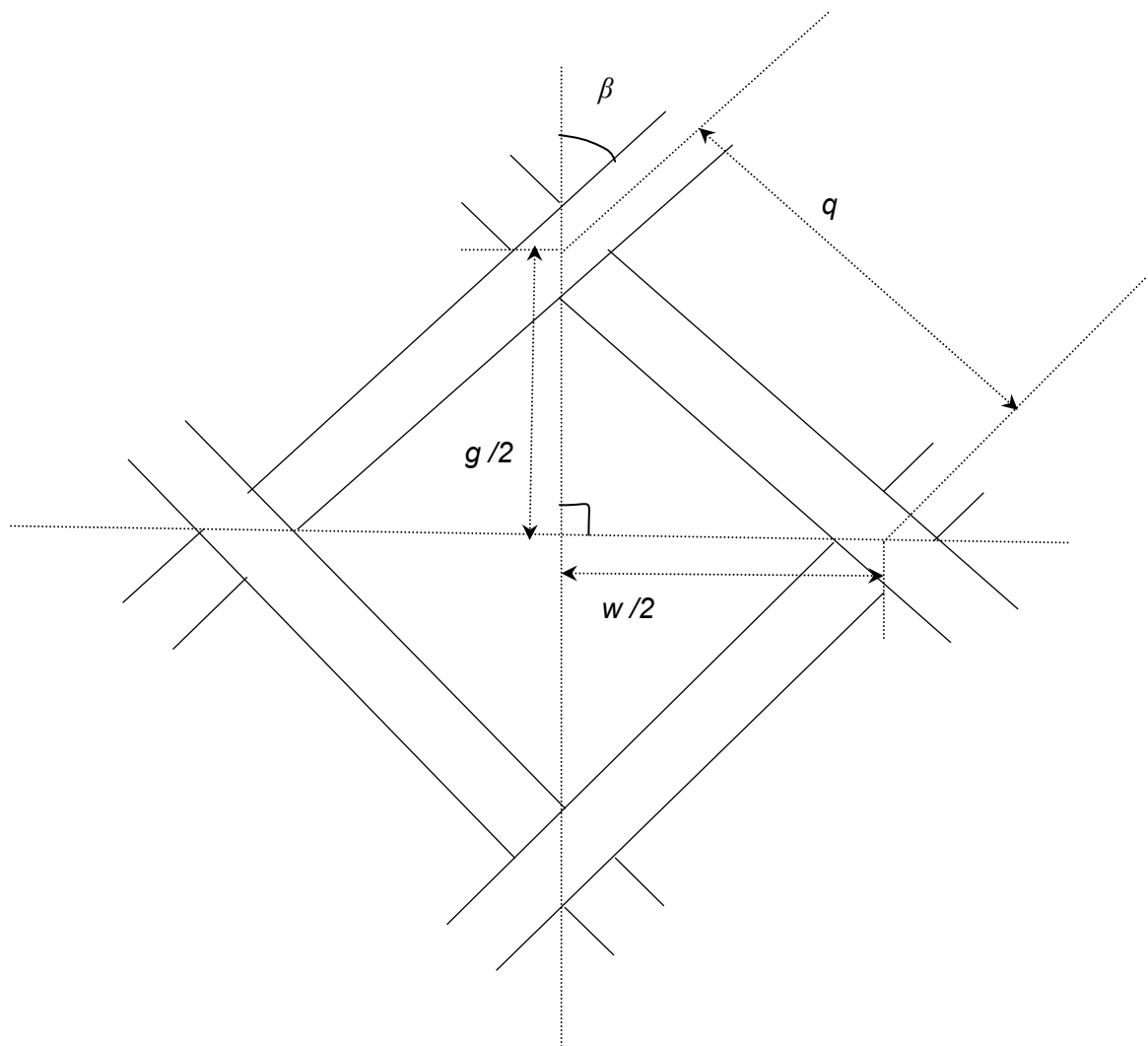


FIGURE 4.3: Diamond trellis as repeating unit.

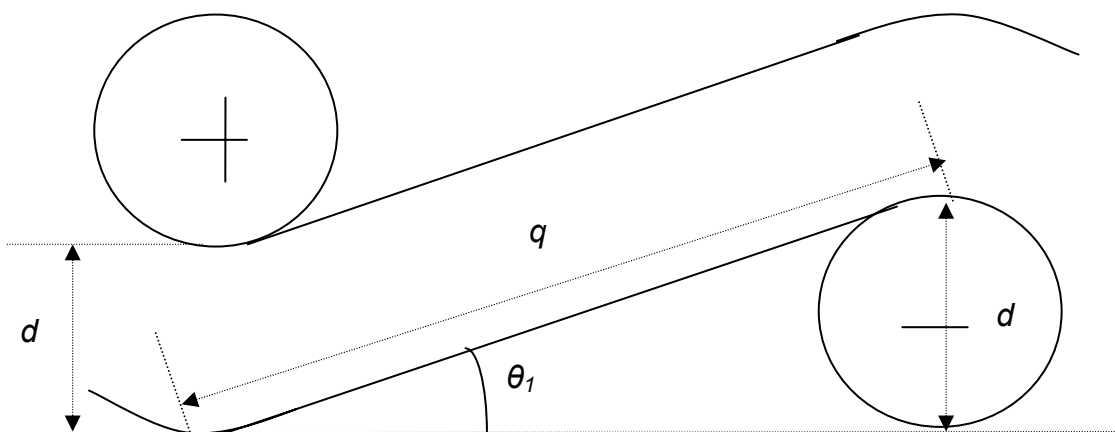


FIGURE 4.4: Cross-section showing 'braid inclination angle'.

Cut and opened braided structure (Figure 4.2) had m monofilaments; $m/2$ heading in one direction and $m/2$ in the other. Diamond trellis (Figure 4.3) was considered as the repeating unit of the braided structure. Monofilaments (m) formed $m/2$ diamond trellises along the width $2\pi r$. Therefore,

$$\text{width of each diamond trellis } w = \frac{2\pi r}{m/2} \quad (4.1)$$

The monofilaments (m) formed $m/2$ diamond trellises along the length l . Length of each diamond trellis is,

$$g = \frac{l}{m/2} \quad (4.2)$$

For certain value of braid angle, the diamond trellis became a rhombus. Hence, total number of diamond trellises in the braided structure of length l

$$= \frac{\text{Total surface area of the braided structure of length } l}{\text{Area of one diamond trellis}} = m^2 / 2 \quad (4.3)$$

From Figure 4.2,

$$\tan \alpha = \frac{l}{2\pi r}$$

$$l = 2\pi r \tan (90 - (\text{braid angle} / 2))$$

Thus, length of fabric braided in one carrier rotation is

$$l = 2\pi r \tan (90 - \beta) \quad (4.4)$$

Due to braiding crimp, monofilaments were inclined at an angle θ_i . Braid inclination angle- θ_l (Figure 4.4) is defined as the angle at which the monofilaments are inclined when the cut and opened braided structure is laid flat. Because of the braid symmetry assumed and similar monofilament diameters, braid inclination angles remain

the same. Braid inclination angle depends on interlacing, filament diameter, braid angle, and braid hanging length (q).

From g , w and Figure 4.3,

$$q = \frac{w/2}{\sin \beta}$$

$$\text{From Figure 4.4, the braid inclination angle} = \theta_l = \sin^{-1} \left(\frac{d}{q} \right) \quad (4.5)$$

All these braid structural parameters are used in strain energy (mechanical) modeling of textile stents.

4.2 Definition of Strain Energy Function

ASSUMPTIONS

- The monofilaments are straight flexible cylinders rigidly joined at the point of their intersection. The monofilaments intersection (Figure 4.5) is repeating unit of the braided structure.
- Braid is extended along monofilament units A_1PA_2 and C_1PC_2 . P and Q show two possible cases of monofilaments intersection in the repeating unit.
- If interfilament force v caused a very small change (d') in the monofilament diameter, it can be assumed that,

$$v = \mu d'$$

Therefore, strain energy of compression is $\frac{v^2 d}{2\mu}$.

Monofilaments bend with flexural rigidity B . The strain energy per unit length of the monofilament is $M^2/2B$.

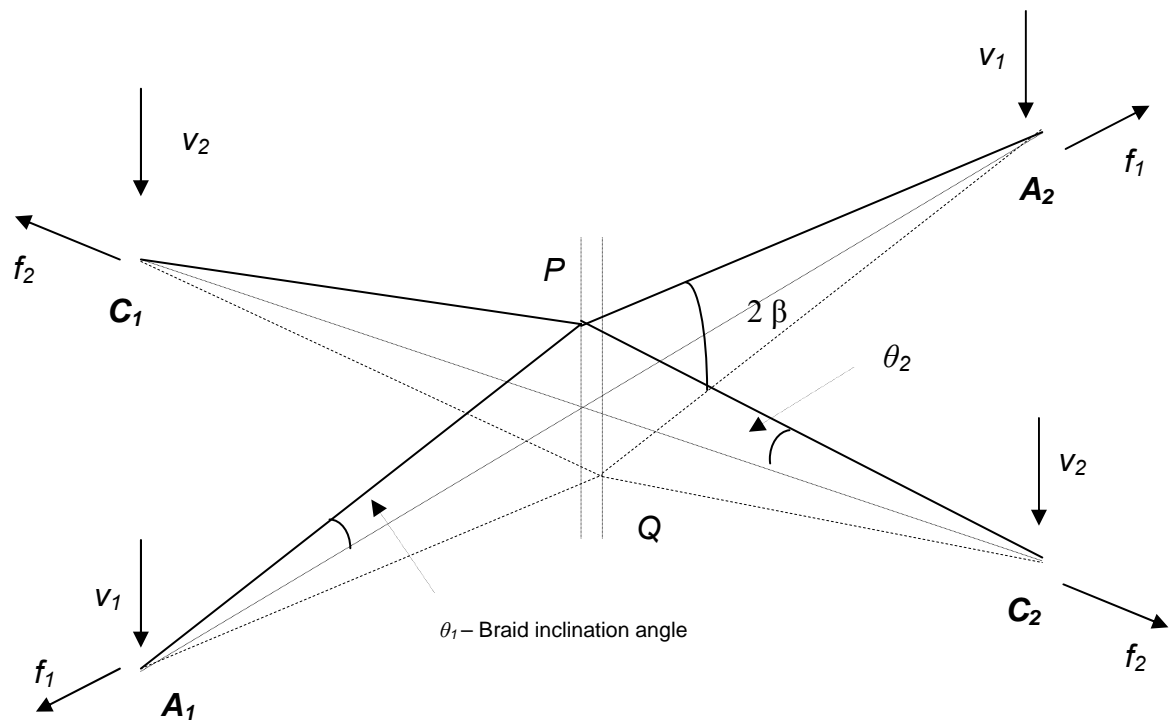


FIGURE 4.5: Monofilaments intersection as a unit of braided structure.

At any point on monofilaments intersection, the tension and shear generated due to deformation were resolved into two components f_I and v_I . For small within structure deformations, the bending moment of any point at a distance a from A_I on A_IP is approximately,

$$(f_I \sin \theta_I - v_I \cos \theta_I) a$$

$$\text{Bending strain energy in } A_IP = \frac{1}{2B_1} \int_0^{x/2} (f_I \sin \theta_I - v_I \cos \theta_I)^2 a^2 da$$

$$E_1 = \frac{(x)^3 (f_I \sin \theta_I - v_I \cos \theta_I)^2}{48 B_1}$$

The bending strain energy in B_IP is given by a similar expression. Total bending strain energy of the unit is

$$U_b = 2 E_1 + 2 E_2$$

$$= \frac{(x)^3 (f_1 \sin \theta_1 - v_1 \cos \theta_1)^2}{24 B_1} + \frac{(y)^3 (f_2 \sin \theta_2 - v_2 \cos \theta_2)^2}{24 B_2} \quad (4.6)$$

Tension in A_IP is

$$T = f_1 \cos \theta_1 + v_1 \sin \theta_1$$

So extension strain energy of A_IP is

$$E_{t1} = \frac{(x)(f_1 \cos \theta_1 + v_1 \sin \theta_1)^2}{4 \lambda_1} \quad (4.7)$$

Hence, total extension strain energy of the unit is

$$U_e = 2 E_{t1} + 2 E_{t2}$$

$$U_e = \frac{(x)(f_1 \cos \theta_1 + v_1 \sin \theta_1)^2}{2 \lambda_1} + \frac{(y)(f_2 \cos \theta_2 + v_2 \sin \theta_2)^2}{2 \lambda_2} \quad (4.8)$$

From compression law assumed, the component of compression strain energy leads to

$$U_c = \frac{v_1^2 d}{\mu} + \frac{v_2^2 d}{\mu} \quad (4.9)$$

From equations 4.6, 4.8, and 4.9, total strain energy of the given monofilaments intersection is $U = U_b + U_e + U_c$.

$$U = \frac{(x)^3 (f_1 \sin \theta_1 - v_1 \cos \theta_1)^2}{24 B_1} + \frac{(y)^3 (f_2 \sin \theta_2 - v_2 \cos \theta_2)^2}{24 B_2} + \frac{(x)(f_1 \cos \theta_1 + v_1 \sin \theta_1)^2}{2 \lambda_1} + \frac{(y)(f_2 \cos \theta_2 + v_2 \sin \theta_2)^2}{2 \lambda_2} + \frac{v_1^2 d}{\mu} + \frac{v_2^2 d}{\mu} \quad (4.10)$$

4.3 Formulation of Interfilament Force

Plane B was assumed to be passing through contact point of monofilaments and parallel to plane A as shown in Figure 4.6. h_1 and h_2 are projections from monofilament centers (O_1 and O_2 respectively) on plane A . To maintain the structural integrity of braid, distance between these two planes has to be same and monofilaments must be in contact with each other.

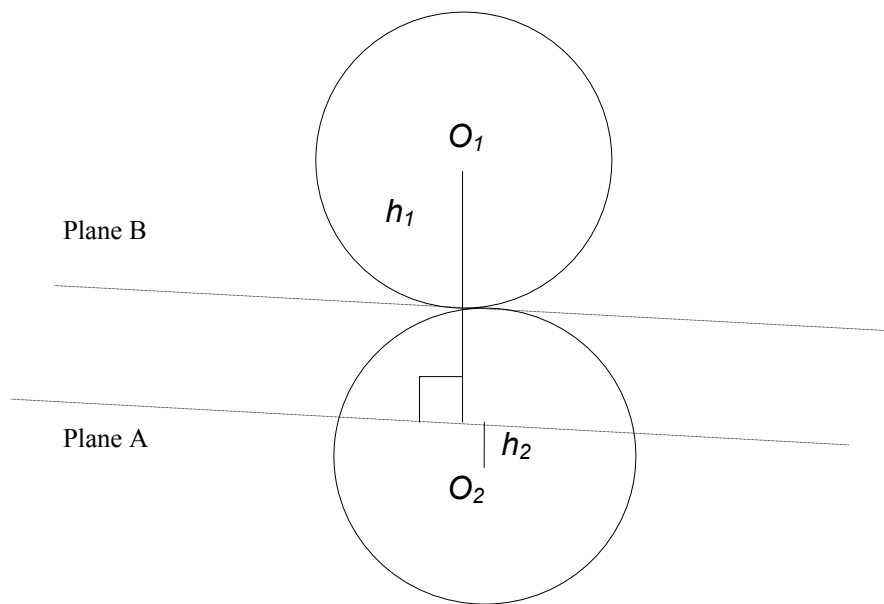


FIGURE 4.6: Cross-section of monofilaments intersection.

Therefore, $h_1 - r_1 = r_2 - h_2$.

$$\delta(h_1 - r_1) + \delta(h_2 - r_2) = 0.$$

Castigliano's theorem [10] can be summarized as

“the first derivative of strain energy with respect to external force is equal to the displacement at the point of application of that force”.

By applying Castigliano's theorem,

$$\begin{aligned} \delta(h_1 - r_1) &= \frac{\delta U}{\delta v_1} \text{ and } \delta(h_2 - r_2) = \frac{\delta U}{\delta v_2} \\ \frac{\delta U}{\delta v_1} + \frac{\delta U}{\delta v_2} &= 0 \end{aligned} \quad (4.11)$$

Differentiating U partially with respect to v_1 and v_2 , and substituting in equation 4.11,

$$\begin{aligned} \frac{\delta U}{\delta v_1} + \frac{\delta U}{\delta v_2} &= \\ \frac{x^3}{24 B_1} (2 v_1 \cos^2 \theta_1 - 2 f_1 \sin \theta_1 \cos \theta_1) + \frac{x}{2 \lambda_1} (2 v_1 \sin^2 \theta_1 + 2 f_1 \cos \theta_1 \sin \theta_1) + \\ \frac{2d}{\mu} v_1 + \frac{y^3}{24 B_2} (2 v_2 \cos^2 \theta_2 - 2 f_2 \sin \theta_2 \cos \theta_2) \\ + \frac{y}{2 \lambda_2} (2 v_2 \sin^2 \theta_2 + 2 f_2 \cos \theta_2 \sin \theta_2) + \frac{2d}{\mu} v_2 &= 0 \end{aligned} \quad (4.12)$$

At some point of deformation, $v = v_1 = v_2$. Putting this in equation 4.12,

$$v = \frac{\left\{ \left(\frac{x^3}{12 B_1} - \frac{x}{\lambda_1} \right) (f_1 \sin \theta_1 \cos \theta_1) \right\} + \left\{ \left(\frac{y^3}{12 B_2} - \frac{y}{\lambda_2} \right) (f_2 \sin \theta_2 \cos \theta_2) \right\}}{\frac{x^3}{12 B_1} (\cos^2 \theta_1) + \frac{x}{\lambda_1} (\sin^2 \theta_1) + \frac{y^3}{12 B_2} (\cos^2 \theta_2) + \frac{y}{\lambda_2} (\sin^2 \theta_2) + \frac{4d}{\mu}} \quad (4.13)$$

Equation 4.13 can quantify inter-filament force v if f_1 and f_2 are known.

4.4 Determination of Braid Extension

Braid extension in a given direction is

$$e_l = \frac{dp}{p} \quad (4.14)$$

Using Castigliano's first theorem,

$$e_l p = dp = \frac{dU}{df_1} \quad (4.15)$$

Therefore,

$$e_l = \frac{1}{p} \frac{dU}{df_1} \quad (4.16)$$

Differentiating U with respect to f , and putting $v = v_l = v_2$,

$$e_l = \frac{1}{p} \left\{ \frac{x^3}{12B_1} f_1 \sin^2 \theta_1 + \frac{x}{\lambda_1} f_1 \cos^2 \theta_1 + \left(\frac{x}{\lambda_1} - \frac{x^3}{12B_1} \right) \frac{\left(\frac{x^3}{12B_1} (f_1 \sin^2 \theta_1 \cos^2 \theta_1) - \frac{x}{\lambda_1} (f_1 \sin^2 \theta_1 \cos^2 \theta_1) + \frac{y^3}{12B_2} (f_2 \sin \theta_1 \cos \theta_1 \sin \theta_2 \cos \theta_2) - \frac{y}{\lambda_2} (f_2 \sin \theta_1 \cos \theta_1 \sin \theta_2 \cos \theta_2) \right)}{\frac{x^3}{12B_1} (\cos^2 \theta_1) + \frac{x}{\lambda_1} (\sin^2 \theta_1) + \frac{y^3}{12B_2} (\cos^2 \theta_2) + \frac{y}{\lambda_2} (\sin^2 \theta_2) + \frac{4d}{\mu}} \right\} \quad (4.17)$$

This is elongation of braid in one direction, not the overall elongation.

4.5 Quantification of Young's Modulus

Suppose F_1 and F_2 are forces per unit area which deform the braided fabric along the monofilaments such as,

$$f_1 = \frac{F_1 p}{n_1} \quad \text{and} \quad f_2 = \frac{F_2 t}{n_2}$$

For textile stent, component of the unit cell had only one monofilament. Therefore, $n_1 = n_2 = 1$. Putting $f_1 = F_1 p$ and $f_2 = F_2 t$ in equation 4.17, e_1 is formulated.

From Hook's law,

$$E_1 = \frac{F_1}{e_1}$$

For simplification, loading in the direction of F_1 was considered, so $F_2 = 0$. All monofilaments used for textile stents were similar, so $B = B_1 = B_2$. The monofilaments were assumed incompressible and inextensible, so μ , λ_1 and λ_2 tend to be infinity. Applying all these,

$$E_1 = \frac{x^3 (\cos^2 \theta_1) + y^3 (\cos^2 \theta_2)}{\frac{x^3 y^3}{12B} \sin^2 \theta_1 \cos^2 \theta_2} \quad (4.18)$$

Equation 4.18 gives Young's modulus of the textile stent by the strain energy model. To calculate Young's modulus, flexural rigidity of monofilaments is necessary. Flexural rigidity is calculated by the approach proposed by Ucar [13]. Ten monofilament samples were tested for flexural rigidity. All necessary calculations were performed with Maple[®] software. The values of Young's modulus calculated by strain energy (mechanical) model were compared to those obtained by strip testing (ASTM[®] D 5035-95) of textile stents (five samples) on Instron.

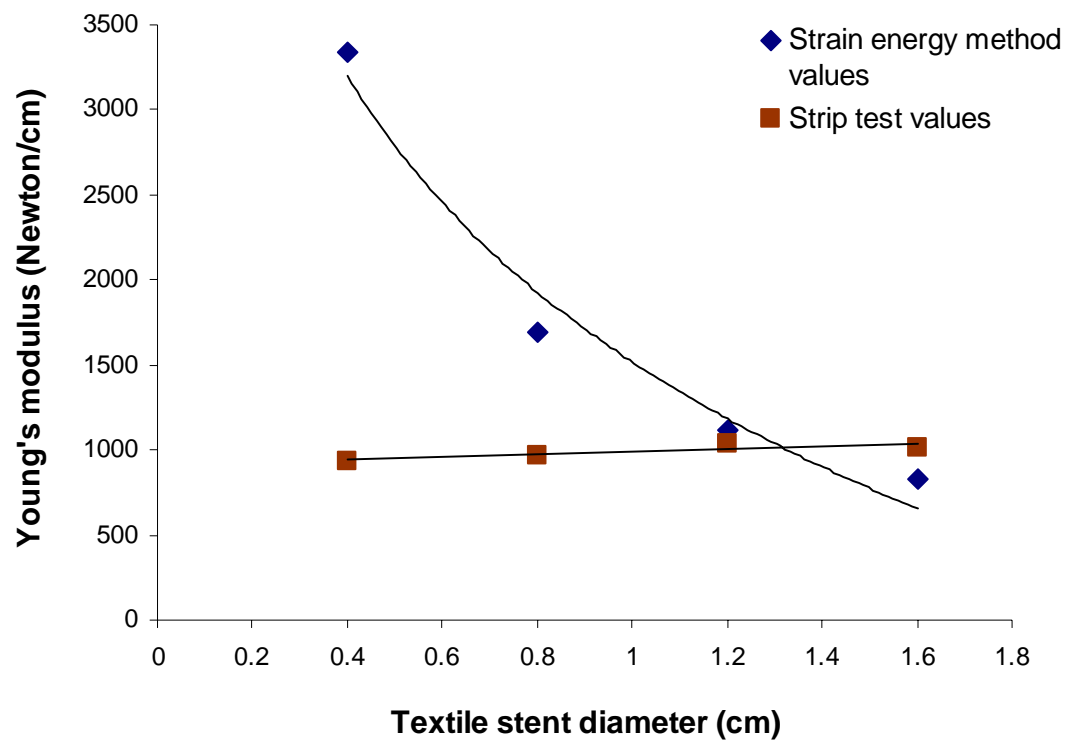


FIGURE 4.7: Comparison of Young's moduli.

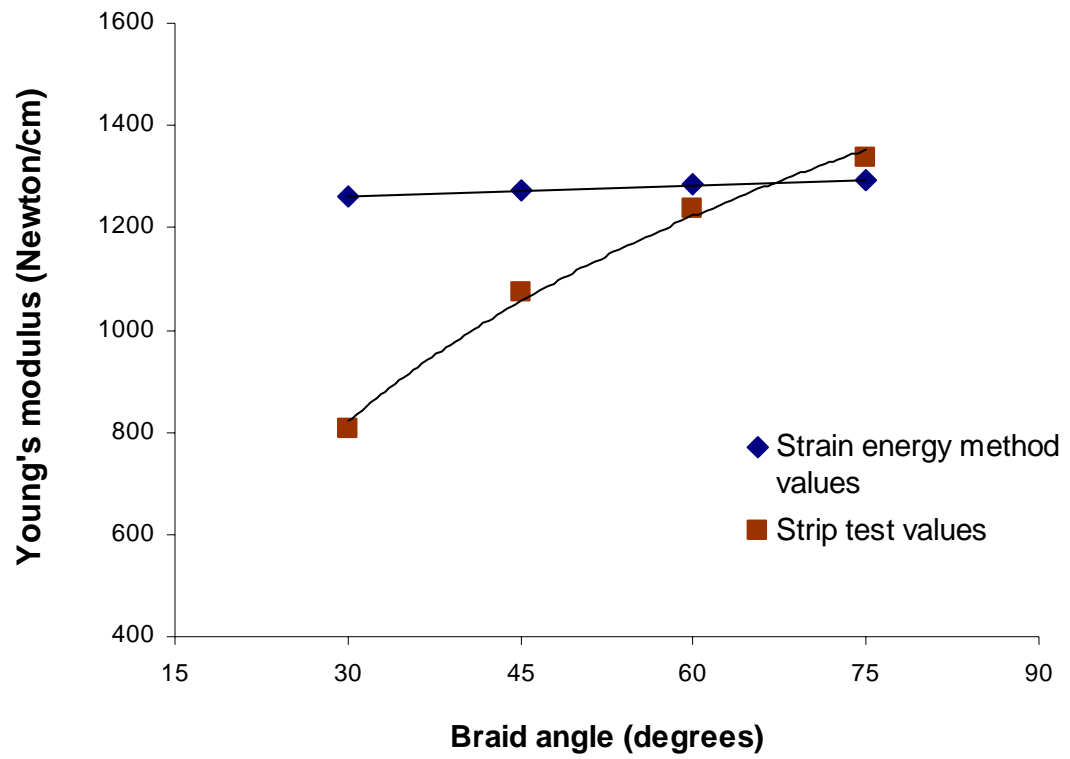


FIGURE 4.8: Comparison of Young's moduli (12 mm textile stents diameter).

Figure 4.7 shows comparison of values of Young's moduli. For calculations of strain energy model, the best samples out of the previously mentioned general linear model were selected. In Figure 4.7, 60° braid angle and 60 minutes heatset textile stents were compared for their Young's modulus. The comparison showed good correlation (adjusted $R^2 = 0.7955$). Agrawal and Clark [2] and Fallone *et al.* [3] also observed similar trend for Young's modulus values for metal stents with respect to diameter. Figure 4.8 shows comparison of Young's moduli for 12 mm textile stents having different braid angles. As strain energy formula and geometry of textile stents were dominated by radius, testing similar diameter textile stents resulted in similar Young's moduli even for different braid angles.

The strain energy (mechanical) model was based on energy stored in the system during deformation. Equation 4.18 determines Young's modulus of textile stents from geometry of the structure and flexural rigidity of monofilaments. It gave similar values for textile stents of different braid angles. Also, textile stents being compared were heatset, but there was no heatset factor in the strain energy model. It was assumed that monofilaments were rigidly joined at the point of their intersection. But after applying load, monofilaments slipped over each other. 'Braid inclination angle' was defined for diamond braid (1/1 intersection), but the approach used to define braid inclination angle may not apply for interlacings other than diamond braid and in that case equation 4.18 will not be able to quantify Young's modulus. The strain energy model could not formulate forces acting on individual monofilaments, so the compression parameter was not calculated. However, strain energy model was useful in understanding the limit of

elasticity of textile stents. Young's modulus values obtained by strain energy model would be helpful in understanding the *in vivo* performance of textile stents.

4.6 Load- Strain Curves of Textile Stents

Figures 4.9, 4.10, 4.11, and 4.12 show stress-strain curves for the textile stents. The initial region of the load-strain curve is defined as 'decrimping strain' (Figure 4.9), where monofilaments were just slipping within the structure. Once the decrimping was over, textile stent started elongating. Higher diameter textile stents showed higher decrimping strain. 'Decrimping strain' was a distinguishing characteristic of textile stents. Self-expanding textile stents need to be crimped while placing on the catheter. Higher decrimping strain will provide higher allowance for decrimping procedure.

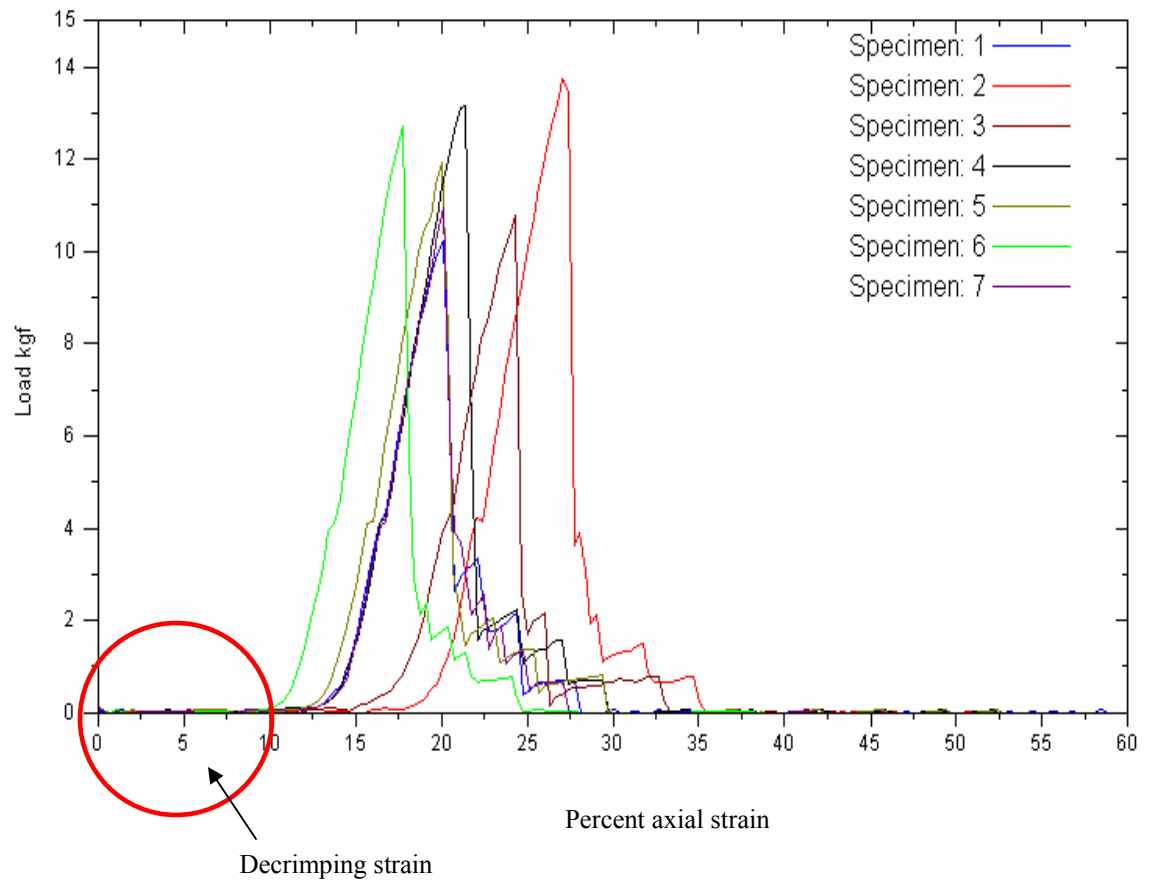


FIGURE 4.9: Load-strain curves (4 mm diameter textile stents).

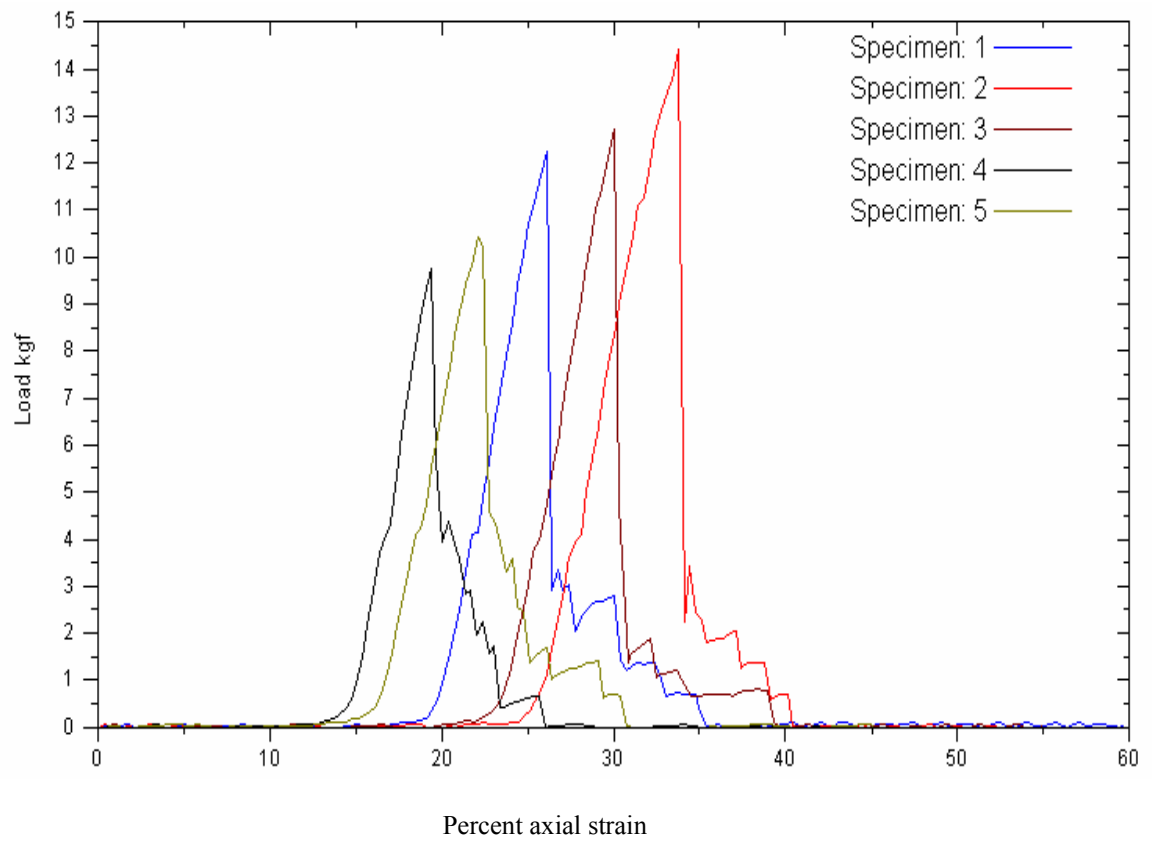


FIGURE 4.10: Load-strain curves (8 mm diameter textile stents).

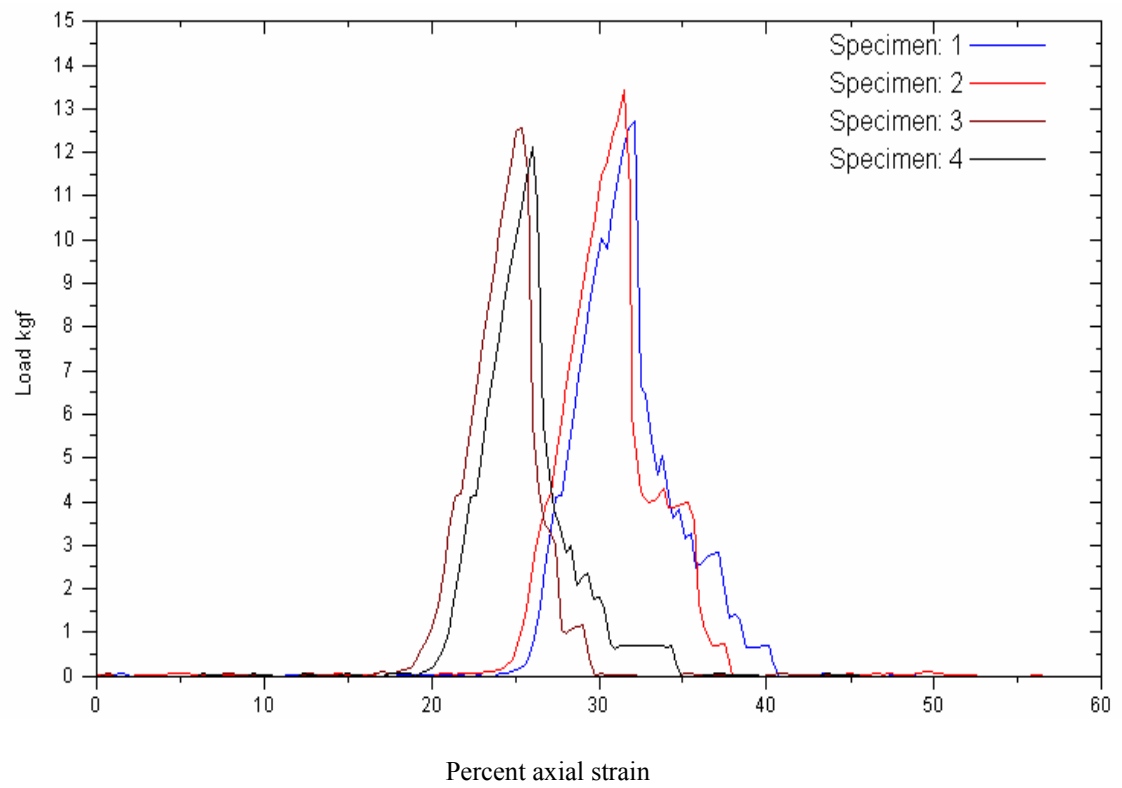


FIGURE 4.11::Load-strain curves (12 mm diameter textile stents).

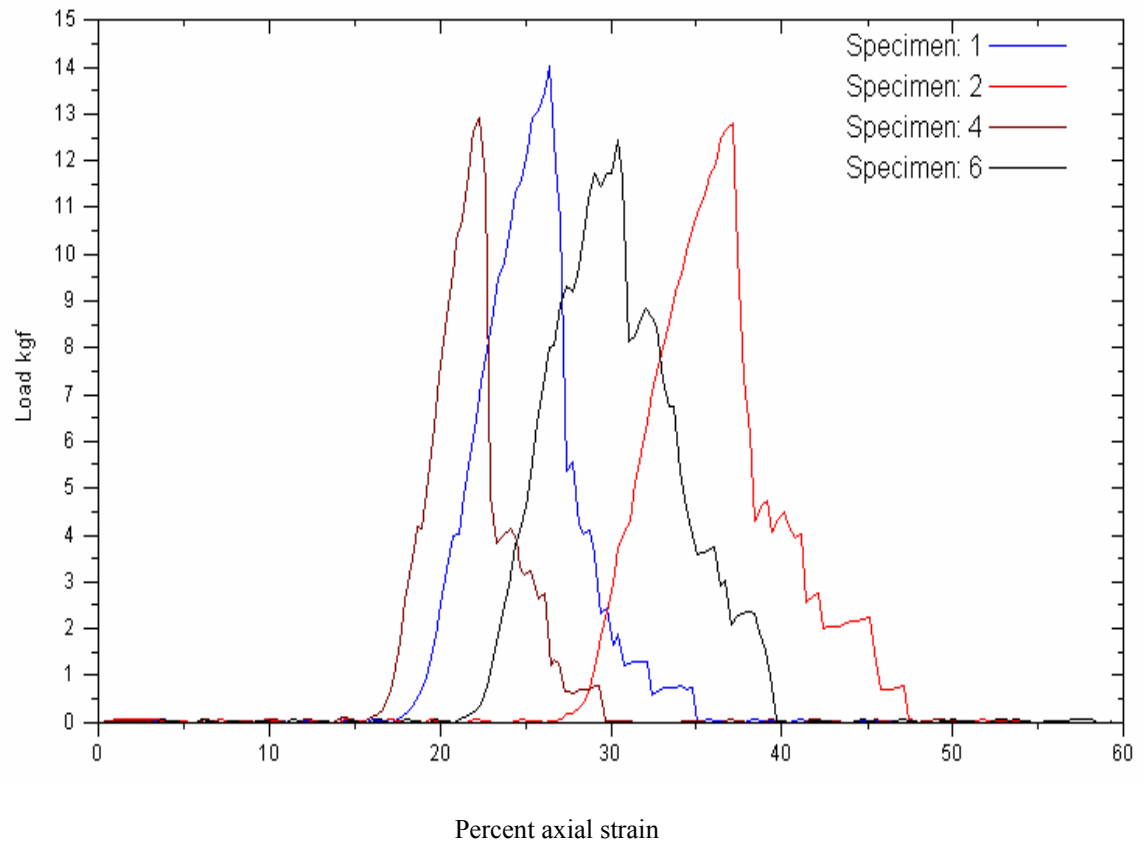


FIGURE 4.12: Load-strain curves (16 mm diameter textile stents).

4.7 Formulation of Compression Force

The strain energy (mechanical) model could not quantify compression related parameters. The objective of empirical model was to formulate, quantify, and predict compression force of textile stents. The empirical model was able to predict compression force of textile stents from any two of the known manufacturing variables. This can become an innovative approach to formulate, quantify, as well as predict a material property from the available pool of parent data. The parent compression force data used in the empirical model were obtained by the novel compression testing (Chapter 3) of textile stents on Instron. The empirical model is explained to quantify the compression force of textile stents from heatset time and textile stent radius.

In Figure 4.13, compression force of textile stents is plotted against heatset time. The equations for different stent radii were in the form of

$$y = mx + C.$$

$$y = 0.0278x + 17.307 \text{ (for 0.3 cm radius)}$$

$$y = 0.0267x + 7.6781 \text{ (for 0.6 cm radius)}$$

$$y = 0.0217x + 6.6646 \text{ (for 0.9 cm radius)}$$

$$y = 0.0144x + 4.8529 \text{ (for 1.27 cm radius)}$$

For all equations,

$$\text{Compression force} = m (\text{heatset time}) + C \quad (4.19)$$

To quantify compression force from equation 4.19, we must know m and C . The respective values of m and C for equations with different textile stent radii are shown in Table 4.2.

TABLE 4.2: Respective values of m and C .

	m	C
0.3	0.0278	17.307
0.6	0.0267	7.6781
0.9	0.0217	6.6646
1.27	0.0144	4.8529

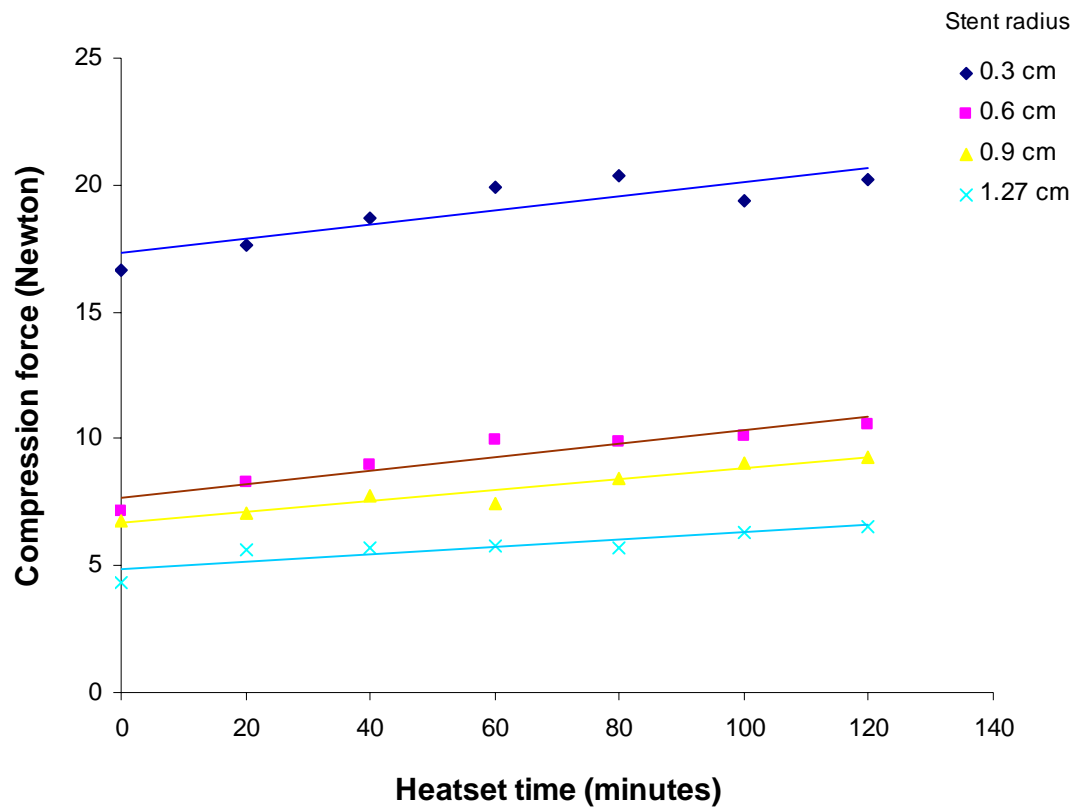


FIGURE 4.13: Trends for 60 degree braid angle textile stents.

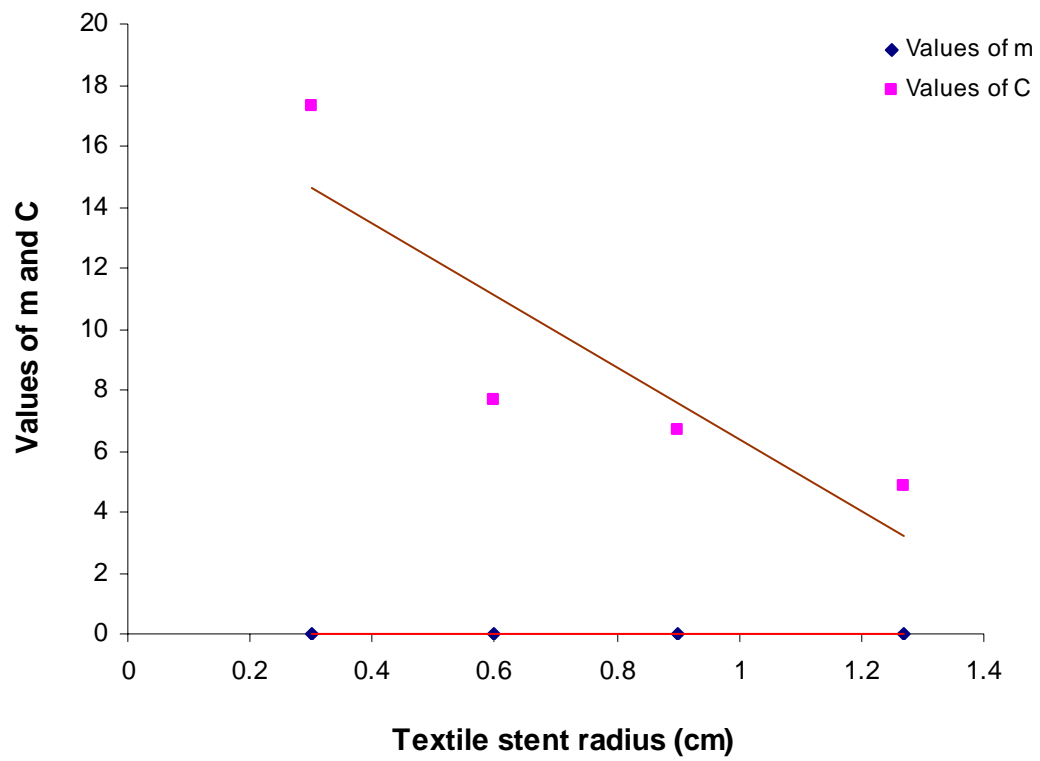


FIGURE 4.14: Trends for m and C .

To formulate m and C , their corresponding values were plotted against four different values of textile stent radii as shown in Figure 4.14.

$$y = -0.0142x + 0.0336 \text{ (for } m\text{)} \quad (4.20)$$

$$y = -11.72x + 18.121 \text{ (for } C\text{)} \quad (4.21)$$

For equations 4.20 and 4.21, y is m and C respectively and x is textile stent radius in cm.

After substituting,

$$m = [-0.0142(\text{radius})] + 0.0336 \quad (4.22)$$

$$C = [-11.72(\text{radius})] + 18.121 \quad (4.23)$$

Substituting m and C in equation 4.19,

Compression Force =

$$\{[(-0.0142 \times \text{radius}) + 0.0336] \times (\text{heatset time})\} + [(-11.72 \times \text{radius}) + 18.121] \quad (4.24)$$

Equation 4.24 formulates the compression force from textile stent manufacturing variables viz. textile stent radius and heatset time. Similar empirical formulae can be obtained from any two manufacturing variables based on the parent data.

4.8 Verification of the Empirical Model

Figure 4.15 shows verification of the empirical model. Values obtained by empirical formula showed closeness to those obtained by experimental ones (parent data). Regression analysis showed *adjusted R²* values: 0.7153 (for 0.3 cm radius), 0.8669 (for 0.6 cm radius), 0.9251 (for 0.9 cm radius), and 0.7198 (for 1.27 cm radius). Correlation between empirical and experimental values was strong for 0.6 cm and 0.9 cm and good for 0.3 cm and 1.27 cm textile stent radii. However, the empirical formula lacks in comprising more than two manufacturing variables. It had no specific material related

factor and was based on trends observed in the parent data. The value of R^2 (coefficient of determination) from the parent data affected accuracy of prediction of the compression force. In addition, parent data were very much necessary to initiate and verify the empirical model. However, the approach was helpful in quantifying and predicting the compression force from known manufacturing variables and parent data.

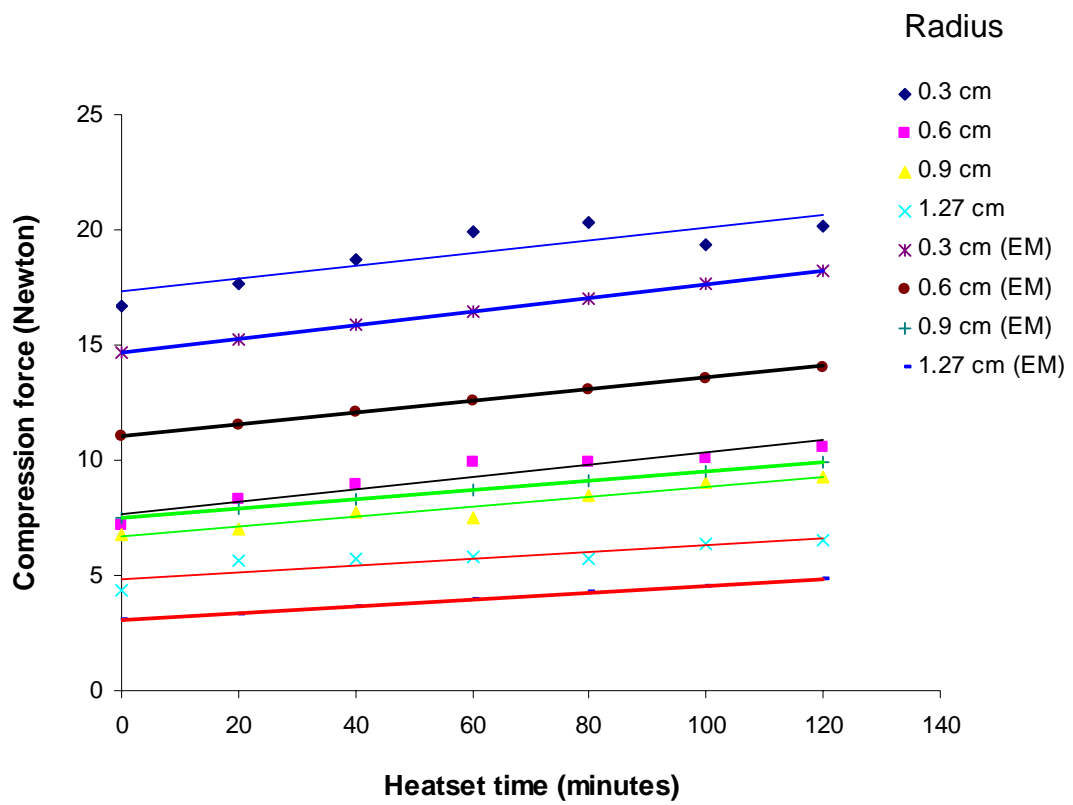


FIGURE 4.15: Verification of the empirical model (EM).

4.9 Literature Cited

1. Adanur, S., and Onal, L, “Analysis of a Novel 3D Hybrid Woven/Knitted Fabric Structure, Part II: Mechanical Model to Predict Modulus and Extension”, *Textile Res. J.*, **74**(10), 865-871 (2004).
2. Agrawal, M., and Clark, H., “Deformation Characteristics of a Bioabsorbable Intravascular Stent”, *Invest. Radiol.*, **27**(12), 1020-1024 (1992).
3. Fallone, B., Wallace, S., and Gianturco, C., “Elastic Characteristics of the Self-Expanding Metallic Stents”, *Invest. Radiol.*, **23**(5), 370-376 (1987).
4. Farsakh, G., Numayr, K., and Hamad, K., “A Micro-mechanical Model for Predicting the Compressive Strength of Fibrous Composite Materials”, *Comp. Sci. Technol.*, **57**, 1415-1422 (1997).
5. Hearle, J., and Shanahan, W., “An Energy Method for Calculations in Fabric Mechanics- Part I: Principles of the Method”, *J. Textile Inst.*, **69**(4), 81-91 (1978).
6. Heirigs, L., and Schwartz, P., “Properties of Small Diameter Aramid Double Braids: Fatigue Lifetime, Strength Retention after Abrasion, and Strength Modeling”, *Textile Res. J.*, **62**(7), 397-402 (1992).
7. Jong, S., and Postle, R., “A General Energy Analysis of Fabric Mechanics Using Optimal Control Theory”, *Textile Res. J.*, 127-135 (1978).
8. Leaf, G., and Kandil, K., “The Initial Load-extension Behavior of Plain Woven Fabrics”, *J. Textile Inst.*, **71**(1), 1-7 (1980).
9. Sagar, T., Potluri, P., and Hearle, J., “Mesoscale Modeling of Interlaced Fiber Assemblies Using Energy Method”, *Comp. Mater. Sci.*, **28**, 49-62 (2003).

10. Shanahan, W., and Hearle, J., “An Energy Method for Calculations in Fabric Mechanics- Part II: Examples of Application of the Method to Woven Fabrics”, *J. Textile Inst.*, **69**(4), 92-100 (1978).
11. Sinoimeri, A., and Drean, J., “Mechanical Behavior of the Plain Weave Structure Using Energy Methods: Fabric Uniaxial Extension”, *Textile Res. J.*, **67**(5), 370-378 (1997).
12. Timoshenko, S., and Gere, J., *Mechanics of Materials*, D. Van Nostrand Company, New York, 1972.
13. Ucar, N., “Prediction of Curling Distance of Dry-relaxed Cotton Plain Knitted Fabrics- Part I: Theoretical Analysis of Moments on the Loop that Force the Fabric to Curl”, *J. Textile Eng.*, **46**(4), 109-117 (2000).
14. Zang, Q., Beale, D., Adanur, S., Broughton, R., and Walker, R., “Structural Analysis of a Two-dimensional Braided Fabric”, *J. Textile Inst.*, **88**(1), 41-52 (1997).

CHAPTER 5

BLOOD FLOW CHARACTERIZATION OF POLYMERIC TEXTILE STENTS

5.1 Rheology of Blood

Human body has 75×10^{12} cells, 206 named bones and approximately 78 milligrams of blood per kilogram of its weight [8, 24]. Blood, regenerative part of it, is a mixed suspension of colloidal proteins. Blood is Newtonian at sufficiently high shear rates. Its viscosity increases markedly at low shear rates; however, its flow behavior is strongly influenced by the volume percentage of red blood cells (hematocrit) and by chemical composition. Fibrinogen and its effect of making red blood cells (RBCs) stick together are primarily responsible for the non-Newtonian behavior of blood at low shear rates. Although, blood is generally found to be non-Newtonian, it does not exhibit viscoelastic behavior [14]. Blood flow in arteries, veins as well as smaller vessels is Newtonian near the wall. However, as one gets closer to the center of the vessel, shear rate approaches to zero and blood exhibits non-Newtonian behavior [6]. The typical Reynolds number range for blood flow in human body varies from 1 in small arterioles to approximately 4000 in the largest artery (aorta) [12]. Reynolds numbers are below 2100 except in the aorta, hence laminar flow is normally assumed in the analysis of blood flow [14].

5.2 Nature of the Blood Flow

Cyclic nature of heart creates pulsatile flows in arteries. Heart empties and fills with blood in alternating cycles called systole and diastole. Blood is pumped out of the heart during systole. Heart rests during diastole where no blood is pumped. Heart pumps blood intermittently, going to zero when the aortic valve is closed. Aorta acts as a reservoir for the high pressure blood during systole and diastole. The nature of pulsatile blood flow is three dimensional. The flow is zero or even reversed in the external carotid, brachial, and femoral arteries [10]. Density of blood is 1050 kg/m^3 . Blood is considered to be incompressible [27].

5.3 Characterization of Blood Flow

The structure and function of the artery wall are modified by the local flow conditions, possibly through an interaction between the flow and artery depending on the level of wall shear stress. Long term hypertension produces medial thickening in arteries. The primary locations of atheroma are carotid artery sinus, coronary arteries, abdominal aorta, and superficial femoral arteries. In each of these arteries there are localized sites where the mean wall shear stress is very low and oscillates between positive and negative directions during the cardiac cycle. Most intimal thickening is found where the average wall shear stress is less than 10 dynes/cm^2 [25]. Arteries of several species including human tend to adjust their diameters to wall shear stress of $10\text{-}20 \text{ dynes/cm}^2$. Wherever the local mean wall shear stress exceeds approximately 10 dynes/cm^2 , the artery tends to be spared from intimal thickening [13]. In addition, velocity distribution, separation phenomena, and turbulence play an important role towards the flow behavior of blood

[26]. The forces due to blood flow in larger arteries not only depend on time, position, and vessel geometry but also vary from species to species [1].

Stents reduce the mass and momentum transport of blood from the parent artery and alter blood flow patterns [19]. Frank *et al.* [7] found that stent strut spacing and thickness significantly affect the blood flow behavior. Thiriet *et al.* [23] observed that the higher the Reynolds number, the greater the shear rate at the inner wall. LaDisa *et al.* [11] observed that reducing the stent strut thickness caused regions subjected to low wall shear stress to decrease by ~87 % and increasing the number of stent struts produced 2.75-fold increase. Other *in vitro* blood flow and stent models [26, 2, 21, 3] showed that hemodynamic disturbances created by stents trigger thrombogenic events, and affect long term patency of artery lumens. *In vitro* blood flow and stent models observed in the literature used different diameter solid rods [22], silicone rubber [18], and acrylic rings [17] to develop the effect of plaque. These researchers considered the plaque to be radially uniform. However, plaque is not longitudinally (Figure 5.1) or radially (Figure 5.2) uniform. An interaction of stent geometry and blood flow plays a critical role towards the gradual development of post-implantation plaque and restenosis.

5.4 Objective

Even after treatment by stents restenosis may be inevitable. The objective of this part of the study is to analyze the blood flow characterization of textile stents which comprise textile stent entrance and exit effects and interactions between textile stent geometry and blood flow in the textile stented artery segment.



FIGURE 5.1: Longitudinally irregular plaque.

Source: www.kaweahdelta.org, access date: May 31, 2005.

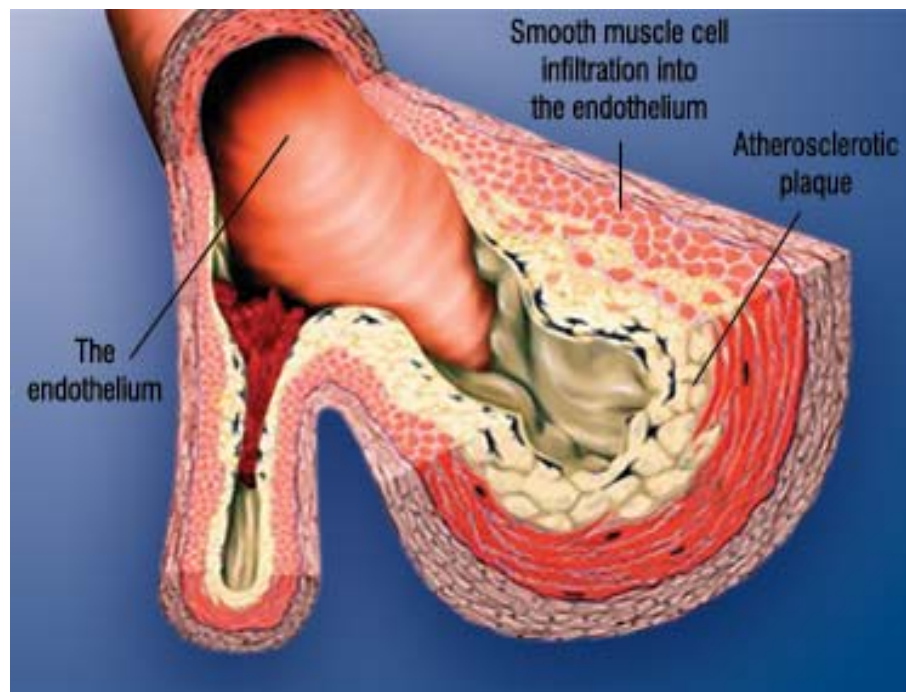


FIGURE 5.2: Radially irregular plaque.

Source: www.lef.org, access date: May 31, 2005.

5.5 Textile Stent Entrance and Exit Effects

The obstruction to the blood flow produced by textile stent monofilaments is similar to the flow situations known as ‘flow over forward and flow over backward facing effects’. The forward and backward facing flow effects related to textile stents are defined as textile stent entrance and textile stent exit effects.

The monofilament intersections act as stagnation points for the blood flow. The pressure due to blood flow is maximum at these stagnation points and gradually decreases as blood flows over the top semicircular part of monofilaments intersection. However, as blood flows over the other side of the top semicircle, it experiences an adverse pressure gradient, which separates it from the surface, creating turbulence. In case of textile stent entrance effect (Figure 5.3), monofilaments intersection inhibits the forward movement of blood adjacent to the monofilaments, creating a separation zone. In case of textile stent exit effects (Figure 5.4), momentum of blood flowing over monofilaments intersection carries blood past corner of monofilaments, creating a separation zone. The separation zones associated with textile stent exit effects are typically smaller than those with entrance effects. To analyze textile stent entrance and exit effects, two-dimensional module of ANSYS® Flotran was used. ANSYS® is a simulation driven, finite element based design development software.

ASSUMPTIONS

- Blood is incompressible and has constant properties and temperature. Its density is 1050 kg/m^3 and viscosity is 4 cP. Blood flow is laminar and its behavior is non-Newtonian.

- Blood velocity is uniform at the inlet and velocity in the direction normal to the inlet (Y- direction) is zero.
- The rigid tube represents an artery and bumps inside the tube represent textile stent monofilament intersections after *in vivo* cell growth. Several monofilament bumps radially placed at a specific distance create similar obstructions as that of textile stent inside an artery. Displacement at all ends of the artery and monofilament bumps is zero.
- Blood flow variations are not deforming textile stents. Artery diameter is uniform. Textile stents follow geometry mentioned in the mechanical model (Chapter 4). Braid angle was 60° for all textile stent combinations; hence distance between bumps remained same.
- Textile stent geometry and blood flow were represented by monofilament diameters (denier) and blood input velocity, respectively.

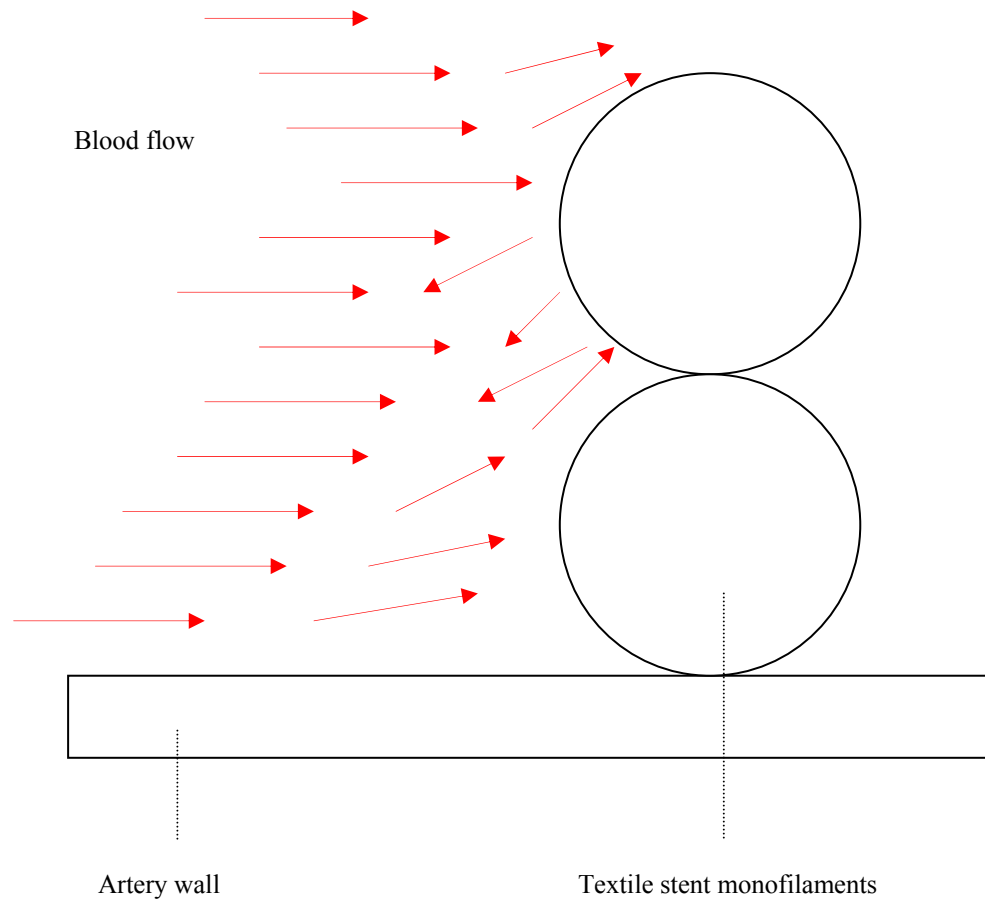


FIGURE 5.3: Textile stent entrance effect.

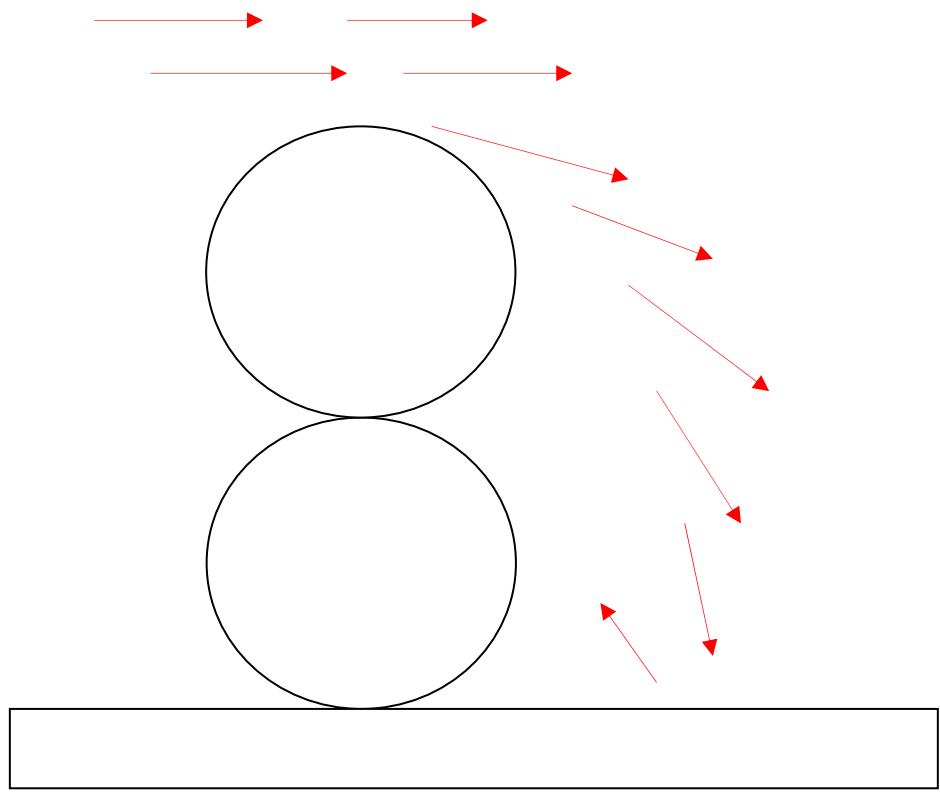
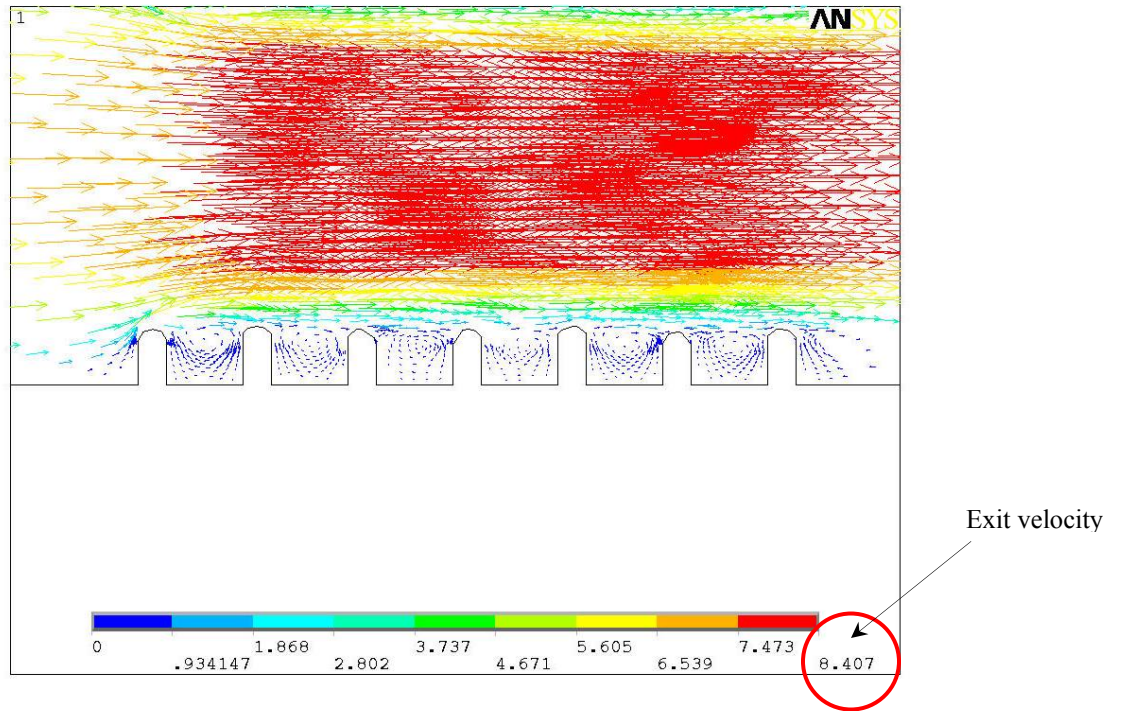
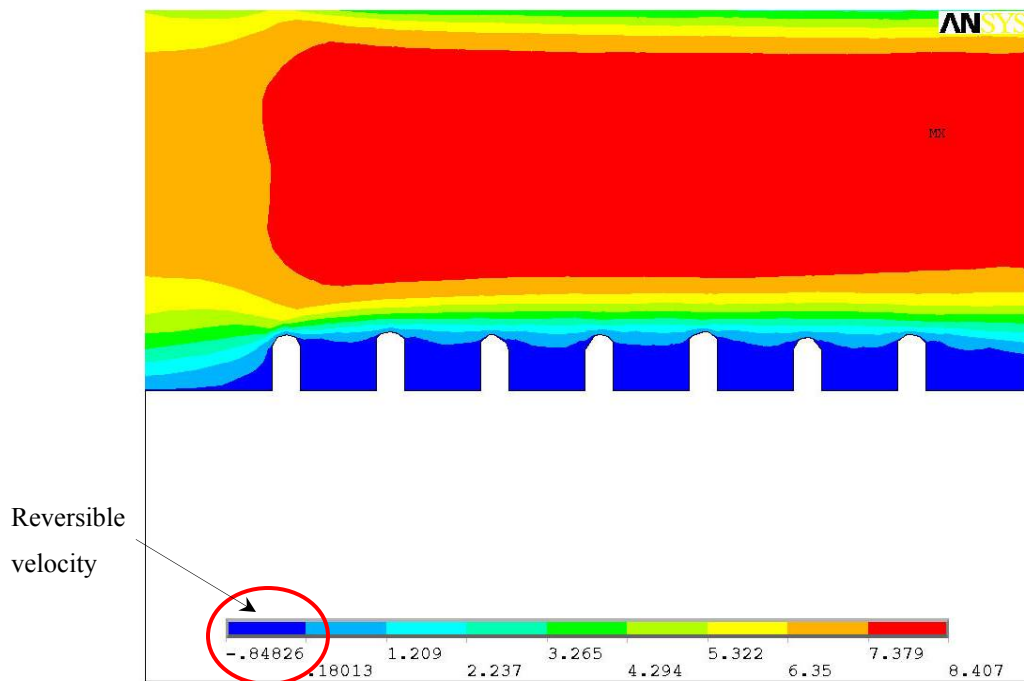


FIGURE 5.4: Textile stent exit effect.

For all ANSYS® results, the direction of blood flow was from left to right. Figure 5.5A shows textile stent entrance and exit effects. Due to sequential arrangement of monofilament bumps, entrance and exit effects of each interacted with the next or previous ones. Interaction of entrance and exit effects developed flow vortices and separation zones. Blood velocity was found to be negative in the region between monofilament bumps. Velocity contours (Figure 5.5B) also show negative and reversible velocities. The reversible flow of blood between monofilament bumps increased the residing time of blood in the textile stented artery segment. ‘Residing time’ is defined as the time taken by blood particles to travel specific axial distance of the textile stented artery segment in the direction of the blood input velocity. ANSYS® results also quantified exit velocity. ‘Exit velocity’ is defined as the maximum velocity of blood after the textile stented artery segment determined by ANSYS® Flotran analysis. Exit velocity is shown in Figure 5.5A.



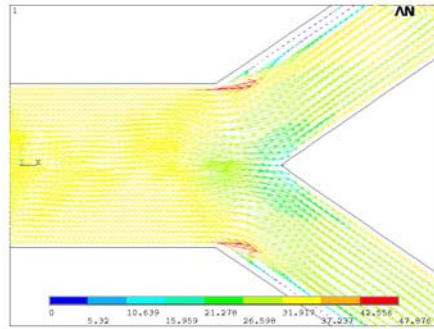
A: Velocity vectors.



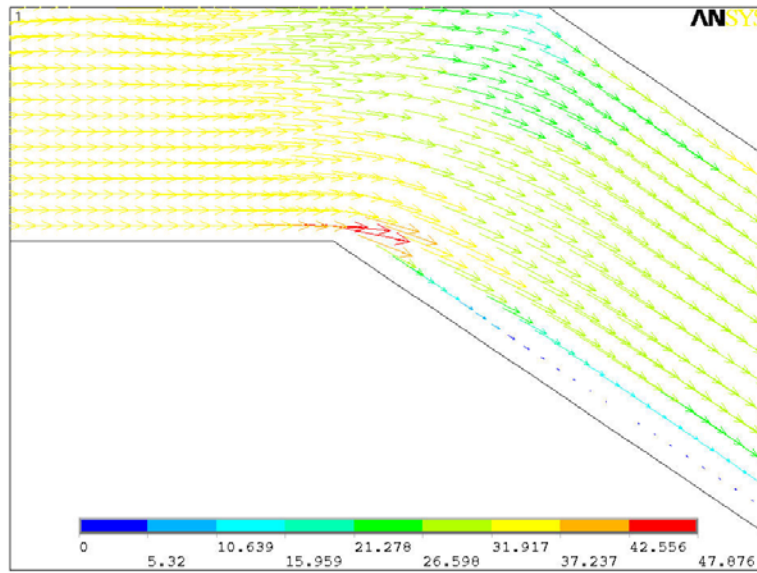
B: Velocity contours.

FIGURE 5.5: Textile stent entrance and exit effects (0.4 cm artery diameter, 600 denier, 6 cm/s).

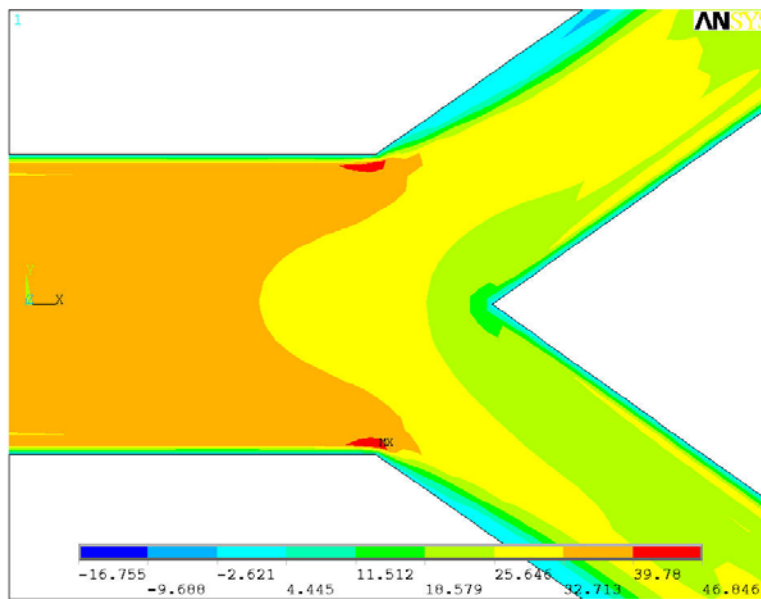
Geometrical model of abdominal aortic bifurcation was also developed and solved in ANSYS[®] to analyze the bifurcated textile stent entrance and exit effects. Figure 5.6 shows blood flow in the human abdominal aortic bifurcation, which is symmetrical. The daughter tubes (left and right common iliac arteries) have the same cross sectional area with an area ratio (ratio of sum of cross sectional areas of daughter tubes to the cross sectional area of the parent tube) of 0.8. The angle of bifurcation is 70° [23]. Blood flow deviates at the bifurcated edges of the abdominal aorta creating reversible flows, even without implantation of a stent. Sections of textile stented aortic bifurcation are shown in Figures 5.7 and 5.8. Similar textile stent entrance and exit effects were observed (Figures 5.7A and 5.7B) for bifurcated textile stents. Reversible velocities and flow vortices were observed within the monofilament bumps. Joint of aortic bifurcation (Figure 5.8) also showed negative velocities between monofilament bumps.



A: Human abdominal aortic bifurcation.

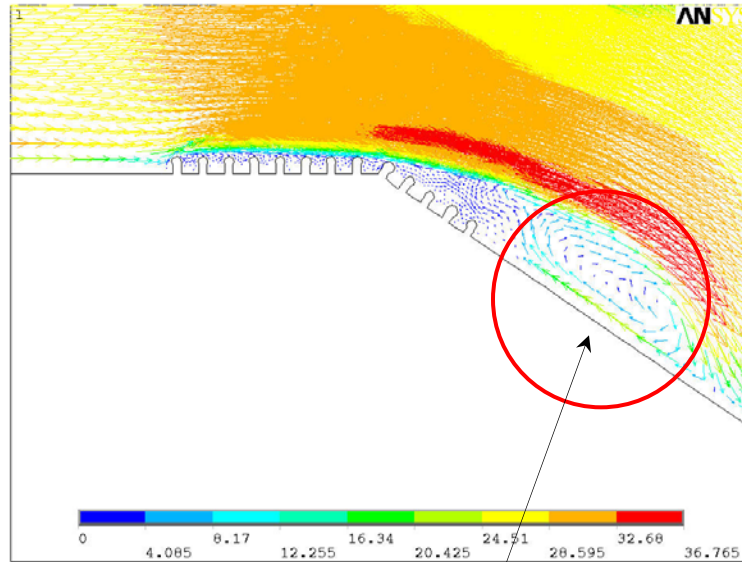
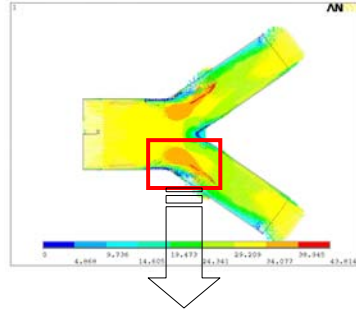


B: Velocity vectors.



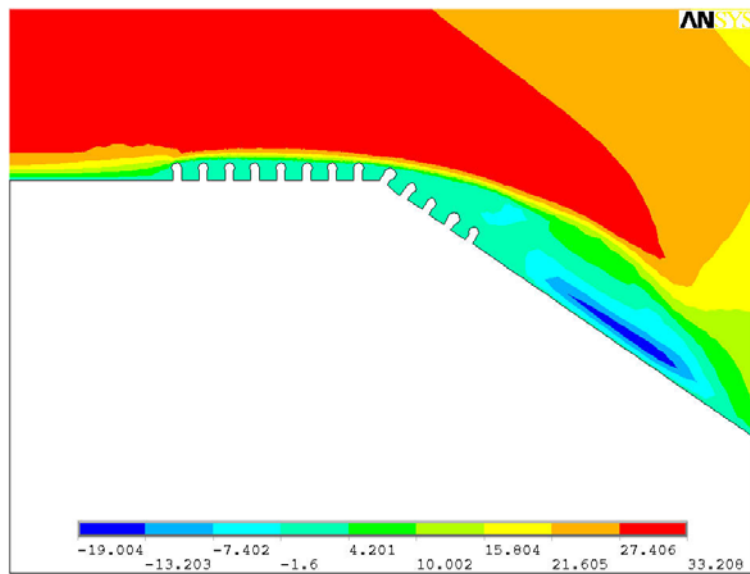
C: Velocity contours.

FIGURE 5.6: Blood flow in the human abdominal aortic bifurcation (blood input velocity= 38 cm/s).



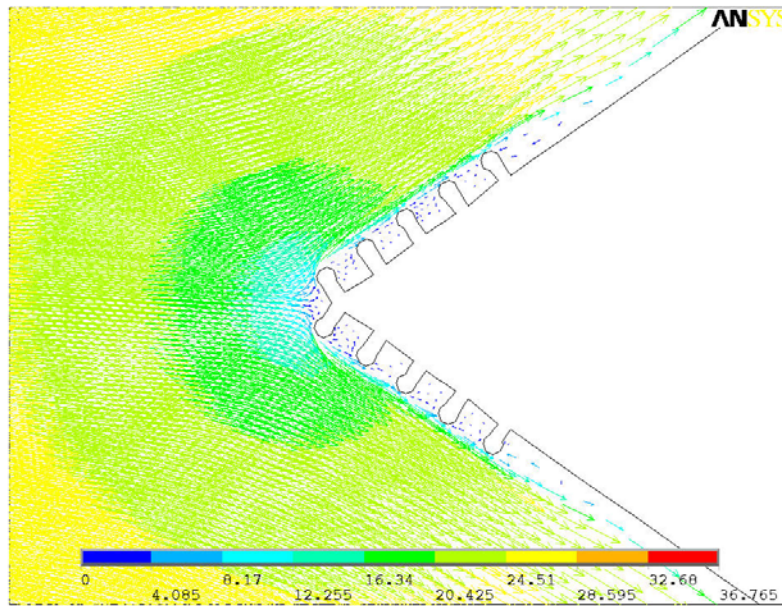
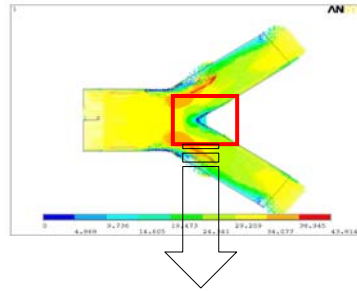
A: Velocity vectors.

Blood flow vortices.

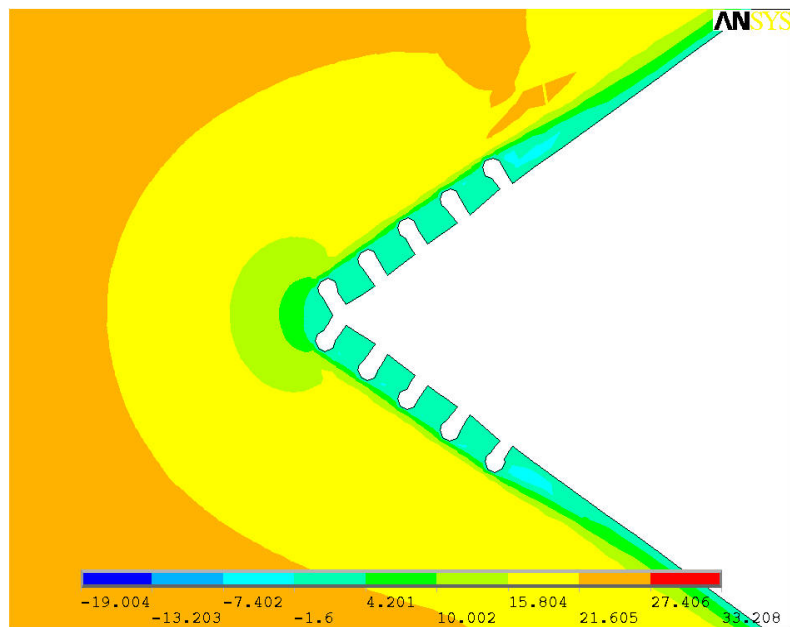


B: Velocity contours.

FIGURE 5.7: Bifurcated textile stent entrance and exit effects (blood input velocity= 28 cm/s).



A: Velocity vectors.

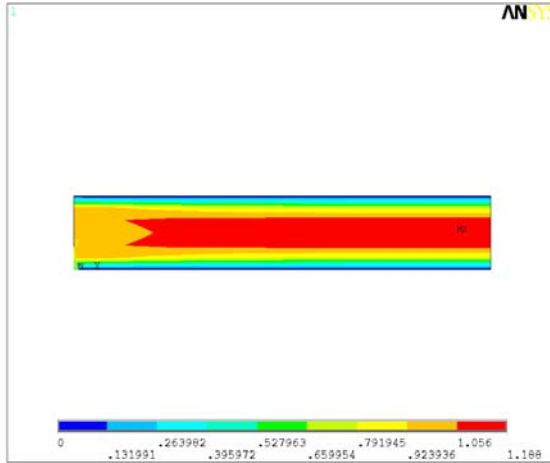


B: Velocity contours.

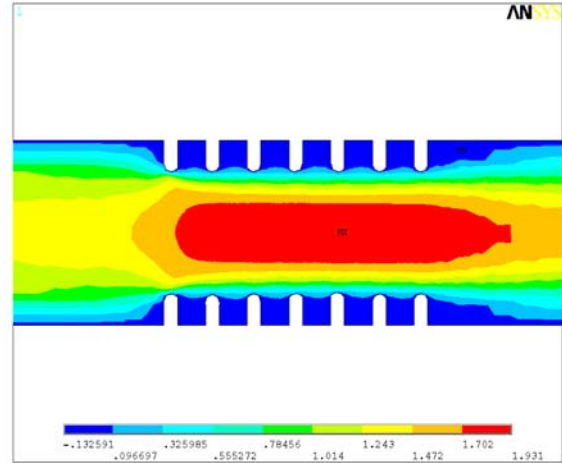
FIGURE 5.8: Joint of textile stented abdominal aortic bifurcation (blood input velocity= 28cm/s).

5.6 Variation of Textile Stent Entrance and Exit Effects

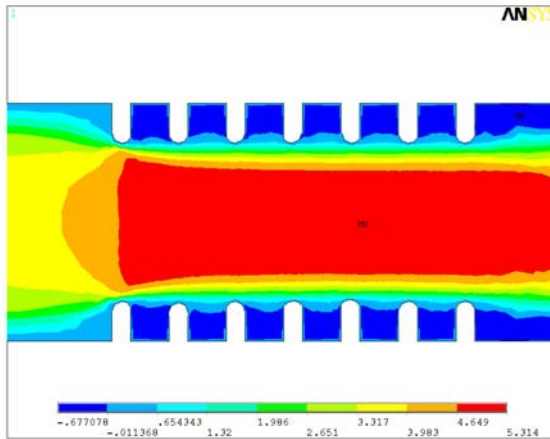
Variation of textile stent entrance and exit effects was determined by varying blood input velocity in ANSYS®. Figure 5.9 shows variation of textile stent entrance and exit effects. Variation was represented by the reduction in ‘minimum velocity’ (Figure 5.9D) in the textile stented artery segment. For 1 cm/s blood input velocity, minimum velocity between the monofilament bumps was -0.1325 cm/s. For 3 cm/s and 6 cm/s blood input velocities, minimum velocities were -0.6770 and -1.627 cm/s, respectively. It was clear that at higher blood input velocities, minimum velocities were also higher, but on negative side. These minimum velocities caused blood flow disturbances and vortices in the textile stented artery segment and were responsible for the severity of textile stent entrance and exit effects. At higher blood input velocity, textile stent entrance and exit effects were severe. Figure 5.9D shows the whole monofilament bumps region with negative velocity. Minimum velocity was observed at the edges of textile stents. Similar variation was observed for different artery diameters and combinations of monofilament deniers and blood input velocities.



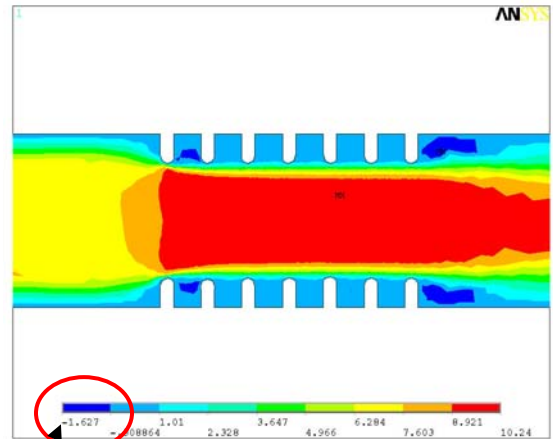
A: Artery without stent
(blood input velocity= 1 cm/s).



B: Blood input velocity = 1 cm/s.



C: Blood input velocity = 3 cm/s.

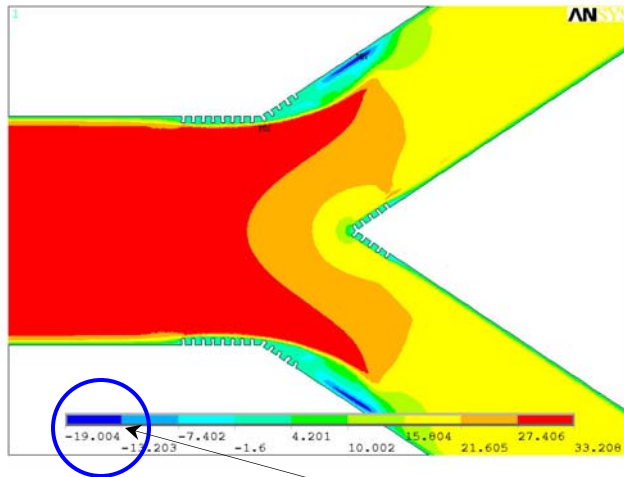


D: Blood input velocity = 6 cm/s.

Minimum velocity

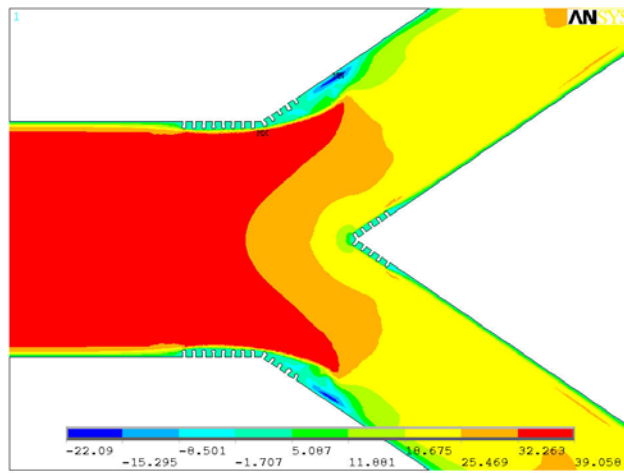
FIGURE 5.9: Variation of textile stent entrance and exit effects (0.4 cm artery diameter, 1100 denier).

Deviation to the direction of blood flow from parent artery to the daughter tubes and introduction of monofilament bumps developed minimum velocities and reversible flows at the ends of bifurcated textile stent. Variation of bifurcated textile stent entrance and exit effects is shown in Figure 5.10. The bifurcated textile stent end region is shown as critical zone in Figure 5.10C. Minimum velocity was reduced as the blood input velocity was increased, making the bifurcated textile stent entrance and exit effects more severe.

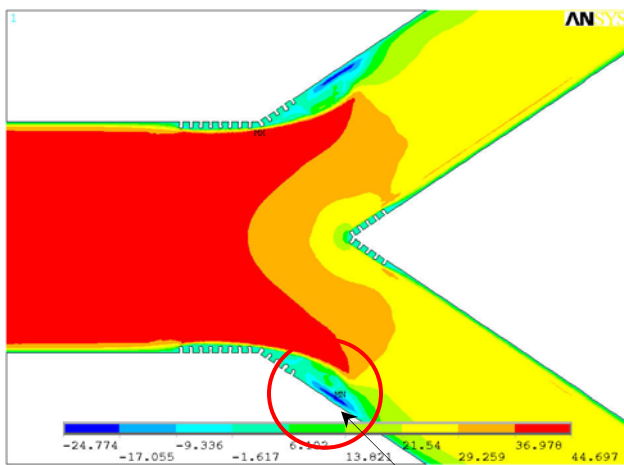


A (blood input velocity= 28 cm/s)

Minimum velocity



B (blood input velocity= 33 cm/s)



C (blood input velocity= 38 cm/s).

Critical zone

FIGURE 5.10: Variation of bifurcated textile stent entrance and exit effects (1100 denier).

5.7 General Linear Model

Textile stent geometry and blood flow were represented by monofilament diameter (denier) and blood input velocity, respectively. A general linear model was developed with five artery diameters (0.4, 0.8, 1.2, 1.6, and 2.5 cm), three monofilament sizes (150, 600, and 1100 denier) and three respective blood input velocities.

$$\text{Total number of combinations} = (\text{level})^{\text{factors}} = 5 \times 3^2 = 45.$$

Lengths of all textile stents were in the range of 6 to 7 cm. Blood input velocities for specific artery diameter were determined from the range of Reynolds number and blood velocities given in the literature [8, 12, 14]. For 0.4, 0.8 and 1.2 cm arteries, Reynolds number should be below 2100. For 1.6 and 2.5 cm arteries Reynolds number should be around 3000 but less than 4000. Blood input velocities viz. 1, 3, and 6 cm/s for 0.4 and 0.8 cm arteries, 8, 10, and 12 cm/s for 1.2 cm artery, 12, 16, and 20 cm/s for 1.6 cm artery, and 28, 33, and 38 cm/s for 2.5 cm artery were selected. All combinations of general linear model were solved for exit velocity using ANSYS® Flotran. Exit velocity was the response variable for statistical analysis.

5.8 Results and Discussion

Exit velocity was taken as the measure of textile stent entrance and exit effects. Figures 5.11- 5.15 show three-dimensional graphs of exit velocity. Peak exit velocities were observed for the combination of highest blood input velocity and thickest monofilament diameter. For all selected artery diameters, increase in exit velocity was observed with an increase in monofilament denier at the same blood input velocity. This was obvious as thicker monofilaments created stronger obstruction to the blood flow,

because of which exit velocity was maximum. It was observed that, larger artery diameters compensated the flow variations and disturbances easily. The regions of flow variations and disturbances caused by the textile stents were less significant for larger diameter arteries.

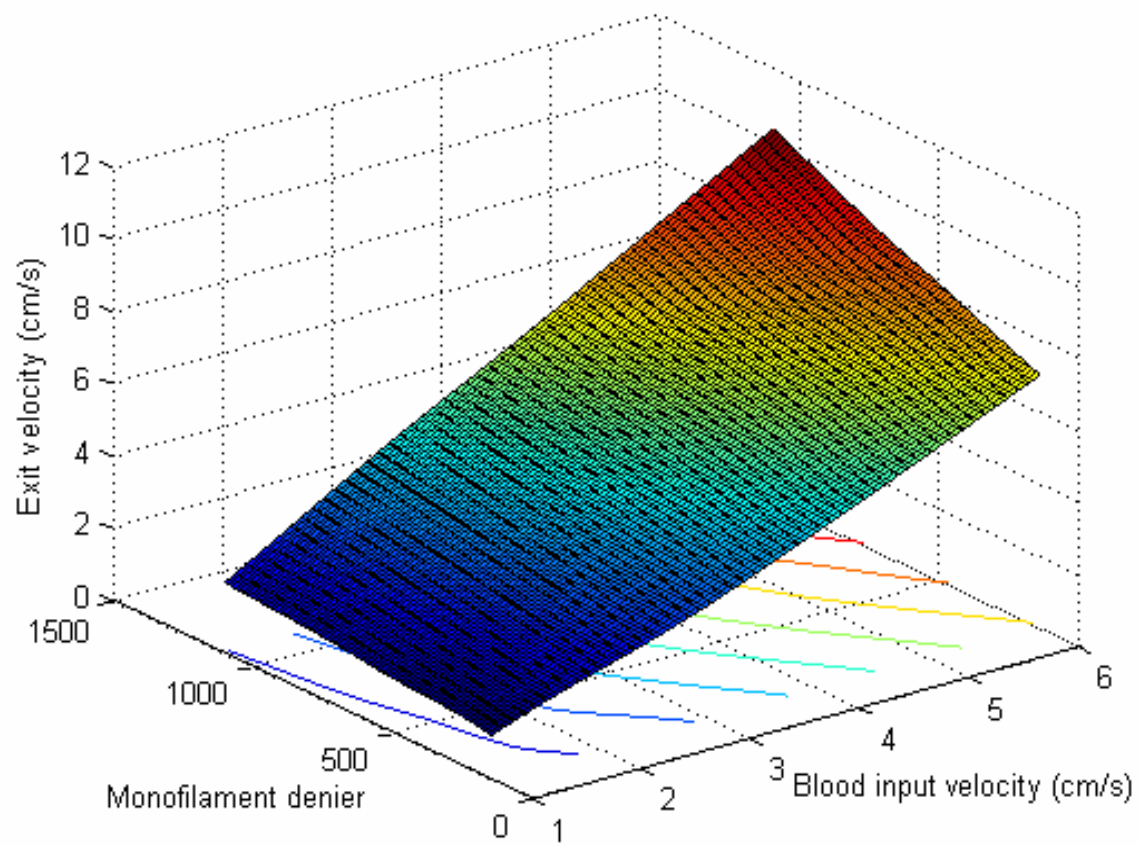


FIGURE 5.11: Three-dimensional graph of exit velocity for artery of 0.4 cm diameter.

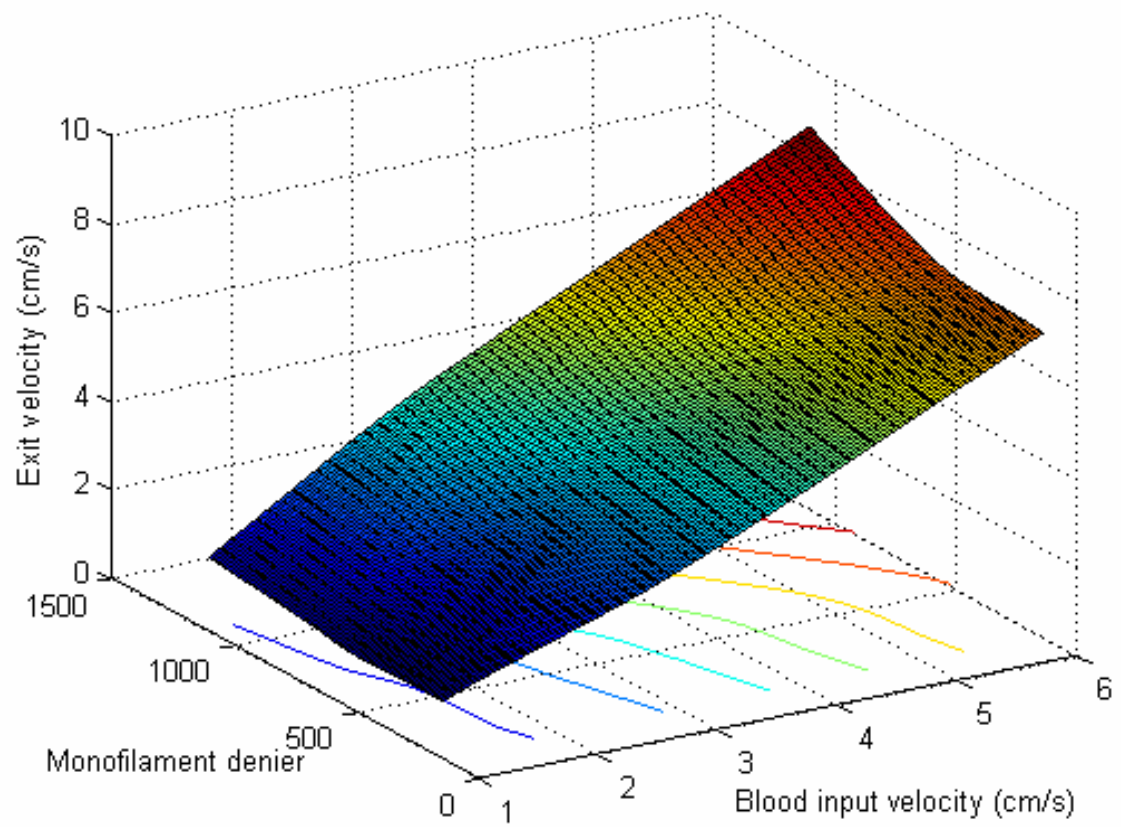


FIGURE 5.12: Three-dimensional graph of exit velocity for artery of 0.8 cm diameter.

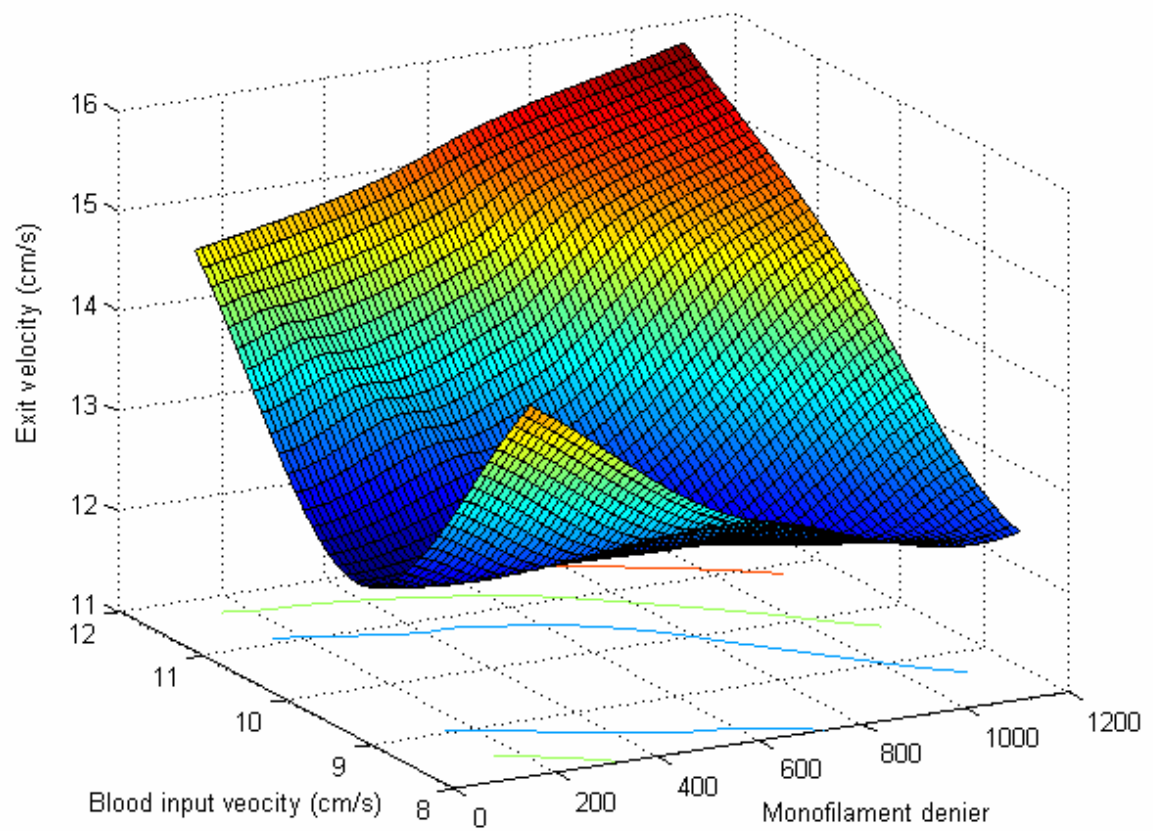


FIGURE 5.13: Three-dimensional graph of exit velocity for artery of 1.2 cm diameter.

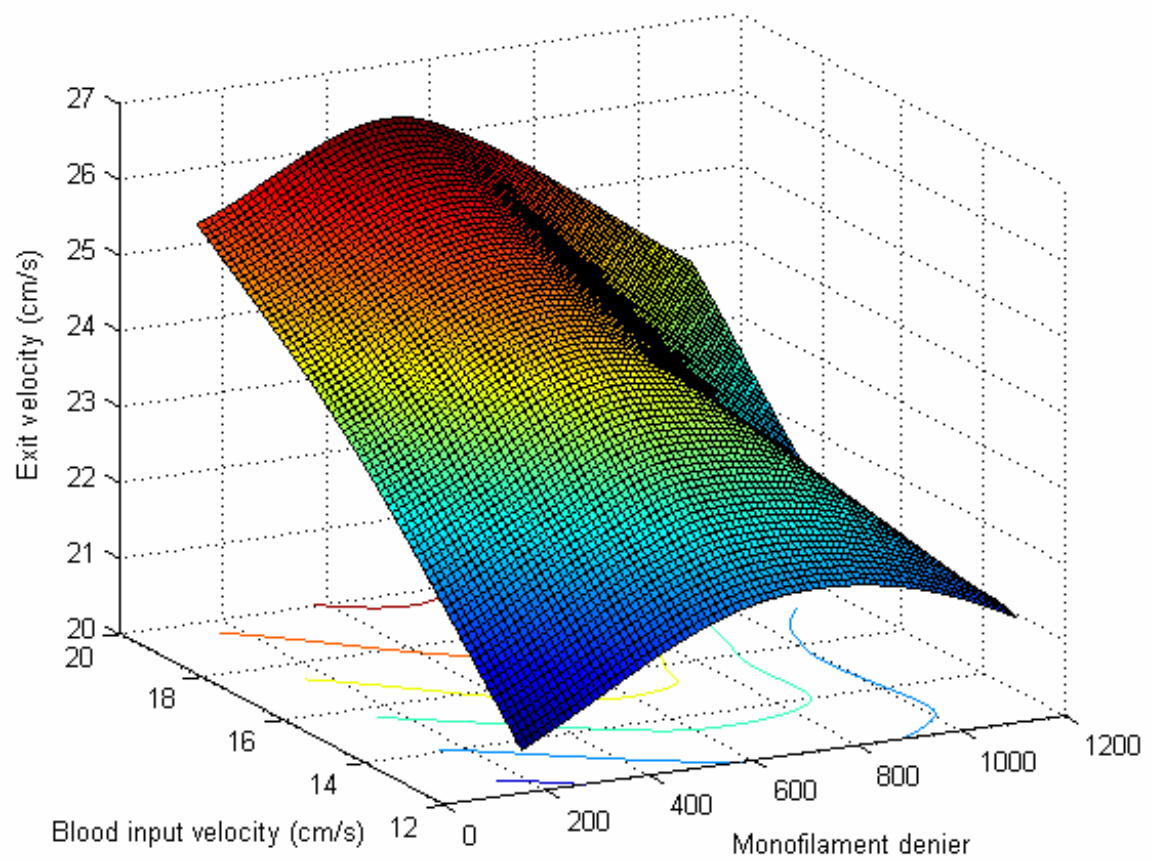


FIGURE 5.14: Three-dimensional graph of exit velocity artery of 1.6 cm diameter.

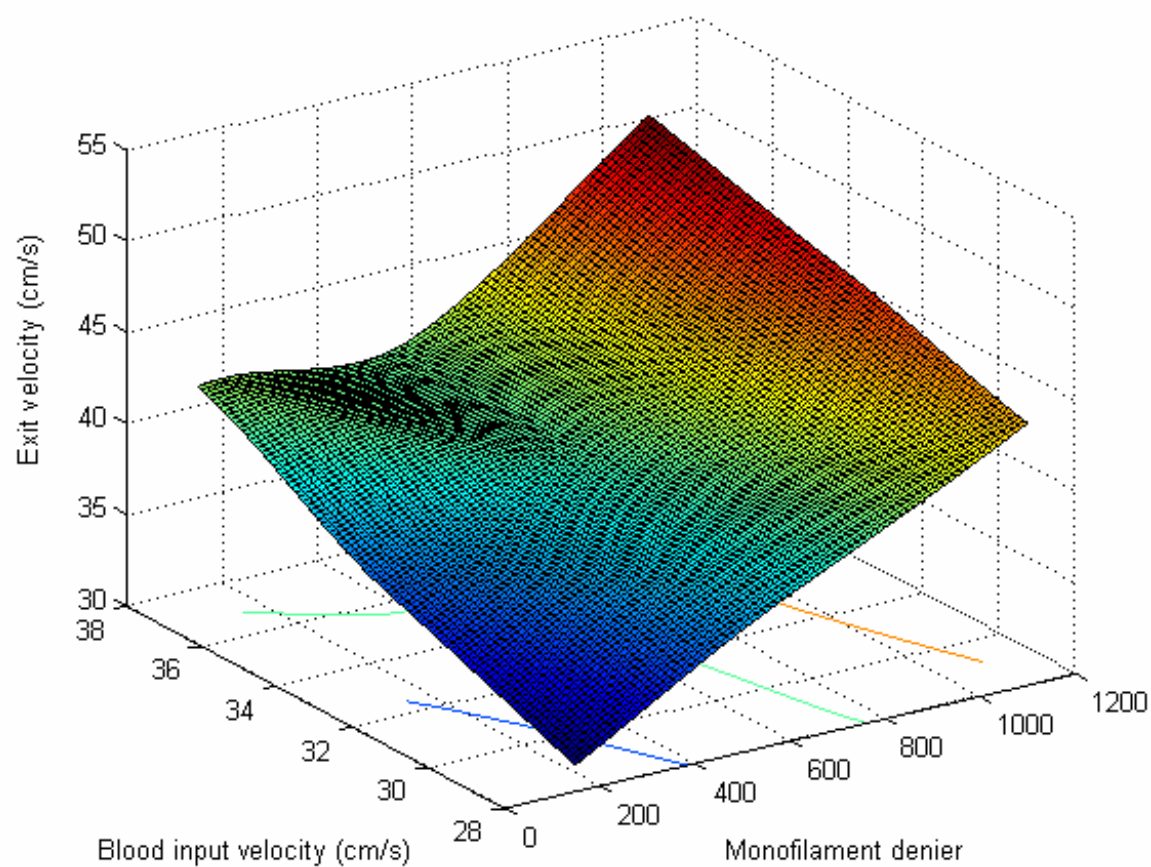


FIGURE 5.15: Three-dimensional graph of exit velocity for artery of 2.5 cm diameter.

Statistical analysis was used to support the ANSYS[®] results. Two-factor ANOVA (analysis of variance) was applied. The response variable was exit velocity and monofilament denier and blood input velocity were factors to be analyzed. Tables 5.1-5.5 show two-factor ANOVA results obtained using Microsoft[®] EXCEL. Two-Factor ANOVA showed statistically significant effect ($p = 0.00051$ for 0.4 cm diameter, $p = 0.00013$ for 0.8 cm diameter, $p = 0.01716$ for 1.2 cm diameter, $p = 0.01240$ for 1.6 cm diameter, $p = 0.0309$ for 2.5 cm diameter) of blood input velocity on exit velocity for all artery diameters. Monofilament denier showed statistically significant effect ($p = 0.04395$ - 0.4 cm, $p = 0.03814$ - 0.8 cm, $p = 0.01491$ - 1.2 cm) on exit velocity except for 1.6 and 2.5 cm arteries. Therefore, less sensitivity of larger diameter arteries to change in monofilament denier was validated by two-factor ANOVA results. It was clear that blood input velocity and thickness of the monofilaments (denier) affect the exit velocity for 0.4, 0.8, and 1.2 cm arteries. As exit velocity was the measure of textile stent entrance and exit effects, it was concluded that textile stent geometry and blood flow in the textile stented artery segment significantly affect textile stent entrance and exit behavior.

TABLE 5.1: Two-factor ANOVA output for 0.4 cm artery diameter.

ANOVA						
<i>Source of Variation</i>	<i>SS</i>	<i>df</i>	<i>MS</i>	<i>F</i>	<i>P-value</i>	<i>F crit</i>
Rows	6.421376	2	3.210688	7.539748	0.043953	6.944272
Columns	73.71034	2	36.85517	86.54802	0.00051	6.944272
Error	1.70334	4	0.425835			
Total	81.83506	8				

TABLE 5.2: Two-factor ANOVA output for 0.8 cm artery diameter.

ANOVA						
<i>Source of Variation</i>	<i>SS</i>	<i>Df</i>	<i>MS</i>	<i>F</i>	<i>P-value</i>	<i>F crit</i>
Rows	2.678893	2	1.339446	8.240076	0.038146	6.944272
Columns	56.34957	2	28.17478	173.3271	0.00013	6.944272
Error	0.650211	4	0.162553			
Total	59.67867	8				

TABLE 5.3: Two-factor ANOVA output for 1.2 cm artery diameter.

ANOVA						
<i>Source of Variation</i>	<i>SS</i>	<i>df</i>	<i>MS</i>	<i>F</i>	<i>P-value</i>	<i>F crit</i>
Rows	0.830354	2	0.415177	0.310646	0.014919	6.944272
Columns	7.559358	2	3.779679	2.828051	0.01716	6.944272
Error	5.345984	4	1.336496			
Total	13.7357	8				

TABLE 5.4: Two-factor ANOVA output for 1.6 cm artery diameter.

ANOVA						
<i>Source of Variation</i>	<i>SS</i>	<i>df</i>	<i>MS</i>	<i>F</i>	<i>P-value</i>	<i>F crit</i>
Rows	6.47116	2	3.23558	4.952332	0.082756	6.944272
Columns	20.84794	2	10.42397	15.95478	0.012408	6.944272
Error	2.613379	4	0.653345			
Total	29.93248	8				

TABLE 5.5: Two-factor ANOVA output for 2.5 cm artery diameter.

ANOVA						
<i>Source of Variation</i>	<i>SS</i>	<i>df</i>	<i>MS</i>	<i>F</i>	<i>P-value</i>	<i>F crit</i>
Rows	200.3574	2	100.1787	33.60815	0.063155	6.944272
Columns	55.83322	2	27.91661	9.365523	0.030966	6.944272
Error	11.92314	4	2.980785			
Total	268.1137	8				

ANSYS® Flotran results showed that when blood flows through textile stented artery segment, it develops a series of entrance and exit effects which interact with each other. Changes in blood flow patterns due to textile stent entrance and exit effects comprise vortex formations and reversible flows. Both these factors increase ‘residing time’ of blood particles and enhance the deposition of platelets (also called as thrombocytes) in the textile stented artery segment during the acute stages of implantation and post-implantation as well. Additionally, platelets can be triggered by the blood flow vortices. Platelets may be activated by intrusion of textile stent monofilaments and the artery wall may be denuded of endothelium due to ballooning or stenting. Thus the textile stented artery segment becomes a site of increased platelet activation. The extent of flow vortices determines the degree to which activated platelets adhere to the artery wall. The adhesion of platelets and other blood particles to the artery wall of the textile stented region generally leads to restenosis. For polymeric textile stents, size of monofilament determines textile stent entrance and exit effects and severity of flow vortices. Two-factor ANOVA analysis showed statistically significant effect of monofilament denier and blood input velocity on exit velocity, ultimately on textile stent entrance and exit effects and restenosis.

Low shear stresses associated with blood flow variations also favor platelet accumulation and adhesion to the artery wall. As the artery wall attempts to adapt itself to this new mechanical environment, the flow patterns caused by textile stent design play a crucial role by influencing regrowth rate of endothelial cells. Also, minuscule movement of monofilaments due to pulsatile blood flow may cause endothelial damage. Previous researchers [5, 4, 16] concluded that metal stent geometry affects blood flow variations

and particle residence time in the stented artery segment. Longest and Kleinstreuer [15] concluded that particle size and near wall hydrodynamic interactions significantly influence blood particle deposition in the stented region. In this study, statistical analysis showed that monofilament denier (thickness) significantly affects textile stent entrance and exit behavior. Blood flow disturbances and vortices caused by monofilament bumps cause activation of platelets. The activated platelets form platelet plugs which trap several other blood particles and cause additional obstructions in the textile stented artery segment, facilitating restenosis.

Textile stent geometry plays a decisive role towards the progression of restenosis. Kastrati *et al.* [9] concluded that different stent designs exhibit different rates of stenosis. Simon *et al.* [20] concluded that endothelial cell coverage may be impaired by the stent wall thickness higher than 75 μ m. The authors mentioned that this impairment may have caused by the flow disturbances created by the specific thickness. Stents used for clinical practice range between 65 – 275 μ m wall thicknesses. Peacock *et al.* [18] concluded that shear stresses from blood flow disturbances were sufficient to delay endothelialization and promote restenosis. Natarajan and Dehghan [17] observed wall shear stresses of 2-3 times around the arterial obstructions than those found in the equivalent normal vessel. In the current study, variation of textile stent entrance and exit effects showed minimum blood velocity at the edges of textile stents and within monofilament bumps. Shear stresses at the edges of textile stents are very low, causing damage to the endothelium and leading to restenosis. Variation in textile stent entrance and exit effects may be directly proportional to the progression of restenosis. All in all, geometry of textile stents and related blood flow variations are responsible for restenosis.

The stress is greatest at the junctions of the arterial tissue and textile stent, where elastic properties of the two are mismatched. As the artery deforms with textile stent, stress in the artery wall adjacent to the monofilaments is elevated, developing a zone of stress concentration. In general, arteries with stents respond with tissue growth to these types of stresses. Polymeric textile stent and artery interactions were not considered in this study. Arteries were assumed as rigid tubes, but human arteries are three-layered, non-homogeneous, non-isotropic, and non-linearly elastic structures. The arteries may move or vibrate due to the flow variations in the textile stented artery segment. Future studies are expected to focus on analyzing the cumulative effect of pulsatile blood flow on blood flow variations in the textile stented artery segment. Three dimensional artery-stent blood flow simulation models will certainly yield more comprehensive results. Blood flow characterization of drug-eluting stents has to be analyzed. However, current study suggests significant guidelines for the blood flow characterization of polymeric textile stents and establishes a relationship between textile stent geometry and restenosis.

5.9 Literature Cited

1. Basmadjian, D., "The Hemodynamic and Embolizing Forces Acting on Thrombi- Part II: The Effect of Pulsatile Blood Flow", *J. Biomech.*, **19**(10), 837-845 (1986).
2. Berry, J., Moore, J., Newman, V., and Routh, W., "In Vitro Flow Visualization in Stented Arterial Segments", *J. Vasc. Invest.*, **3**(2), 63-68 (1997).
3. Berry, J., Santamarina, A., Moore, J., Roychowdhury, S., and Routh, W., "Experimental and Computational Flow Evaluation of Coronary Stents", *Ann. Biomed. Eng.*, **28**(4), 386-398 (2000).
4. Cao, J., and Rittgers, S., "Particle Motion within In Vitro Models of Stenosed Internal Carotid and Left Anterior Descending Coronary Arteries", *Ann. Biomed. Eng.*, **26**(2), 190-199 (1998).
5. Folie, B., and McIntire, L., "Mathematical Analysis of Mural Thrombogenesis- Concentration Profiles of Platelets Activating Agents and Effects of Viscous Shear Flow", *Biophys. J.*, **56**(6), 1121-1141 (1989).
6. Fournier, R., *Basic Transport Phenomena in Biomedical Engineering*, Taylor and Francis, Philadelphia PA, 1999.
7. Frank, A., Walsh, P., and Moore, J., "Computational Fluid Dynamics and Stent Design", *Artif. Org.*, **26**(7), 614-621 (2002).
8. Guyton, A., and Hall, J., *Textbook of Medical Physiology*, Saunders, Philadelphia PA, Tenth edition, 2000.
9. Kastrati, A., Mehilli, J., Dirschinger, J., Pache, J., Ulm, K., Schuhlen, H., Seyforth, M., Schmitt, C., Blasini, R., Neumann, F., and Schomig, A., "Restenosis after Coronary Placement of Various Stent Types", *Am. J. Cardiol.*, **87**(1), 34-39 (2001).

10. Ku, D., "Blood Flow in Arteries", *Annu. Rev. Fluid Mech.*, **29**, 399-434 (1997).
11. LaDisa, J., Olson, L., Guler, I., Hettrick, D., Audi, S., Kersten, J., Warltier, D., and Pagel, P., "Stent Design Properties and Deployment Ratio Influence Indexes of Wall Shear Stress: A 3-Dimensional Computational Fluid Dynamics Investigation within a Normal Artery", *J. Appl. Physiol.*, **97**(1), 424-430 (2004).
12. Lee, T., Liao, W., and Low, H., "Numerical Simulation of Turbulent Flow through Series Stenoses", *Int. J. Numer. Meth. Fluids*, **42**, 717-740 (2003).
13. Lieber, B., and Giddens, D., "Post-Stenotic Core Flow Behavior in Pulsatile Flow and its Effect on Wall Shear Stress", *J. Biomech.*, **25**(6), 597-605 (1990).
14. Lightfoot, E., *Transport Phenomena and Living Systems*, Wiley, New York, 1972.
15. Longest, P., and Kleinstreuer, C., "Comparison of Blood Particle Deposition Models for non-parallel Flow Domains", *J. Biomech.*, **36**(3), 421-430 (2003).
16. Moore, J., and Berry, J., "Fluid and Solid Mechanical Implications of Vascular Stenting", *Ann. Biomed. Eng.*, **30**(4), 498-508 (2002).
17. Natarajan, S., and Dehghan, M., "A Numerical and Experimental Study of Periodic Flow in a Model of a Corrugated Vessel with Application to Stented Arteries", *Med. Eng. Phys.*, **22**(8), 555-566 (2000).
18. Peacock, J., Hankins, S., Jones, T., and Lutz, R., "Flow Instabilities Induced by Coronary Artery Stents: Assessment with an In Vitro Pulse Duplicator", *J. Biomech.*, **28**(1), 17-26 (1995).
19. Sadasivan, C., Leiber, B., Lopes, D., Ringer, A., and Hopkins, L., "Modeling of Angiographic Dye Washout from Cerebral Aneurysms Before and After Stenting: An Index of Stent Efficacy", The Proceedings of 2001 ASME International

Mechanical Engineering Congress and Exposition, **51**, New York, USA, 2001, pp 261-262.

20. Simon, C., Palmaz, J., and Sprague, E., "Influence of Topography on Endothelialization of Stents: Clues for New Designs", *J. Long-term Effects Med. Impl.*, **10**(1), 143-151 (2000).
21. Sprague, E., Luo, J., and Palmaz, J., "Human Aortic Endothelial Cell Migration onto Stent Surfaces under Static and Flow Conditions", *J. Vasc. Intervent. Radiol.*, **8**(1), 83-92 (1997).
22. Sukavaneshvar, S., Rosa, G., and Solen, K., "Enhancement of Stent-Induced Thromboembolism by Residual Stenoses: Contribution of Hemodynamics", *Ann. Biomed. Eng.*, **28**(2), 182-193 (2000).
23. Thiriet, M., Pares, C., Saltel, E., and Hecht, F., "Numerical Simulation of Steady Flow in a Model of the Aortic Bifurcation", *J. Biomech. Eng.*, **114**(1), 40-49 (1992).
24. Tortora, G., and Grabowski, S., *Principles of Anatomy and Physiology*, Wiley, Hoboken NJ, Tenth Edition, 2003.
25. Wootton, W., and Ku, D., "Fluid Mechanics of Vascular Systems, Diseases, and Thrombosis", *Annu. Rev. Biomed. Eng.*, **1**, 299-329 (1999).
26. Yee, L., Kadambi, J., and Wernet, M., "Investigation of Flow Characteristics in a Coronary Artery Stent", The Proceedings of ASME FEDSM'03 4th ASME_JSME Joint Fluids Engineering Conference", Honolulu, Hawaii, USA, 2003, pp 889-900.
27. Young, D., "Fluid Mechanics of Arterial Stenoses", *J. Biomech. Eng.*, **101**, 157-175 (1979).

CHAPTER 6

CONCLUSIONS AND RECOMMENDATIONS

6.1 Conclusions

- Current study focused on prototyping and modeling of braided structures to be used as stents, hence called ‘polymeric textile stents’. The objective was to establish guidelines for commercial manufacturing of polymeric textile stents which can become major substitutes for metal stents. Prototypes of polymeric textile stents and bifurcated textile stents were manufactured with textile machinery.
- Manufacturing variables namely braid angle, braid diameter, and heatset time showed statistically significant effect ($p= 0.0001$) on compression force of textile stents.
- A chart was compiled which categorizes factors affecting the performance of textile stents.
- Strong correlation ($adjusted R^2= 0.9999$) was observed between radial and *in vitro* (unidirectional) compressions of textile stents.

- Agreement between values of Young's modulus of textile stents derived by the mechanical model (strain energy method) to those of the experimental was good (*adjusted R*²= 0.7955). Load-strain curves were obtained by strip testing of textile stents on Instron.
- Empirical model showed strong correlation between empirical and experimental values of compression force for 0.6 cm (*adjusted R*²= 0.8669) and 0.9 cm (*adjusted R*²= 0.9251) textile stents radii.
- Two-factor ANOVA analysis showed statistically significant effect (*p* = 0.00051 for 0.4 cm artery diameter, *p* = 0.00013 for 0.8 cm artery diameter, *p* = 0.01716 for 1.2 cm artery diameter, *p* = 0.01240 for 1.6 cm artery diameter, *p* = 0.0309 for 2.5 cm artery diameter) of blood input velocity on exit velocity. Monofilament denier also showed statistically significant effect (*p* = 0.04395 for 0.4 cm diameter, *p* = 0.03814 for 0.8 cm diameter, *p* = 0.01491 for 1.2 cm diameter) on exit velocity for artery diameters except 1.6 and 2.5 cm.
- Blood flow characterization of polymeric textile stents was helpful in understanding restenosis. Application of textile stents as a substitute to metal stents is feasible.

6.2 Recommendations

In vitro stent-artery-plaque simulator is recommended for future studies. The proposed model is a closed flow system (Figure 6.1) with a pump (such as one from Vivitro Systems Inc., Canada) producing pulsatile flows same as those by the human heart, a reservoir for the artificial blood, pressure controller and indicator, and the stent-artery-plaque simulator (Figure 6.2A). Proposed stent-artery-plaque simulator includes an

artificial artery, textile stent implanted inside the artery and artificial plaque generators. The artificial plaque generators are radially placed, moveable, and can be controlled individually (Figure 6.2B) to cause the desired plaque effect in the textile stented artery segment. Artificial blood can be flown through the flow model. The flow variations in the textile stented region can be observed by the intravascular ultrasound (IVUS) camera. The proposed model is an ideal simulator of the *in vivo* stent-artery-plaque interactions.

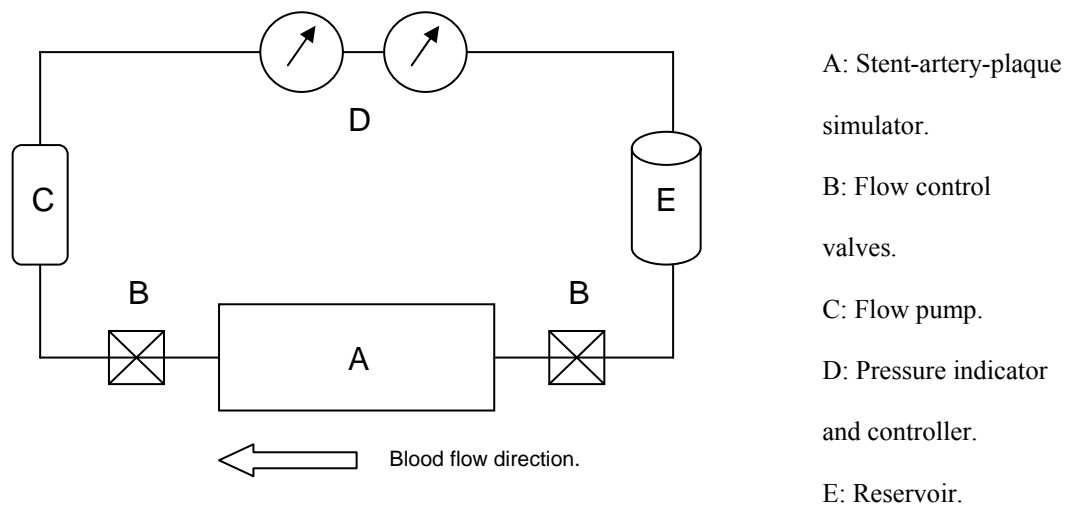


FIGURE 6.1: Proposed flow model.

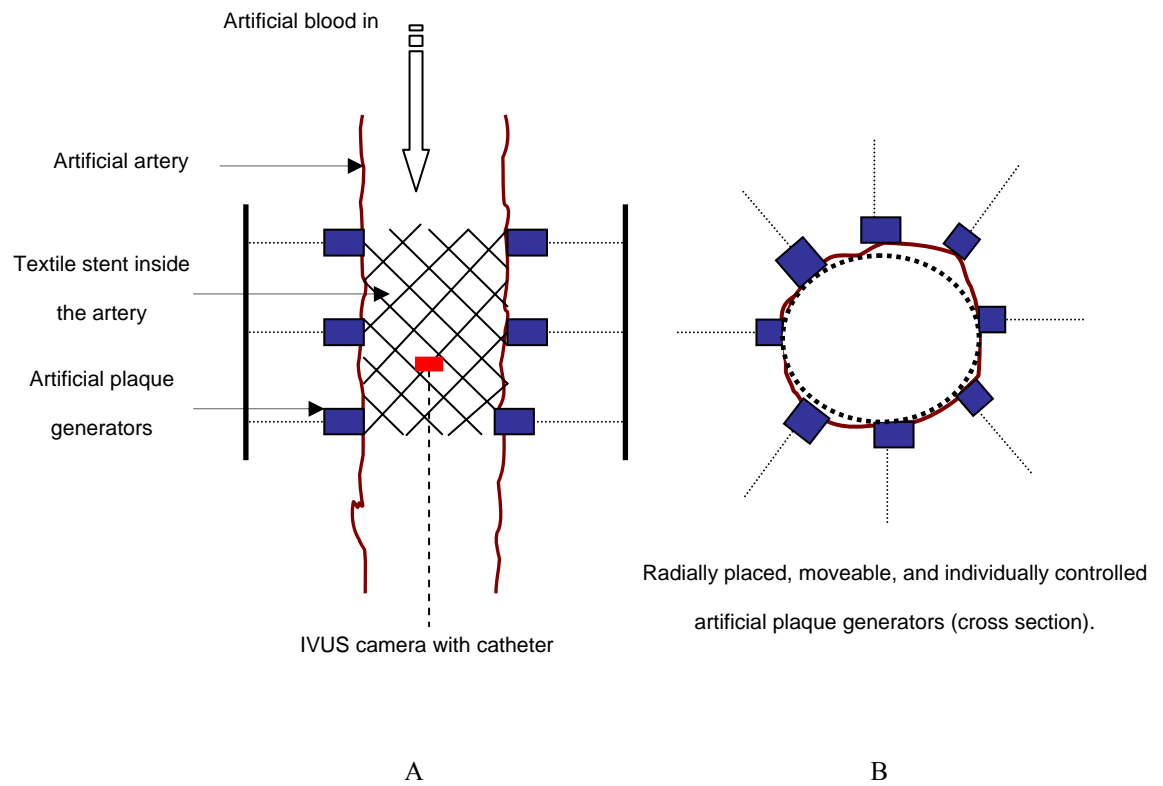


FIGURE 6.2: Proposed *in vitro* stent-artery-plaque simulator.

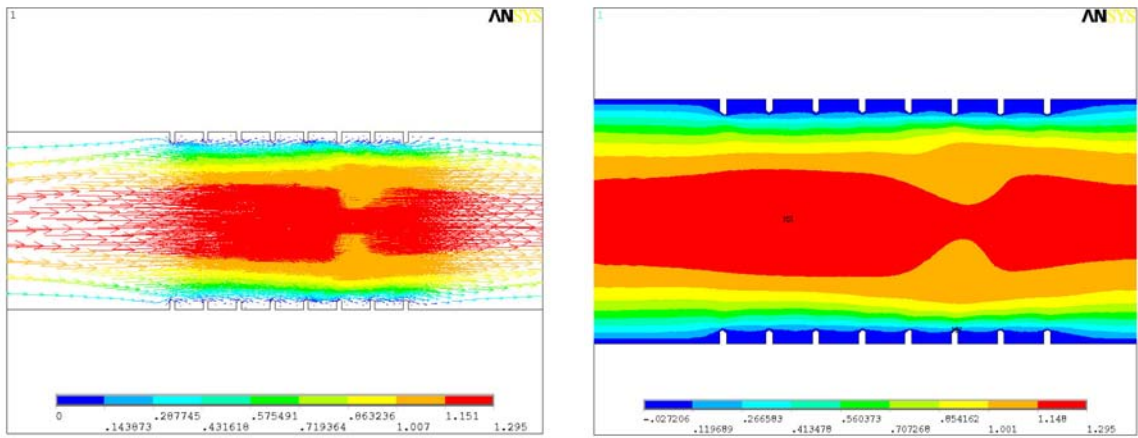
6.3 Future Challenges

The following challenges should be addressed in the future research towards commercialization of polymeric textile stents.

- Develop crimping technique for textile stents.
- Avoid fraying at the ends of textile stents.
- Sterilization and packing of textile stents.
- *In vivo* implantation of textile stents.

APPENDICES

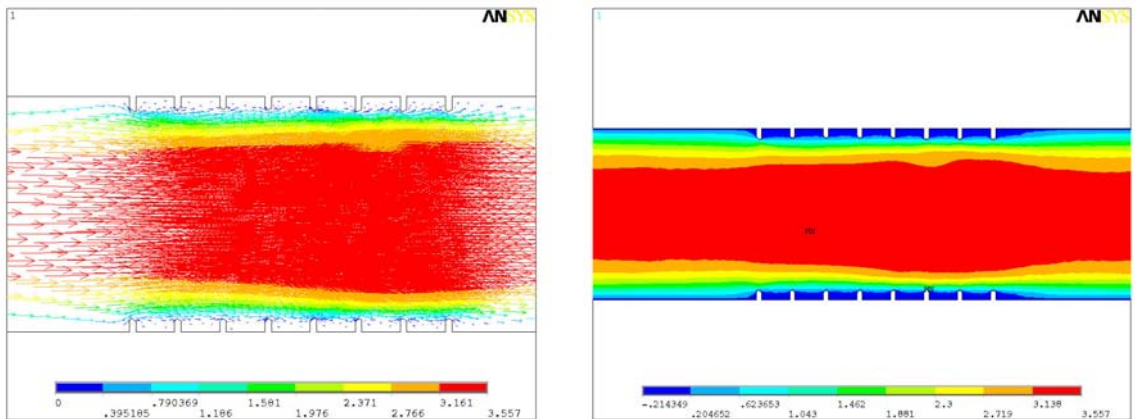
A.1 Exit Velocity Results for 0.4 cm Artery Diameter Combinations



A: Vector plot.

B: Contour plot.

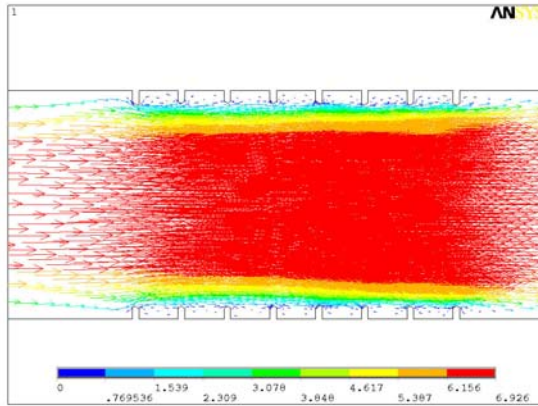
FIGURE A.1: Exit velocity for combination of 0.4 cm, 150 denier, and 1 cm/s.



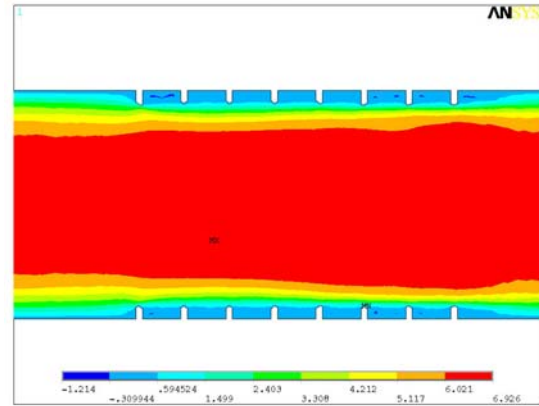
A: Vector plot.

B: Contour plot.

FIGURE A.2: Exit velocity for combination of 0.4 cm, 150 denier, and 3 cm/s.

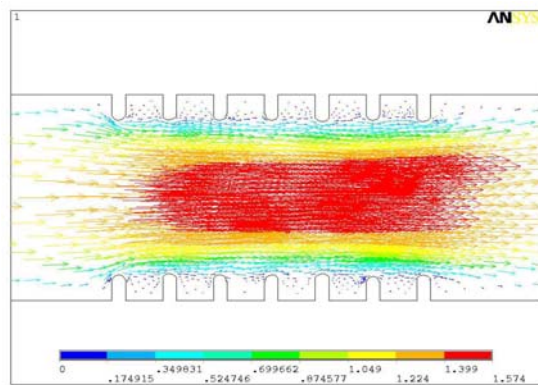


A: Vector plot.

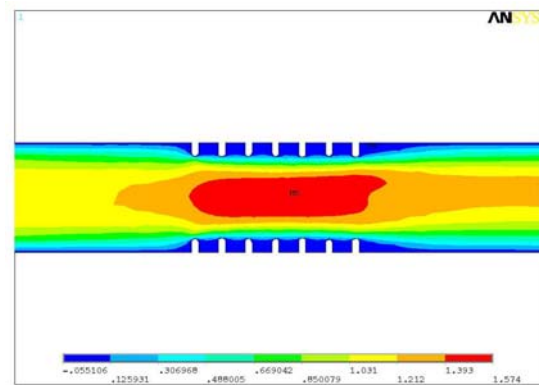


B: Contour plot.

FIGURE A.3: Exit velocity for combination of 0.4 cm, 150 denier, and 6 cm/s.

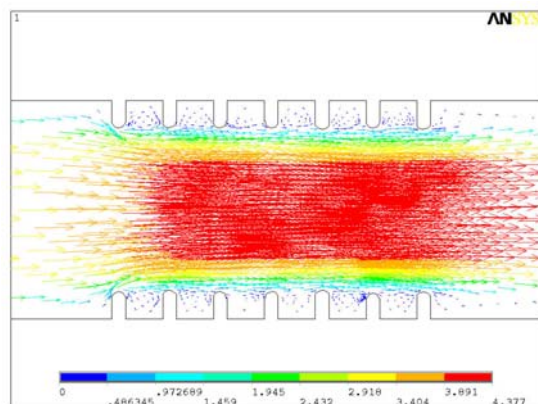


A: Vector plot.

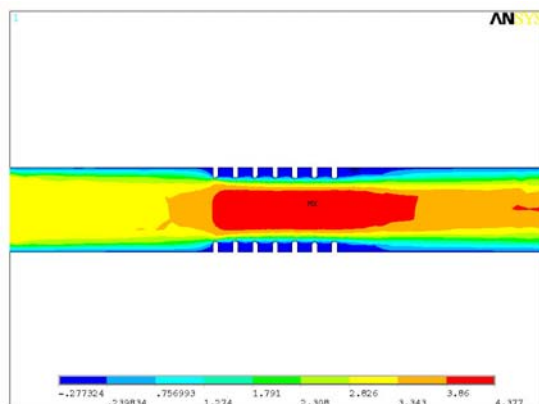


B: Contour plot.

FIGURE A.4: Exit velocity for combination of 0.4 cm, 600 denier, and 1 cm/s.

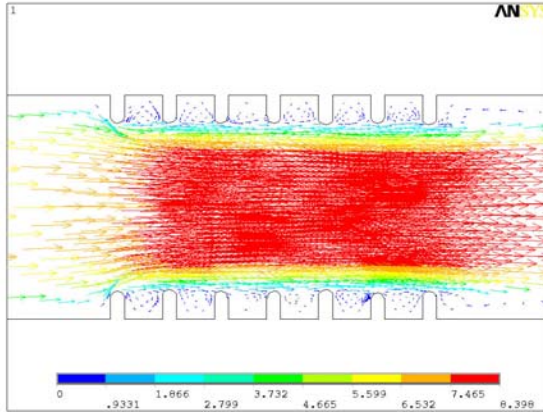


A: Vector plot.

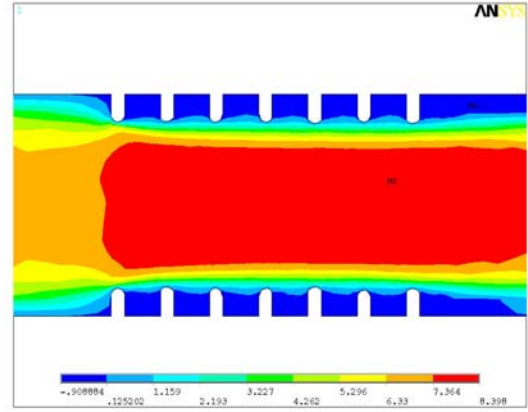


B: Contour plot.

FIGURE A.5: Exit velocity for combination of 0.4 cm, 600 denier, and 3 cm/s.

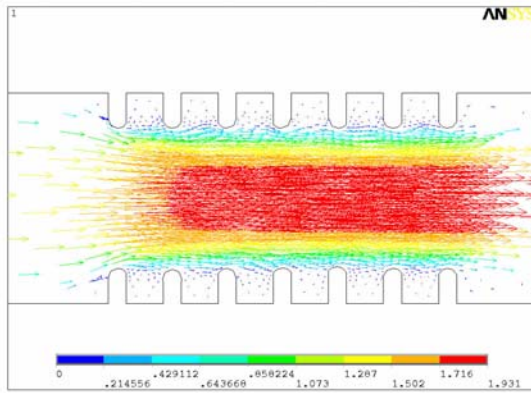


A: Vector plot.

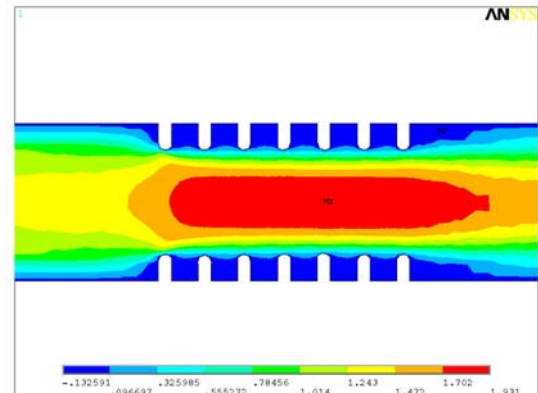


B: Contour plot.

FIGURE A.6: Exit velocity for combination of 0.4 cm, 600 denier, and 6 cm/s.

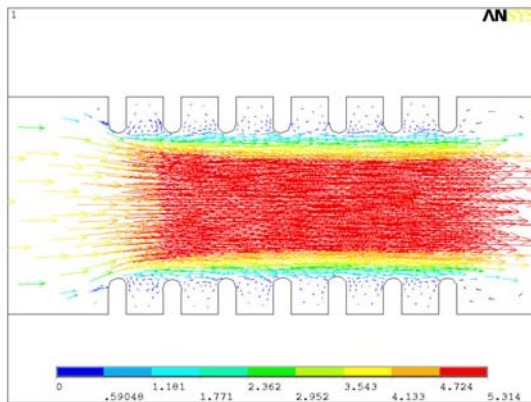


A: Vector plot.

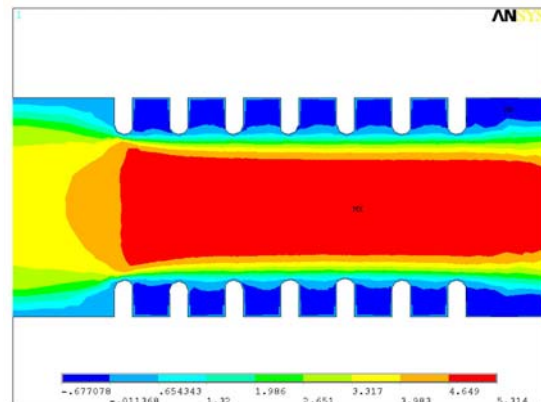


B: Contour plot.

FIGURE A.7: Exit velocity for combination of 0.4 cm, 1100 denier, and 1 cm/s.

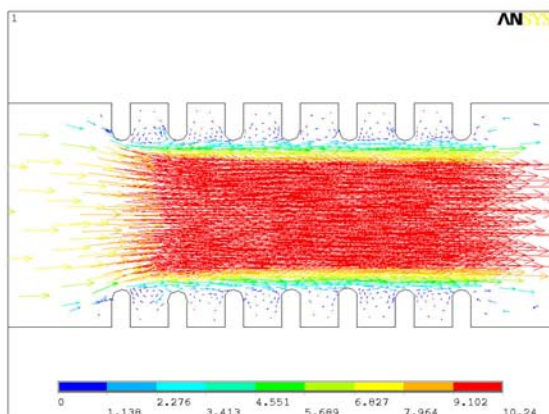


A: Vector plot.

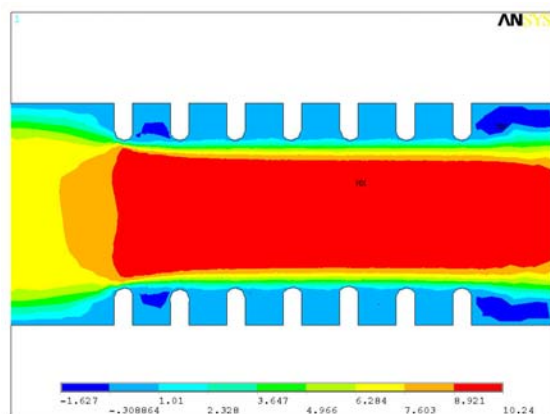


B: Contour plot.

FIGURE A.8: Exit velocity for combination of 0.4 cm, 1100 denier, and 3 cm/s.



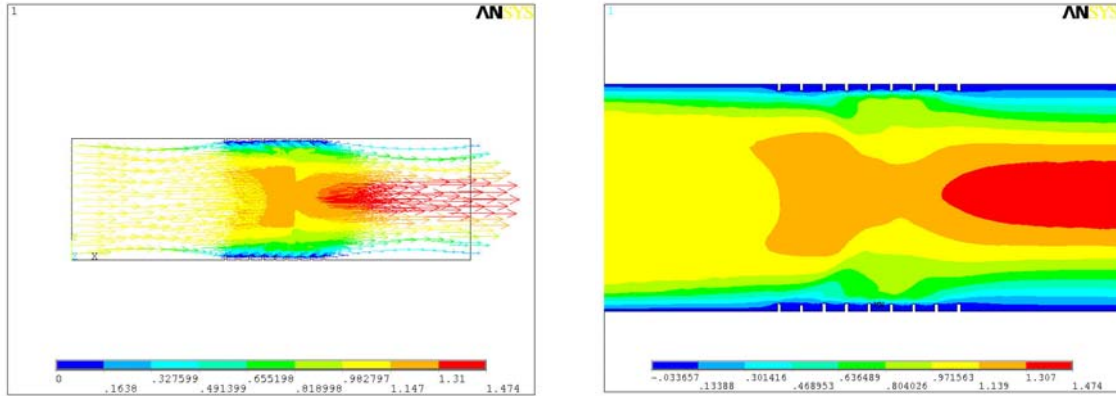
A: Vector plot.



B: Contour plot.

FIGURE A.9: Exit velocity for combination of 0.4 cm, 1100 denier, and 6 cm/s.

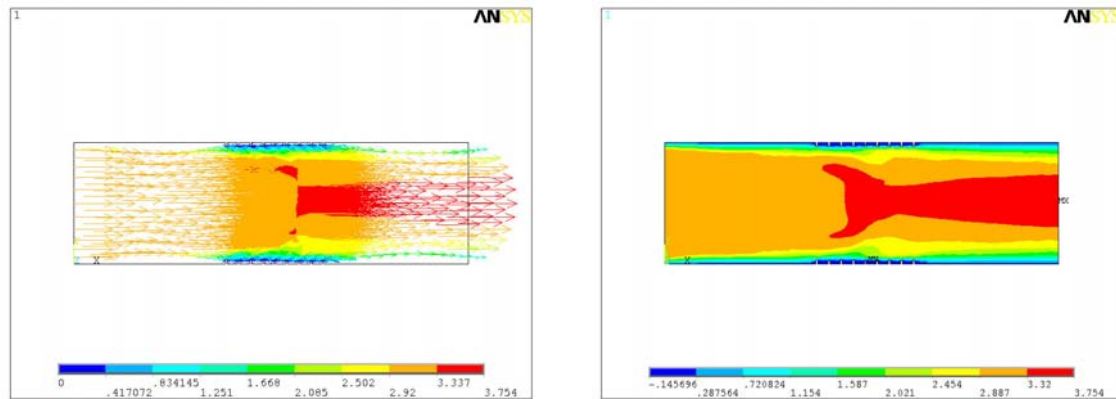
A.2 Exit Velocity Results for 0.8 cm Artery Diameter Combinations



A: Vector plot.

B: Contour plot.

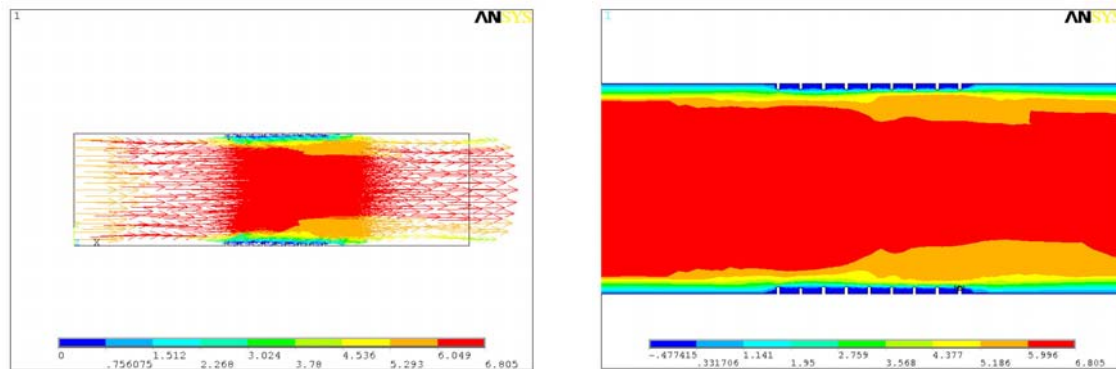
FIGURE A.10: Exit velocity for combination of 0.8 cm, 150 denier, and 1 cm/s.



A: Vector plot.

B: Contour plot.

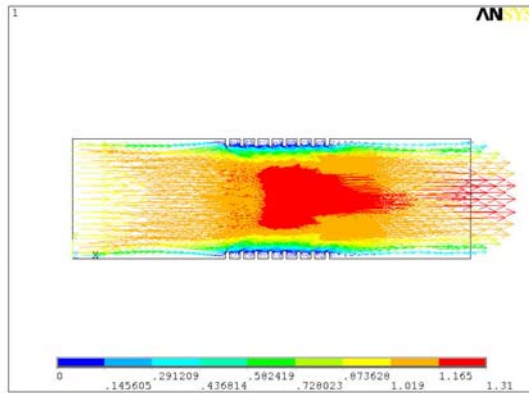
FIGURE A.11: Exit velocity for combination of 0.8 cm, 150 denier, and 3 cm/s.



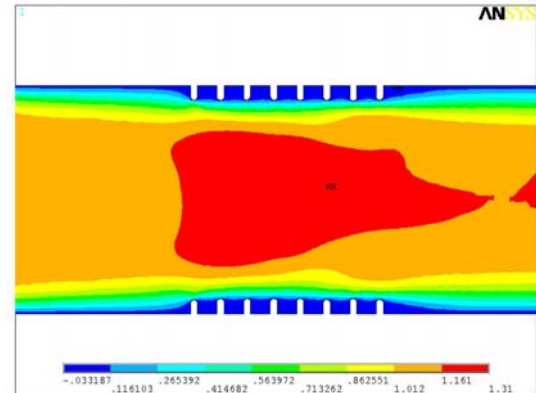
A: Vector plot.

B: Contour plot.

FIGURE A.12: Exit velocity for combination of 0.8 cm, 150 denier, and 6 cm/s.

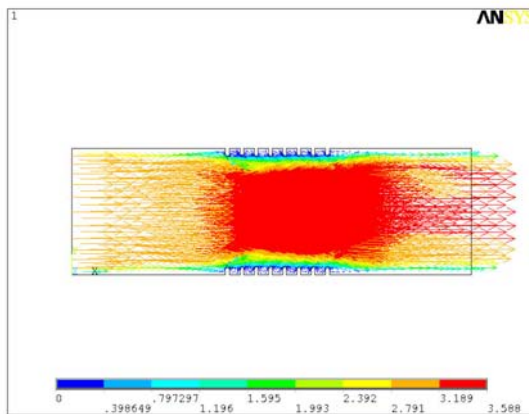


A: Vector plot.

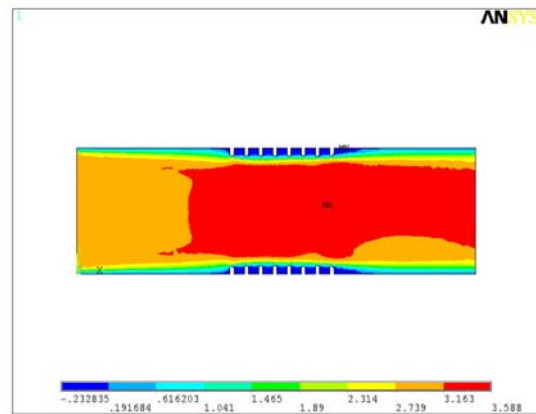


B: Contour plot.

FIGURE A.13: Exit velocity for combination of 0.8 cm, 600 denier, and 1 cm/s.

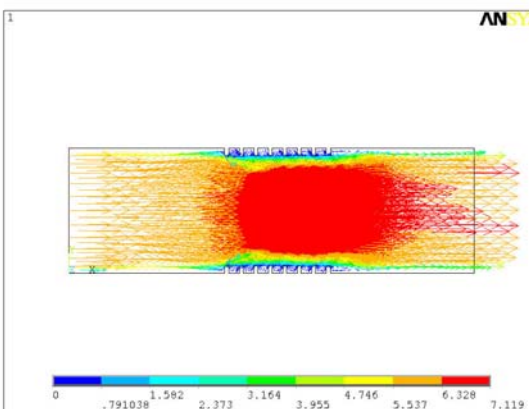


A: Vector plot.

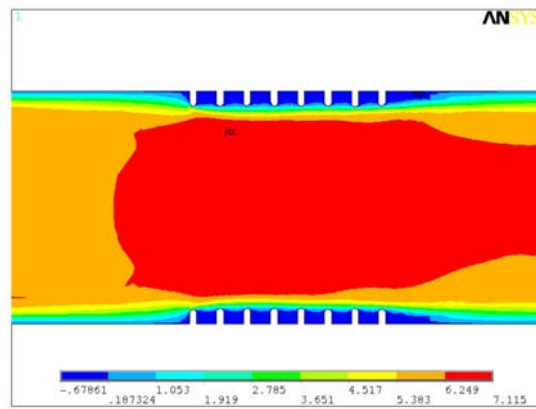


B: Contour plot.

FIGURE A.14: Exit velocity for combination of 0.8 cm, 600 denier, and 3 cm/s.

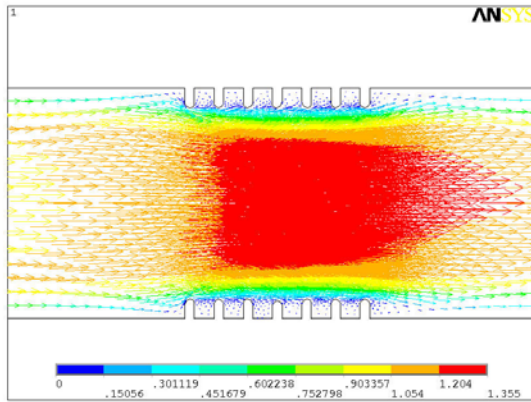


A: Vector plot.

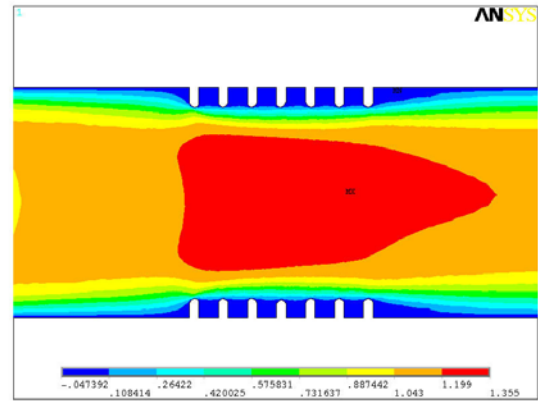


B: Contour plot.

FIGURE A.15: Exit velocity for combination of 0.8 cm, 600 denier, and 6 cm/s.

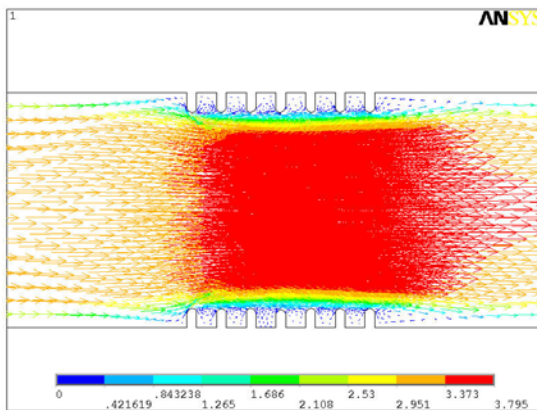


A: Vector plot.

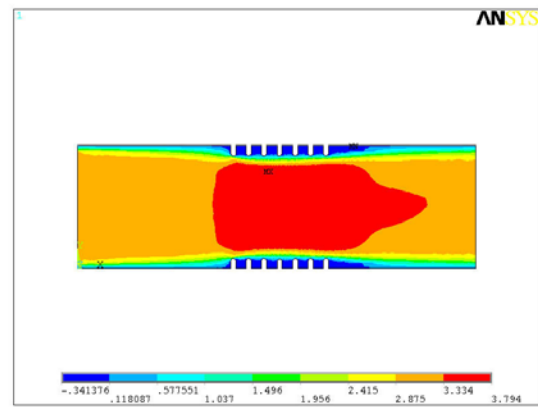


B: Contour plot.

FIGURE A.16: Exit velocity for combination of 0.8 cm, 1100 denier, and 1 cm/s.

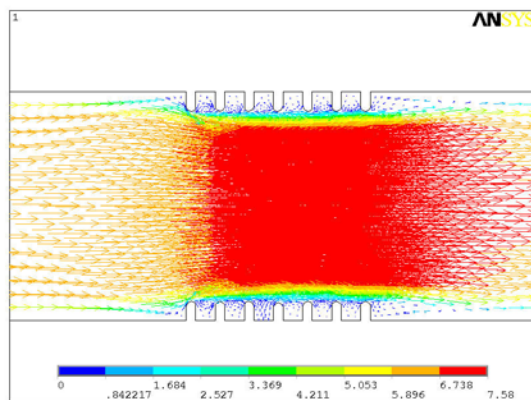


A: Vector plot.

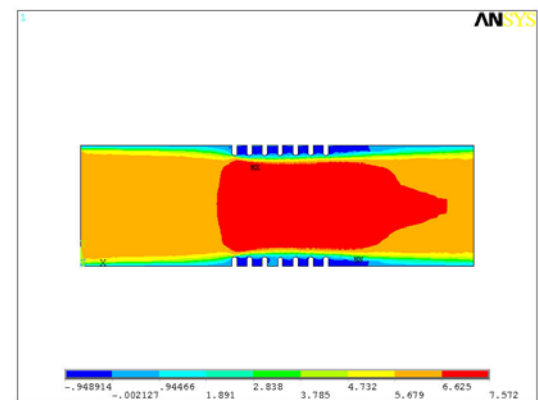


B: Contour plot.

FIGURE A.17: Exit velocity for combination of 0.8 cm, 1100 denier, and 3 cm/s.



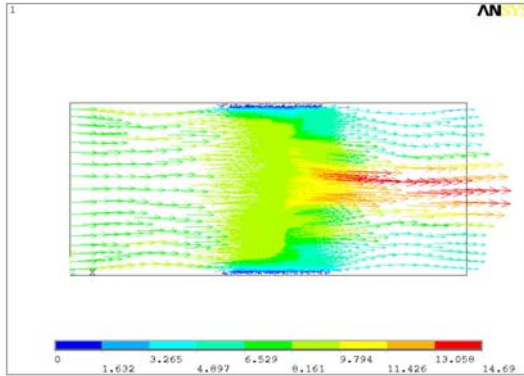
A: Vector plot.



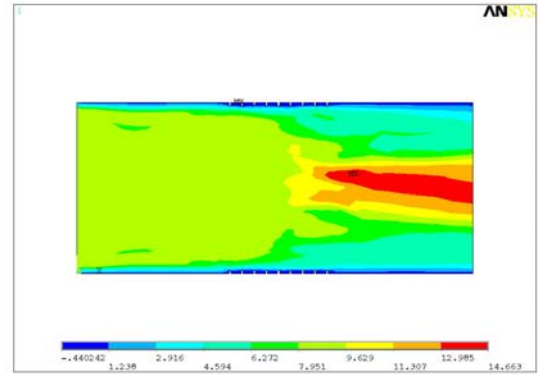
B: Contour plot.

FIGURE A.18: Exit velocity for combination of 0.8 cm, 1100 denier, and 6 cm/s.

A.3 Exit Velocity Results for 1.2 cm Artery Diameter Combinations

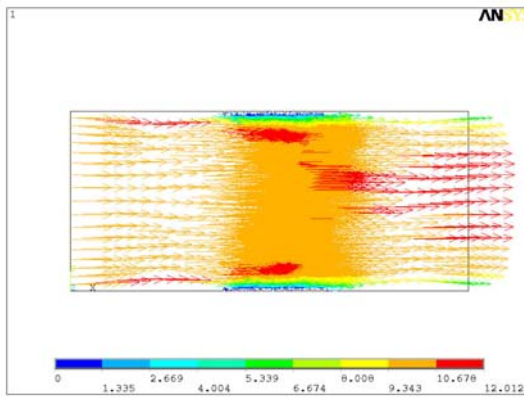


A: Vector plot.

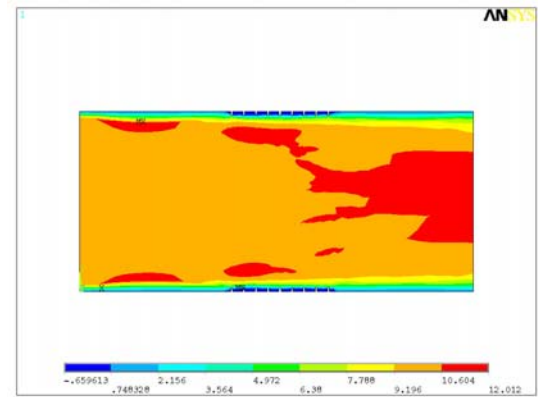


B: Contour plot.

FIGURE A.19: Exit velocity for combination of 1.2 cm, 150 denier, and 8 cm/s.

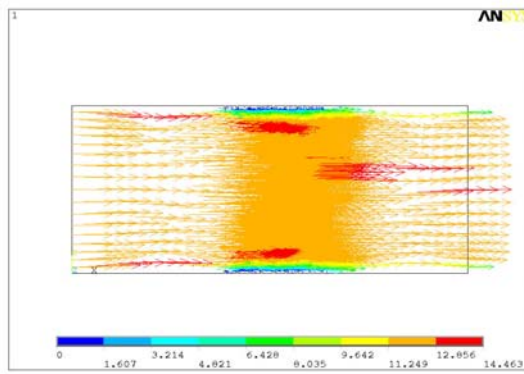


A: Vector plot.

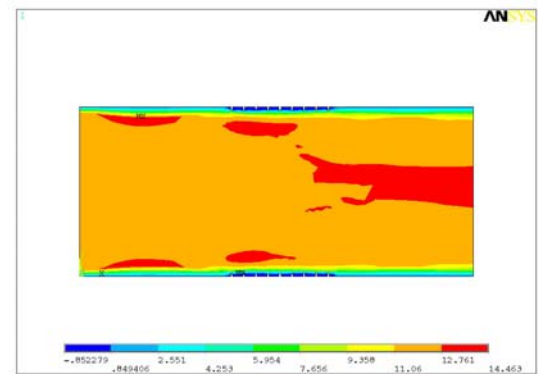


B: Contour plot.

FIGURE A.20: Exit velocity for combination of 1.2 cm, 150 denier, and 10 cm/s.

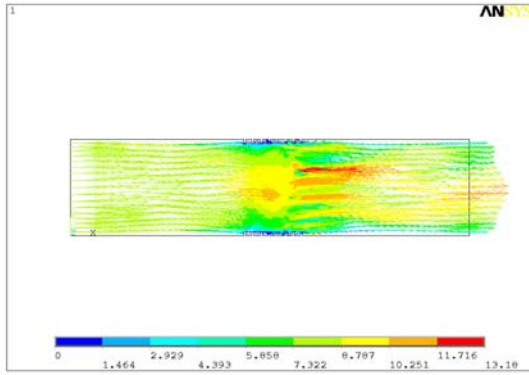


A: Vector plot.

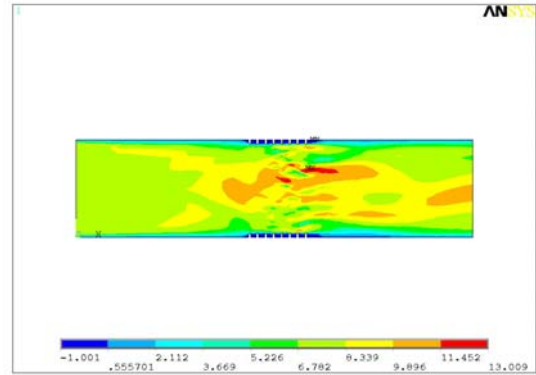


B: Contour plot.

FIGURE A.21: Exit velocity for combination of 1.2 cm, 150 denier, and 12 cm/s.

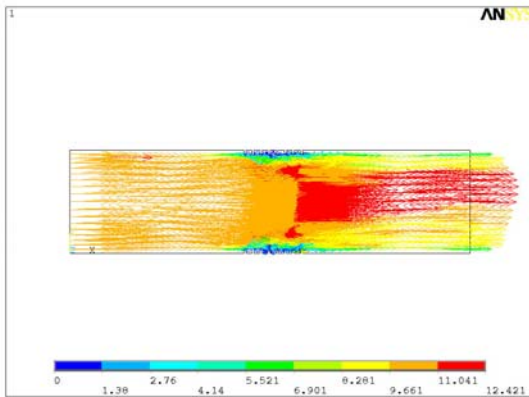


A: Vector plot.

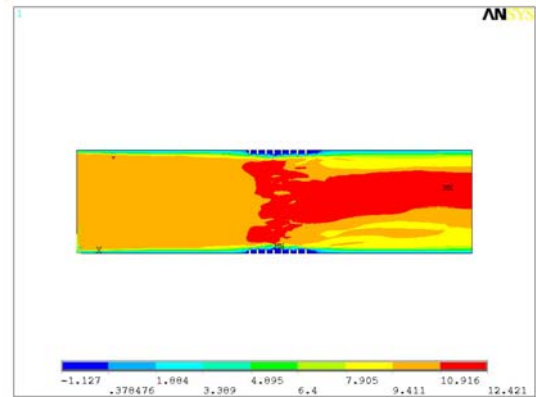


B: Contour plot.

FIGURE A.22: Exit velocity for combination of 1.2 cm, 600 denier, and 8 cm/s.

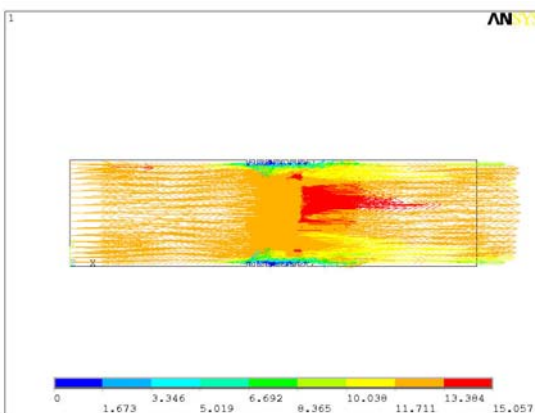


A: Vector plot.

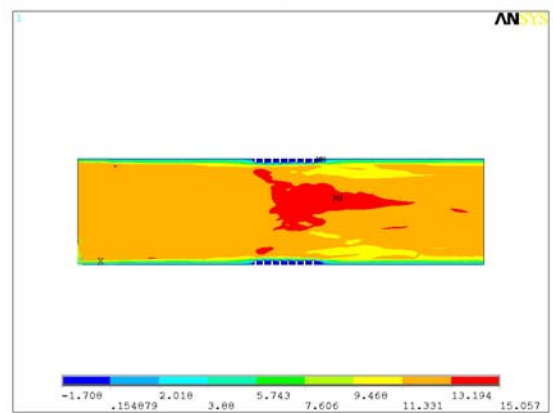


B: Contour plot.

FIGURE A.23: Exit velocity for combination of 1.2 cm, 600 denier, and 10 cm/s.

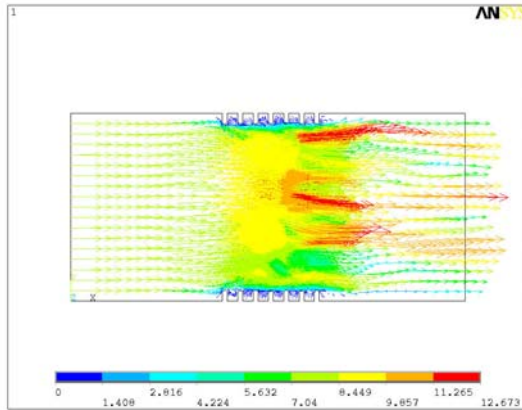


A: Vector plot.

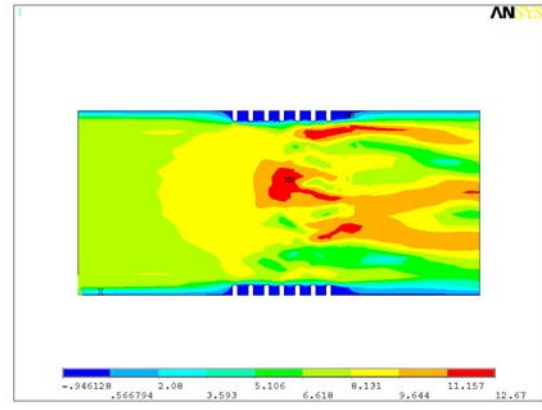


B: Contour plot.

FIGURE A.24: Exit velocity for combination of 1.2 cm, 600 denier, and 12 cm/s.

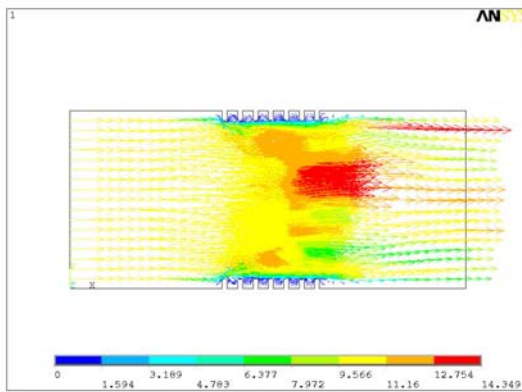


A: Vector plot.

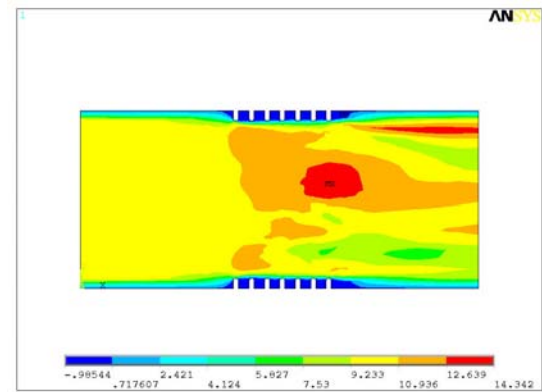


B: Contour plot.

FIGURE A.25: Exit velocity for combination of 1.2 cm, 1100 denier, and 8 cm/s.

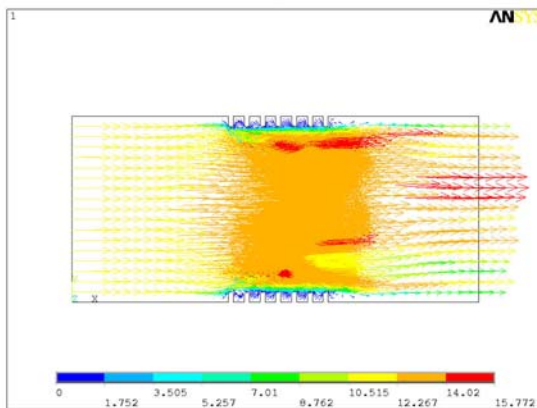


A: Vector plot.

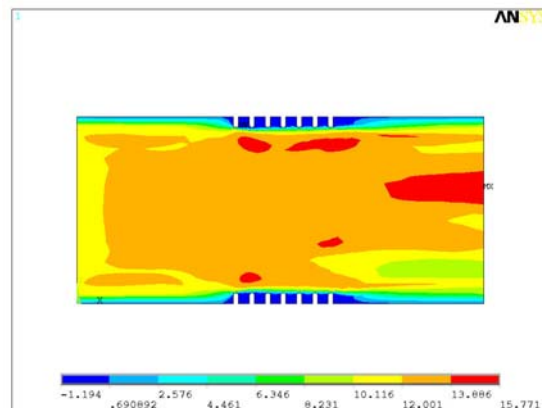


B: Contour plot.

FIGURE A.26: Exit velocity for combination of 1.2 cm, 1100 denier, and 10 cm/s.



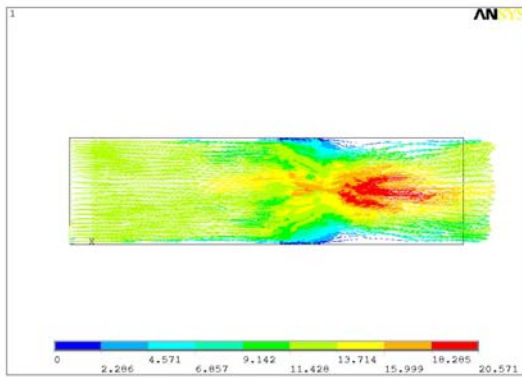
A: Vector plot.



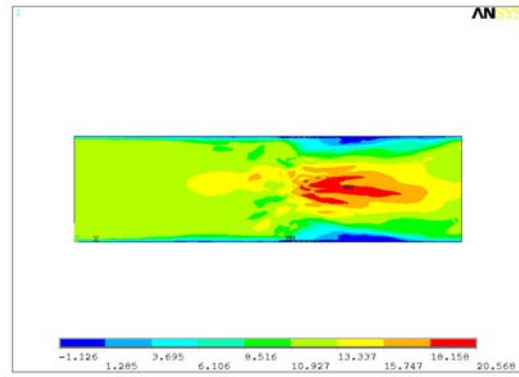
B: Contour plot.

FIGURE A.27: Exit velocity for combination of 1.2 cm, 1100 denier, and 12 cm/s.

A.4 Exit Velocity Results for 1.6 cm Artery Diameter Combinations

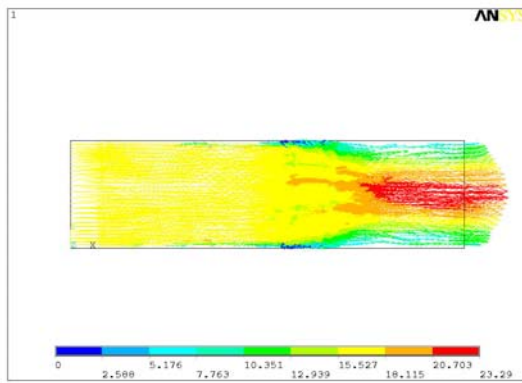


A: Vector plot.

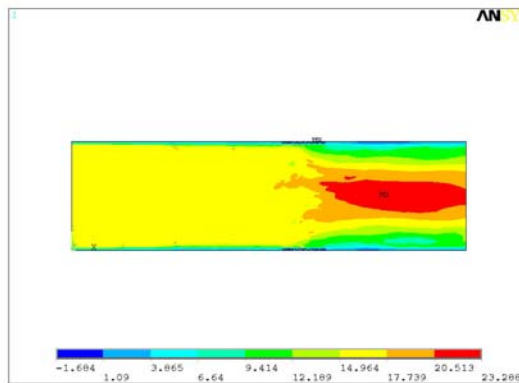


B: Contour plot.

FIGURE A.28: Exit velocity for combination of 1.6 cm, 150 denier, and 12 cm/s.

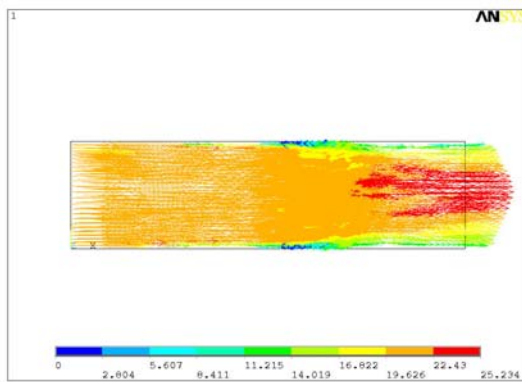


A: Vector plot.

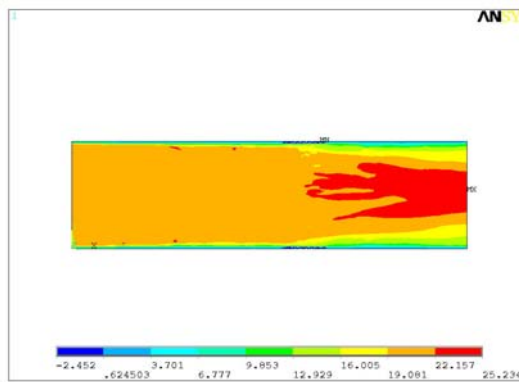


B: Contour plot.

FIGURE A.29: Exit velocity for combination of 1.6 cm, 150 denier, and 16 cm/s.

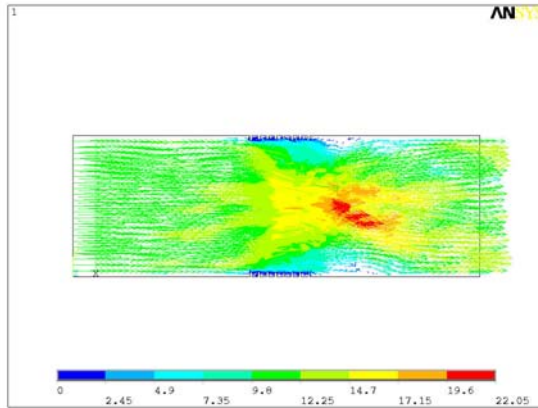


A: Vector plot.

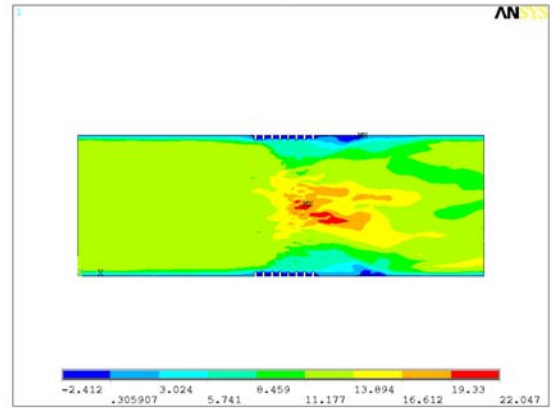


B: Contour plot.

FIGURE A.30: Exit velocity for combination of 1.6 cm, 150 denier, and 20 cm/s.

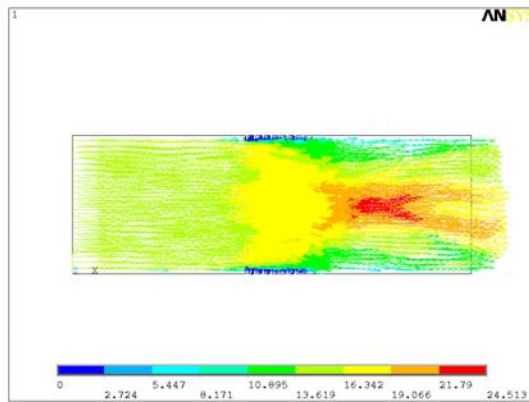


A: Vector plot.

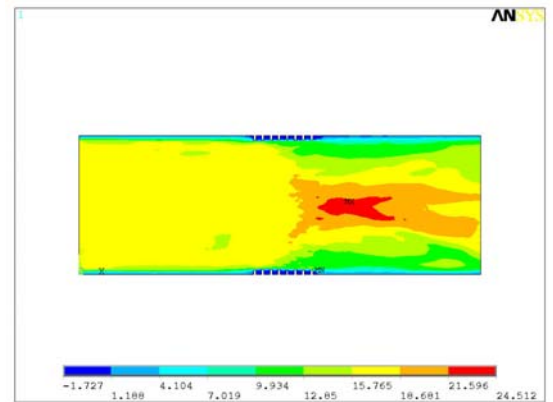


B: Contour plot.

FIGURE A.31: Exit velocity for combination of 1.6 cm, 600 denier, and 12 cm/s.

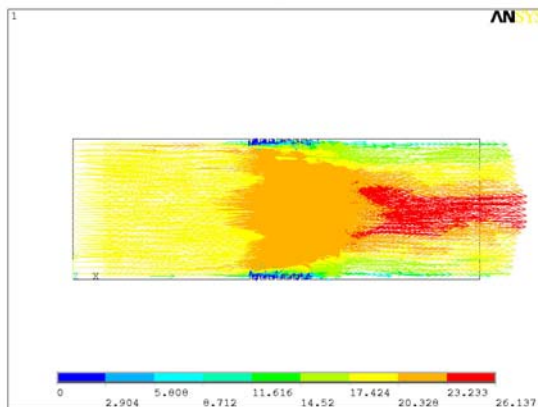


A: Vector plot.

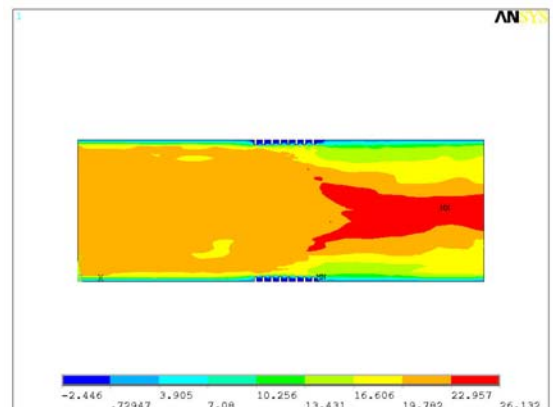


B: Contour plot.

FIGURE A.32: Exit velocity for combination of 1.6 cm, 600 denier, and 16 cm/s.

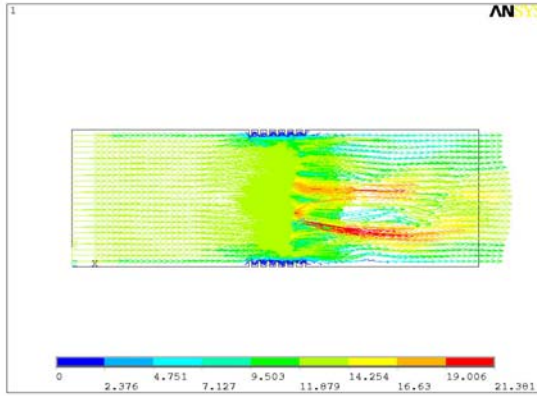


A: Vector plot.

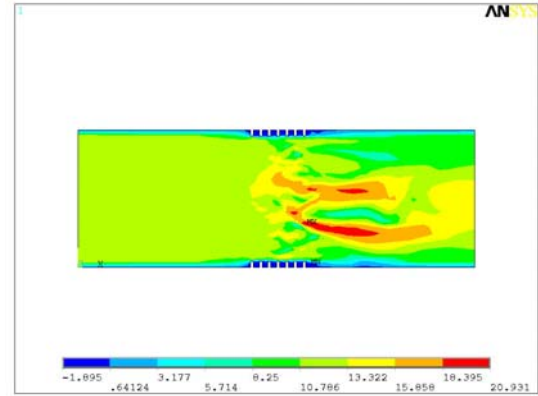


B: Contour plot.

FIGURE A.33: Exit velocity for combination of 1.6 cm, 600 denier, and 20 cm/s.

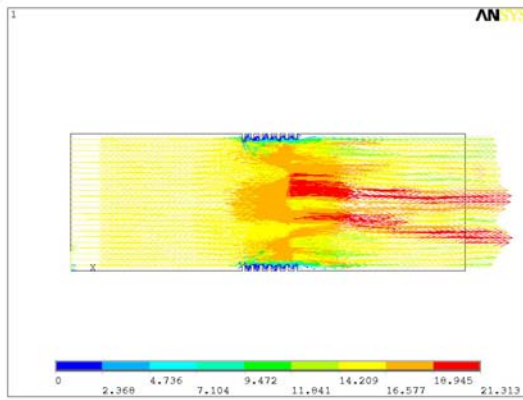


A: Vector plot.

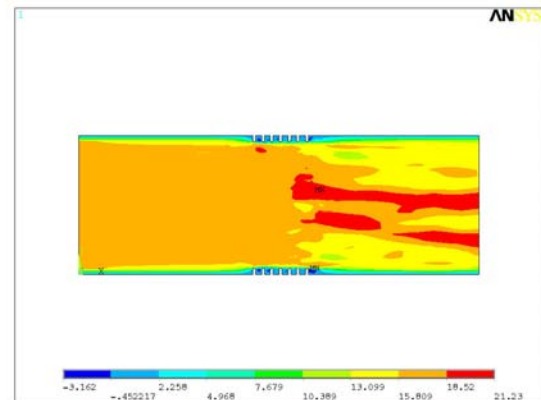


B: Contour plot.

FIGURE A.34: Exit velocity for combination of 1.6 cm, 1100 denier, and 12 cm/s.

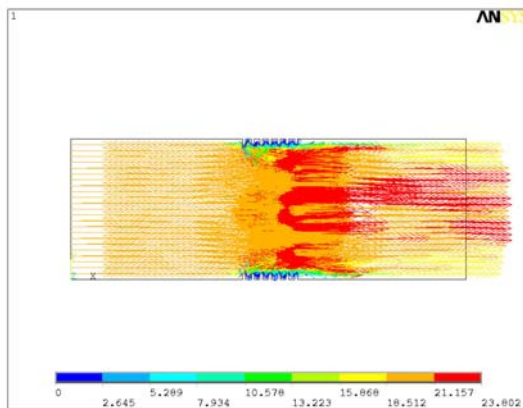


A: Vector plot.

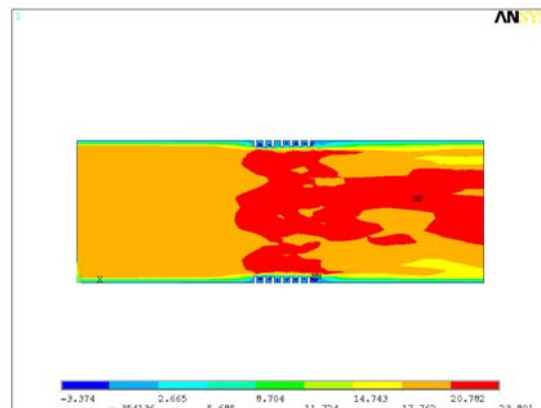


B: Contour plot.

FIGURE A.35: Exit velocity for combination of 1.6 cm, 1100 denier, and 16 cm/s.



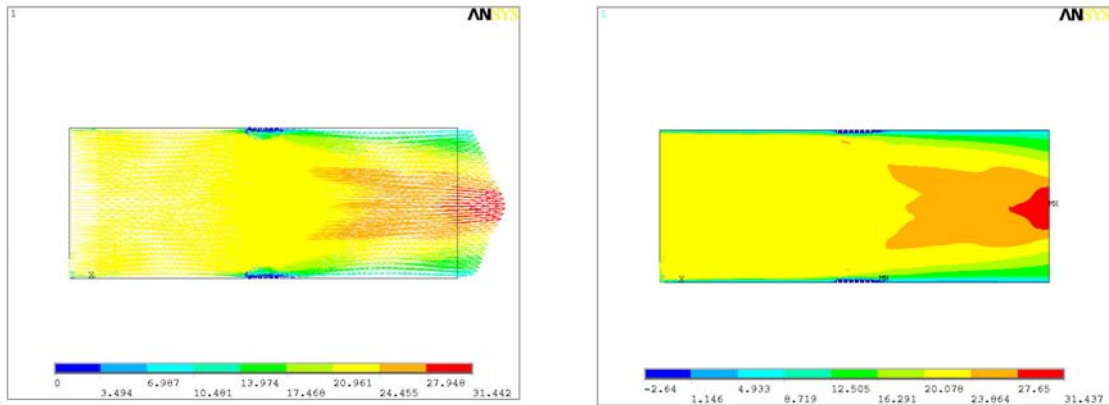
A: Vector plot.



B: Contour plot.

FIGURE A.36: Exit velocity for combination of 1.6 cm, 1100 denier, and 20 cm/s.

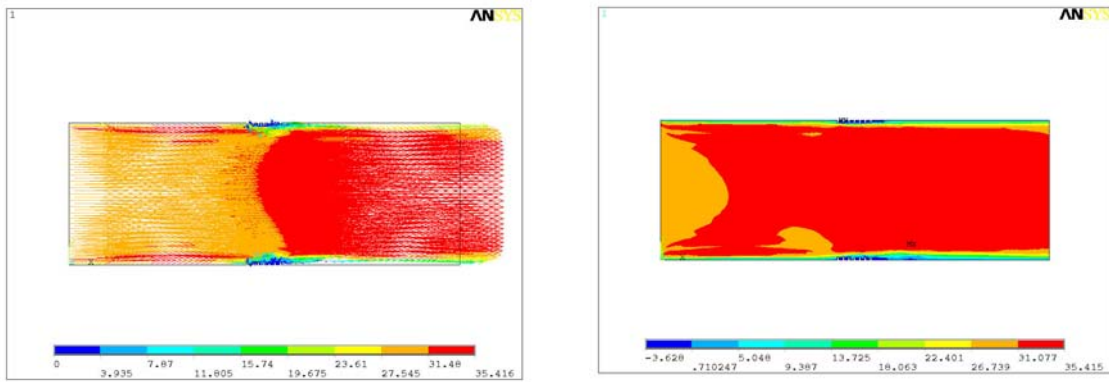
A.5 Exit Velocity Results for 2.5 cm Artery Diameter Combinations



A: Vector plot.

B: Contour plot.

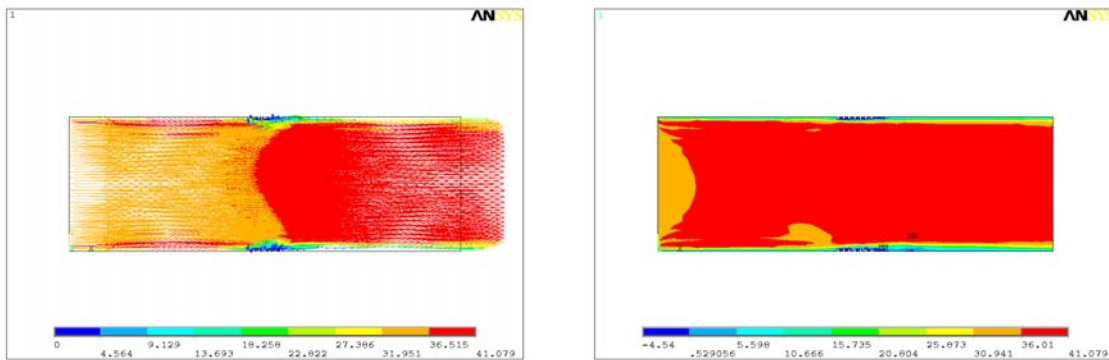
FIGURE A.37: Exit velocity for combination of 2.5 cm, 150 denier, and 28 cm/s.



A: Vector plot.

B: Contour plot.

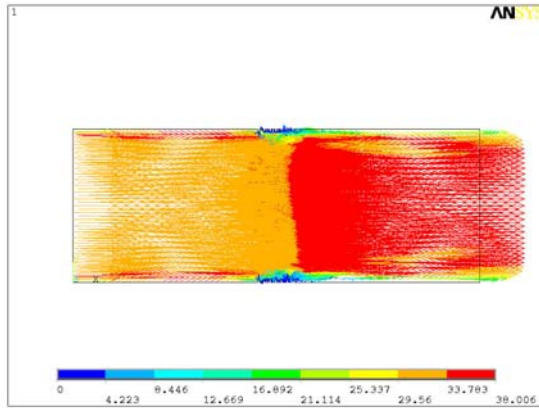
FIGURE A.38: Exit velocity for combination of 2.5 cm, 150 denier, and 33 cm/s.



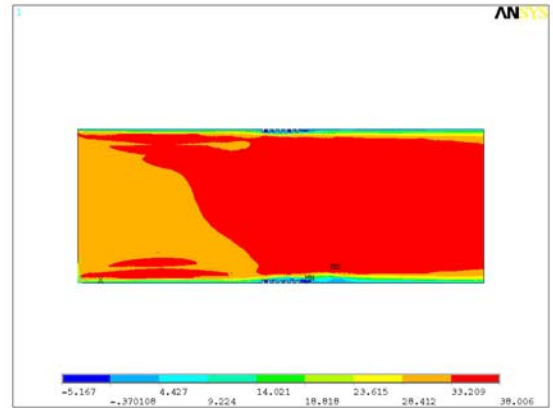
A: Vector plot.

B: Contour plot.

FIGURE A.39: Exit velocity for combination of 2.5 cm, 150 denier, and 38 cm/s.

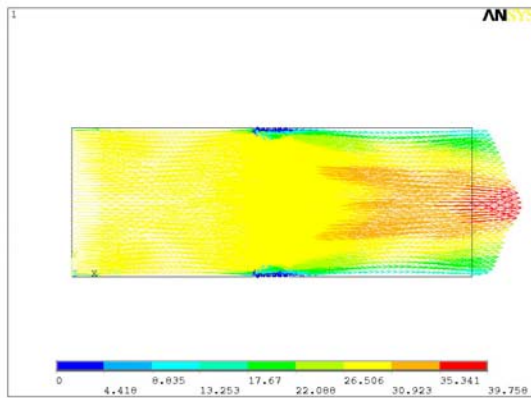


A: Vector plot.

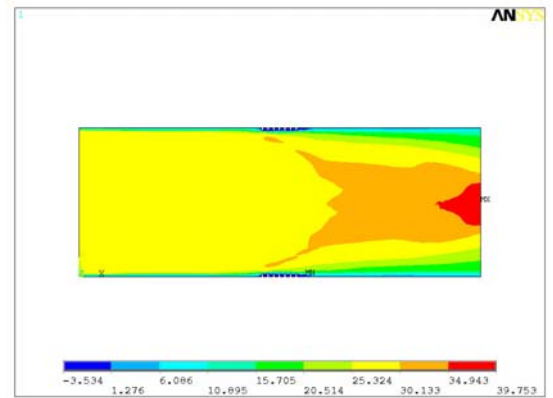


B: Contour plot.

FIGURE A.40: Exit velocity for combination of 2.5 cm, 600 denier, and 28 cm/s.

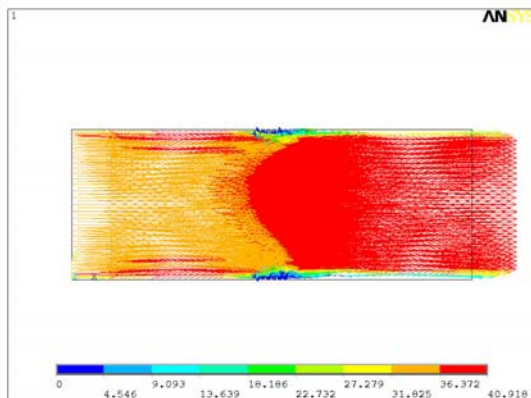


A: Vector plot.

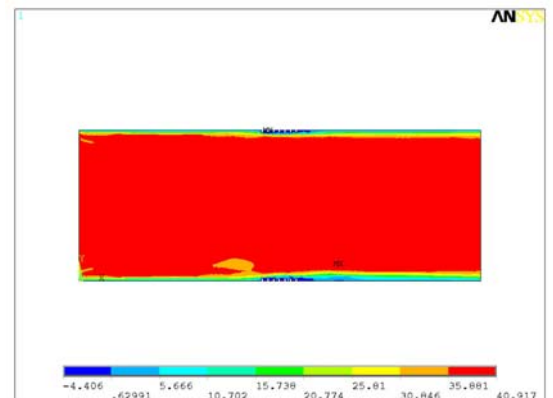


B: Contour plot.

FIGURE A.41: Exit velocity for combination of 2.5 cm, 600 denier, and 33 cm/s.

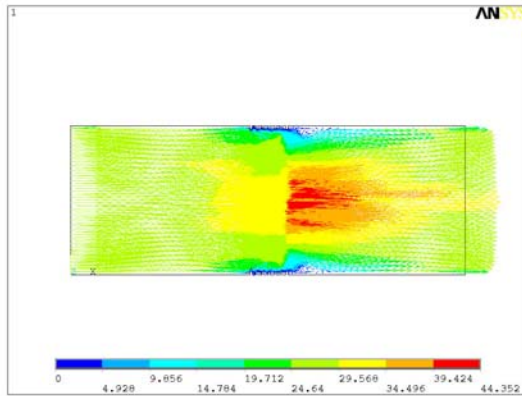


A: Vector plot.

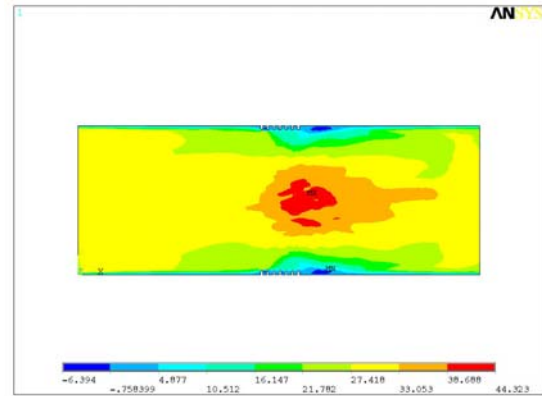


B: Contour plot.

FIGURE A.42: Exit velocity for combination of 2.5 cm, 600 denier, and 38 cm/s.

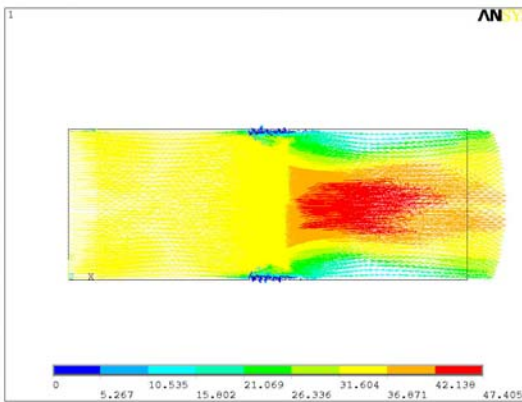


A: Vector plot.

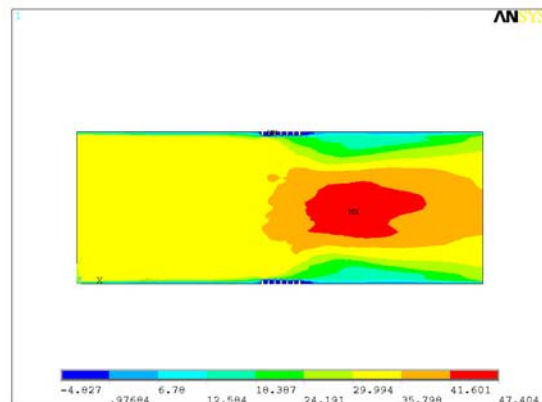


B: Contour plot.

FIGURE A.43: Exit velocity for combination of 2.5 cm, 1100 denier, and 28 cm/s.

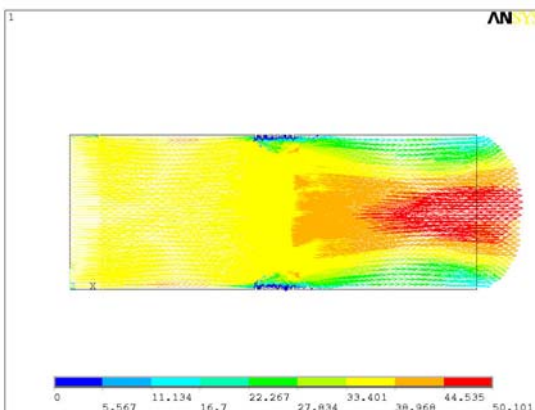


A: Vector plot.

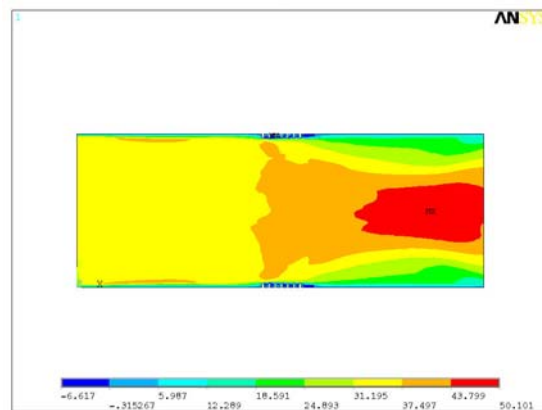


B: Contour plot.

FIGURE A.44: Exit velocity for combination of 2.5 cm, 1100 denier, and 33 cm/s.



A: Vector plot.



B: Contour plot.

FIGURE A.45: Exit velocity for combination of 2.5 cm, 1100 denier, and 38 cm/s.

A.6 Prototype Manufacturing of Braided Hand

To explore other applications of braided structures, a prototype of braided hand was manufactured using the Wardwell braiding machine (Figure A.46). Polyester monofilaments and rectangular wooden mandrels were used. A procedure similar to that described for manufacturing of bifurcated braided structures was followed. The braided hand prototype had a wrist further divided into five fingers. Figures A.47 and A.49 show braided structures manufactured with 16 and 12 monofilaments, respectively. The procedure below was followed:

- The wrist was braided with 64 monofilaments (7.5 cm mandrel).
- After that, the thumb was braided with 16 monofilaments (Figures A.46 and A.48). More monofilaments were used for the thumb because it is thick (2.54 cm mandrel).
- After braiding the thumb, those 16 monofilaments were broken and the bobbins were removed from the machine.
- The remaining 48 bobbins were rearranged on the machine (Figure A.50), 12 in 4 quadrants. A 3.81 cm structure was braided for each finger. Four fingers were braided separately, each with 12 monofilaments (Figures A.48 and A.49). Care was taken to avoid breaking or entangling of monofilaments.

The making of wrist, thumb and four fingers was shown to be feasible.

RECOMMENDATIONS

- The initial part of braided hand has to be braided carefully; transition regions should be braided with proper care.
- Ergonomic and real hand imitating mandrels will certainly improve the appearance of braided hand (Figure A.51 and A.53).

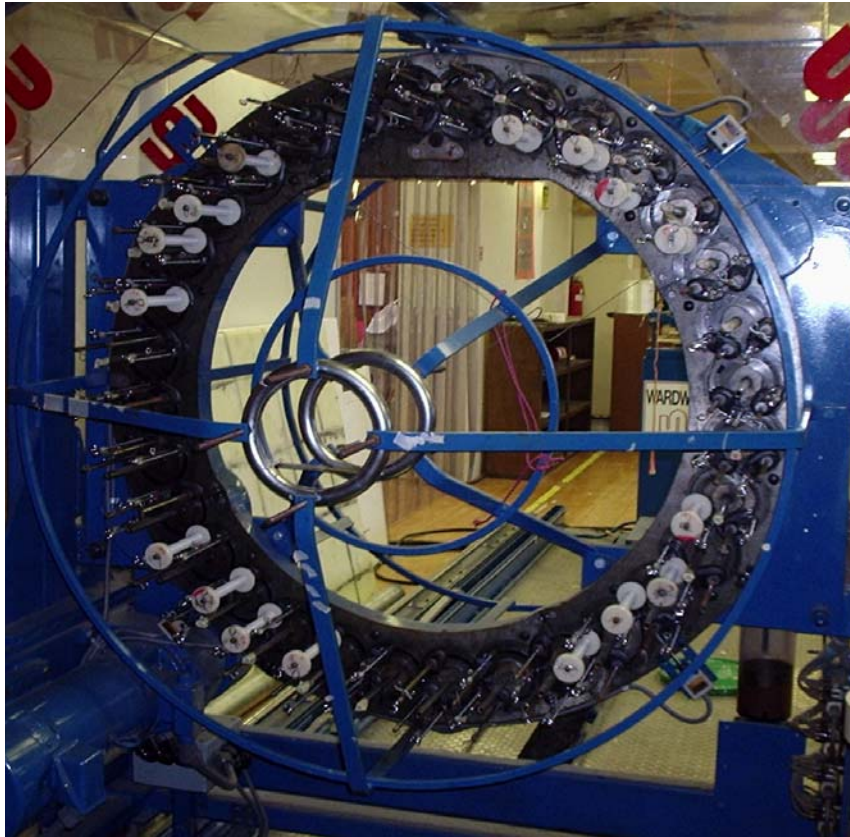


FIGURE A.46: Making braided structure with 16 monofilaments.



FIGURE A.47: Sixteen monofilaments braided structure made on 64 spindle machine.

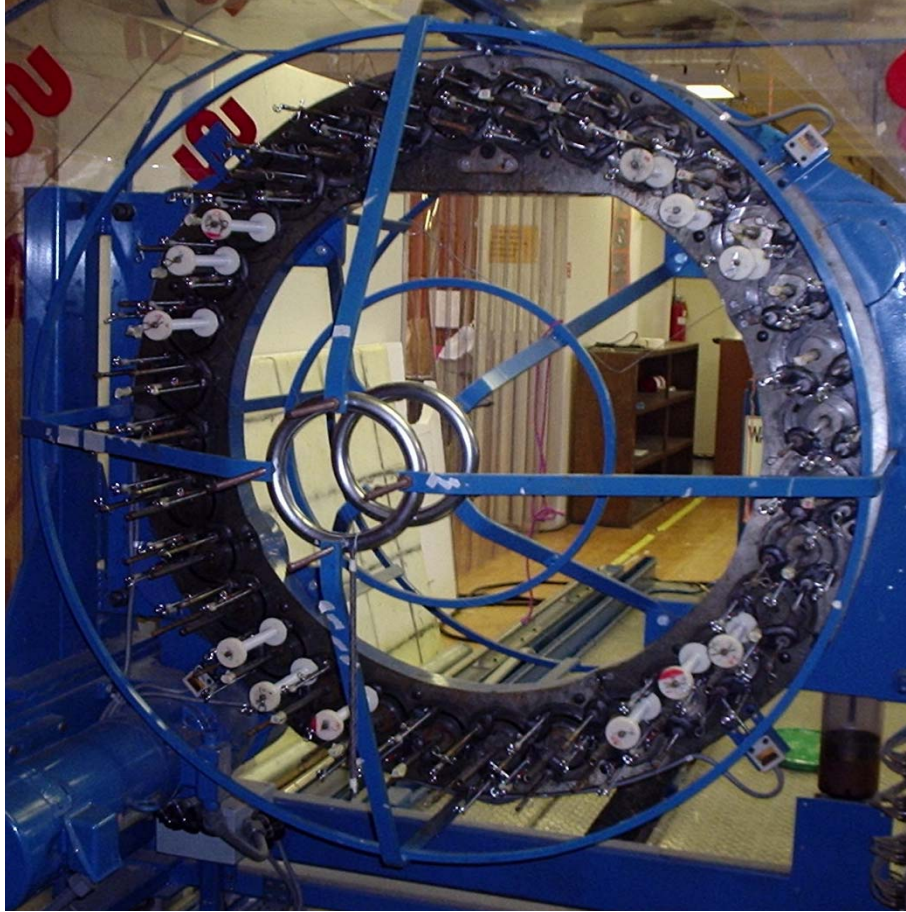


FIGURE A.48: Making braided structure with 12 monofilaments.



FIGURE A.49: Twelve monofilaments braided structure made on 64 spindle machine.

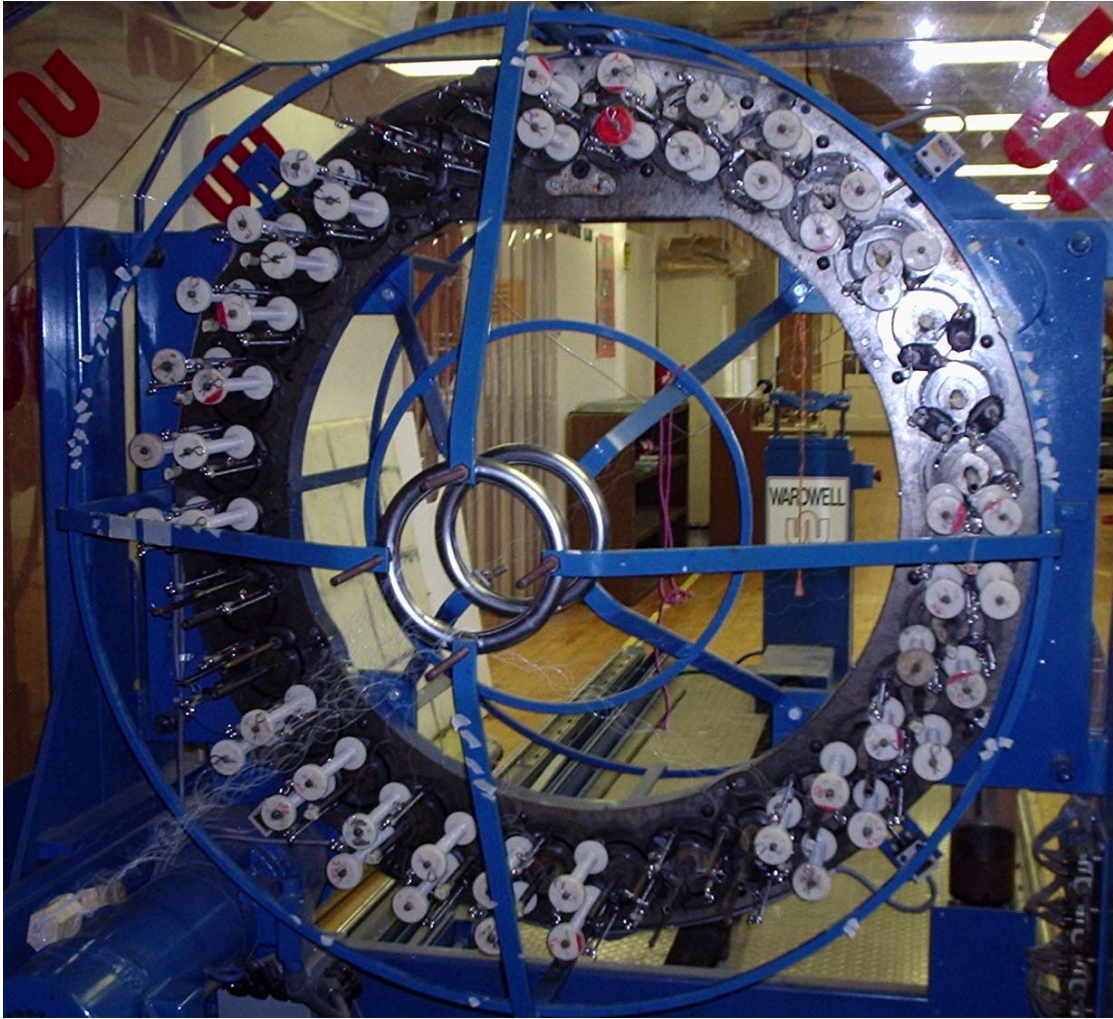


FIGURE A.50: Making braided structure with 48 monofilaments.



FIGURE A.51: Human hand.

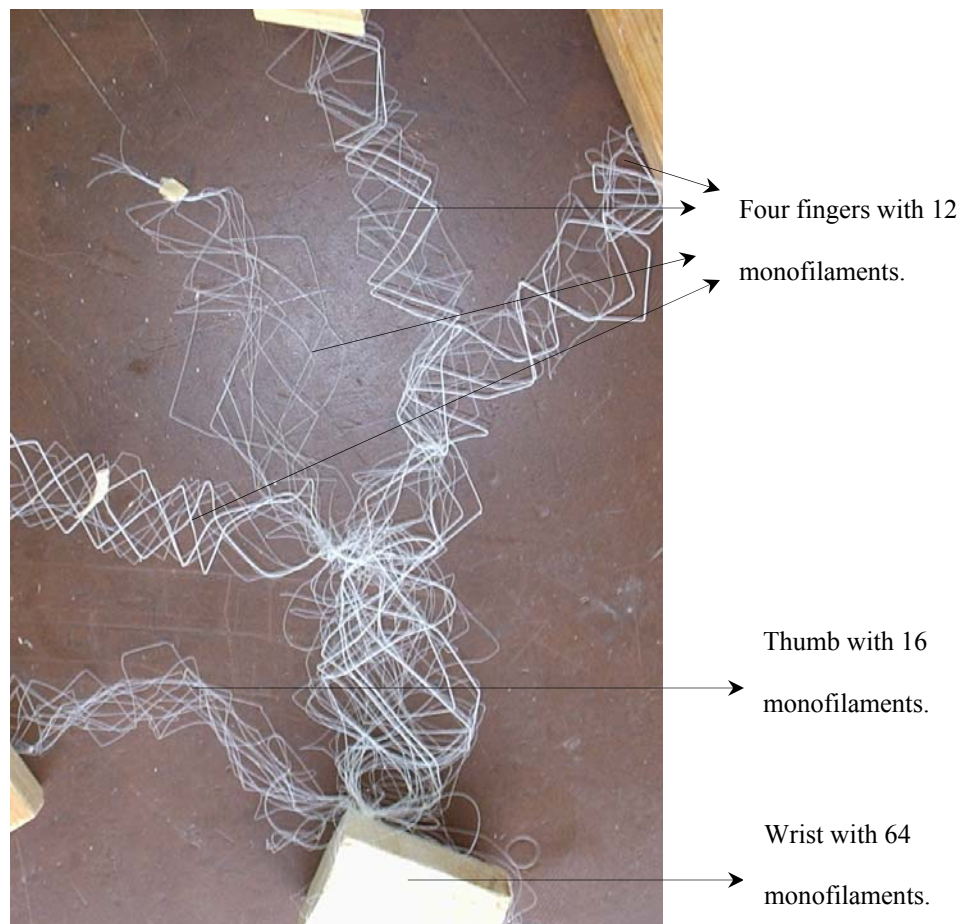


FIGURE A.52: Braided hand prototype.

A.7 Terminology Used

Reference: <http://cancerweb.ncl.ac.uk/omd/>, access date: March 20, 2005.

Anastomosis: An opening developed or created between two normally separate organs by surgical, traumatic or pathological means.

Anatomy: Study of the structure of the body and relationship between its parts.

Aneurysm: A sac formed by the dilatation of the wall of a vessel.

Angioplasty: An operational method to remove blockage of an artery of a person who has angina.

Artery: Thick tubes that carry blood from heart to other parts of the body.

Atherosclerosis: The progressive narrowing and hardening of the arteries over time.

Blood: A circulating tissue composed of a fluid portion (plasma) with suspended formed elements (red blood cells, white blood cells, platelets).

Carotid artery: An artery located in the front of neck that carried blood from heart to brain.

Catheter: A tubular, flexible surgical instrument which can be inserted inside the arteries or veins for various purposes.

Cholesterol: A fatlike steroid found in animal fats and oils, in bile, blood, brain tissue, milk, yolk of egg, myelin sheaths of nerve fibers, the liver, kidneys and adrenal glands.

Coronary: A medical condition in which the flow of blood to the heart is blocked by a blood clot or relating to the arteries that supply blood to the muscles of the heart.

Dilatation: The condition, as of an orifice or tubular structure, of being dilated or stretched beyond the normal dimensions.

Embolism: Sudden blockage of an artery by a clot or foreign material which has been brought to site by the blood current.

Femoral: Pertaining to the femur or thigh.

Graft: Portion of a lesion in the body.

Grafting: The procedure of inserting or implanting a portion of lesion in the body.

Iliac: Pertaining to or in the region of ilium or dorsal bone of the pelvis.

Implantation: The insertion or grafting of living, biological, inert or radioactive material into the body.

Intimal: Relating to the intima or inner layer of a vessel.

Invasive: Involving puncture or incision of the skin for insertion of an instrument or foreign material into the body.

In vitro: Biological processes or reactions happening outside the body in artificial conditions.

In vivo: Inside the living body.

Lesion: Any pathological or traumatic discontinuity of tissue or loss of function of a part.

Magnetic Resonance Imaging: A special imaging technique used to image internal structures of the body.

Morbidity: A diseased condition or state or the incidence of a disease.

Mortality: The death rate.

Patency: The state of being open, especially referred to lumens of arteries and veins.

Physiology: The study of how living organisms function.

Prosthesis: An artificial substitute used for a missing body part or organ.

Restenosis: Recurrence of stenosis after corrective surgery; renarrowing of a structure following the removal or reduction of a previous narrowing.

Stenosis: Narrowing of a duct or canal.

Stent: A tube made of metal or plastic that is inserted into a vessel or passage to keep the lumen open and prevent closure due to a stricture or external compression.

Strut: In general, any piece of a frame which resists thrust or pressure in the direction of its own length.

Thrombosis: The formation, development or presence of thrombus.

Thrombus: An aggregation of blood factors, primarily platelets and fibrin with entrapment of cellular elements, frequently causing vascular obstruction at the point of its formation.

Vein: Blood vessel that returns blood from microvasculature to the heart.

Vessel: Body fluid carrying system.